# Copyright Warning & Restrictions

The copyright law of the United States (Title 17, United States Code) governs the making of photocopies or other reproductions of copyrighted material.

Under certain conditions specified in the law, libraries and archives are authorized to furnish a photocopy or other reproduction. One of these specified conditions is that the photocopy or reproduction is not to be "used for any purpose other than private study, scholarship, or research." If a, user makes a request for, or later uses, a photocopy or reproduction for purposes in excess of "fair use" that user may be liable for copyright infringement,

This institution reserves the right to refuse to accept a copying order if, in its judgment, fulfillment of the order would involve violation of copyright law.

Please Note: The author retains the copyright while the New Jersey Institute of Technology reserves the right to distribute this thesis or dissertation

Printing note: If you do not wish to print this page, then select "Pages from: first page # to: last page #" on the print dialog screen

# DYNAMIC STRESS CONCENTRATIONS ABOUT AN ELLIPTICAL DISCONTINUITY IN AN ELASTIC SOLID

BY

KENNETH ROY SCHROLL

A DISSERTATION

PRESENTED IN PARTIAL FULFILLMENT OF

THE REQUIREMENTS FOR THE DEGREE

OF

DOCTOR OF ENGINEERING SCIENCE IN MECHANICAL ENGINEERING

AT

NEWARK COLLEGE OF ENGINEERING



Newark, New Jersey
1970

APPROVAL OF DISSERTATION

DYNAMIC STRESS CONCENTRATIONS ABOUT AN ELLIPTICAL DISCONTINUITY IN AN ELASTIC SOLID

BY

KENNETH ROY SCHROLL

FOR

DEPARTMENT OF MECHANICAL ENGINEERING

NEWARK COLLEGE OF ENGINEERING

BY

FACULTY COMMITTEE

APPROVED: _____ Chairman

_____

_____

_____

_____

NEWARK, NEW JERSEY

1970

## ABSTRACT

The redistribution of dynamic stresses caused by the presence of an elliptical discontinuity in an infinite isotropic homogeneous elastic solid is examined. The solutions are obtained for the special cases of the rigid immovable inclusion and the vacuous cavity inclusion, and numerical results are presented.

The solutions to the wave equations in elliptical coordinates are expressed in series of the elliptical geometry eigenfunctions. Application of the boundary conditions, vanishing displacements for the rigid immovable inclusion and vanishing stresses for the cavity inclusion, yields in each case two infinite sets of linear algebraic equations for the expansion coefficients of the series solutions.

The incident shear or compressional waves are generated by a line source of excitation whose location with respect to the inclusion may vary. Parametric studies are carried out to determine the influence of ellipse eccentricity, source location and frequency as well as Poisson's ratio with regard to the stresses on the discontinuity boundary.

It is found that the source location does not greatly affect the stress intensity over the range studied. Increasing the ellipse eccentricity causes pronounced increases in the stresses for certain propagation directions of the incident waves. Also the stresses are dependent upon the frequency and are in general maximized at frequencies where the wave length greatly exceeds the dimensions of the discontinuity. Poisson's ratio does not appear to be a critical parameter in the determination of stress intensities.

TABLE OF CONTENTS

## LIST OF SYMBOLS

| Symbol | Definition |
|---|---|
| $x$ | Abscissa of Cartesian Coordinate System |
| $y$ | Ordinate of Cartesian Coordinate System |
| $a$ | Interfocal Separation in Elliptical Coordinate System |
| $\xi$ | Coordinate Label Designating Family of Ellipses |
| $\eta$ | Coordinate Label Designating Family of Hyperbolas |
| $t$ | Time |
| $\omega$ | Circular Frequency |
| $\phi$ | Compressional Wave Displacement Potential |
| $\psi$ | Shear Wave Displacement Potential |
| $k$ | Circular Geometry Wave Number |
| $\gamma_c$ | Elliptical Coordinate Compressional Wave Number |
| $\gamma_s$ | Elliptical Coordinate Shear Wave Number |
| $\lambda$ | Wave Length |
| $ce_m$ | Even Periodic Mathieu Function |
| $se_m$ | Odd Periodic Mathieu Function |
| $Mc_m^{(j)}$ | Even Radial Mathieu Function of $j^{th}$ Kind |
| $Ms_m^{(j)}$ | Odd Radial Mathieu Function of $j^{th}$ Kind |
| $\xi_b$ | Elliptical Coordinate Number Coinciding with Inclusion Boundary |
| $u$ | x Component of Displacement |
| $v$ | y Component of Displacement |
| $\nu$ | Poisson's Ratio |
| $\sigma_x, \sigma_y, \sigma_z$ | Normal Stress Components in Cartesian Coordinates |
| $\rho$ | Density |

| Symbol | Definition |
|---|---|
| $\tau_{ij}$ | Tensor Stress Components |
| $u_i$ | Tensor Displacement Components |
| $\varepsilon_{ij}$ | Tensor Strain Components |
| $\mu$ | Shear Modulus of Elasticity |
| $\delta_{ij}$ | Kronecker Delta |
| $u_\xi$ | $\xi$ Displacement Component |
| $u_\eta$ | $\eta$ Displacement Component |
| $e_{ijk}$ | Alternating Tensor |
| $g$ | Elliptical Metric Tensor Component = $\frac{a^2}{4}(\cosh^2\xi - \cos^2\eta)$ |
| $\tau_{\xi\xi}$ | Radial Stress in Elliptic Coordinates |
| $\tau_{\xi\eta}$ | Shear Stress in Elliptical Coordinates |
| $\tau_{\eta\eta}$ | Tangential or Hoop Stress in Elliptical Coordinates |
| $\tau_{zz}$ | Out of Plane Normal Stress Component |
| $B_m$-$I_m$ | Expansion Coefficients |
| $H_o'$ | Hankel Function of First Kind of Order Zero |
| $\xi_o$ | Radial Coordinate of Wave Source Point |
| $\eta_o$ | Angular Coordinate of Wave Source Point |
| ${}^e\phi_n^k$, ${}^o\phi_n^k$ | Compressional Wave Partial Potentials |
| ${}^e\psi_n^k$, ${}^o\psi_n^k$ | Shear Wave Partial Potentials |
| $B$ | Length of Minor Axis of Elliptical Inclusion |
| $A$ | Length of Major Axis of Elliptical Inclusion |
| $R_o$ | Distance from Inclusion Center to Wave Source Point |
| $R_b$ | Distance from Inclusion Center to Inclusion Boundary Measured in Direction of $R_o$ |

## LIST OF FIGURES

# I. INTRODUCTION

## A. Elastic Wave Diffraction and Dynamic Stresses

It has been known at least since the nineteenth century that an intensification of stress occurs in the vicinity of discontinuities such as holes, cracks, and solid impurities in otherwise homogeneous materials. The theory of elasticity had been well developed by the turn of the nineteenth century beginning with the work of Robert Hooke in the last quarter of the seventeenth century. The phenomenon of elastic wave propagation was examined in the early part of the last century by men such as Navier and Poisson and later by Stokes and Kelvin.[1] It is interesting to note that these investigations were motivated in part by an interest in the transmission of light which was believed to take place in an elastic ether.[2] Also occurring in the latter part of the last century was the development of theories of stress concentrations for holes in plates based on the elasticity theory. However, this work dealt solely with static studies, and it has been only since the middle of the twentieth century that dynamic stress concentrations have been considered in detail.

## B. Static Studies

In 1898, Kirsh obtained the solution for the stress concentrations about a circular hole in a stretched plate.[3] His method of

---

[1]H. Kolsky, Stress Waves in Solids (New York, 1963), p. 14.

[2]Ibid., pp. v-vi.

[3]G. Kirsh, V.D.I., Vol. 42 (1898).

solution was essentially a semi-inverse method, part of which consisted of determining a potential function from which the stresses were derived. The governing differential equation to be satisfied by the potential function was the equation of compatibility in cylindrical coordinates. His results showed that the maximum tensile stress was equal to three times the uniform stress applied at the ends of the plate. Kirsh's solution has been verified many times by strain measurements under experimental conditions.[4]

The solution for the stretched plate containing an elliptical hole was presented by Inglis and Kolosoff[5] in 1913 and 1914, respectively. Kolosoff employed a technique involving complex stress potentials, the governing equation being the biharmonic equation. His results further confirmed those of Kirsh and indicated that as the elliptical hole became more and more slender, the maximum stresses increased without bound. This problem provided valuable insights into the closely related problem of crack development and propagation and the resultant failures of materials.

Another major contribution to the theory of static stress concentrations was made by Southwell and Gough in 1926, when they presented the solution for the stresses around a spherical cavity in a bar subjected to a uniform tension.[6] Again the problem was

---

[4]S. Timoshenko and J. N. Goodier, Theory of Elasticity (New York, 1951), p. 80.

[5]G. Kolosoff, Z. Math. Physik, Vol. 62 (1914).

[6]R. V. Southwell and H. J. Gough, Phil. Mag. (Jan., 1926), p. 71.

solved in terms of a potential function, and the results indicated that the maximum stress on the spherical cavity was about twice as great at the uniform tensile stress for most materials.

The first investigator to treat rigid inclusions rather than cavities was Goodier.[7] He considered gaseous inclusions, perfectly rigid inclusions, and systems representing slag globules in steel and reinforcing rods in concrete. His method of solution consisted of solving the displacement equations of equilibrium by means of a potential function in cylindrical or spherical coordinates. Goodier treated a perfect infinite solid subjected to a uniform static stress at infinity. His numerical results indicated that the maximum stress was approximately equal to twice the uniform stress for most materials and that rigid inclusions caused no appreciable intensification of shear. Also, in agreement with Saint Venant's principle, he determined (as did the aforementioned investigators) that at a distance of about four diameters away from the inclusion, the stress distribution varied from the uniform stress value by no more than about one percent. Thus it was found that the increase of stress caused by geometrical discontinuities was of a very localized nature. Also it was known experimentally that crack propagation and ultimately failure often originated at the boundaries of material imperfections such as those represented by the geometric shapes then being studied analytically.

---

[7]J. N. Goodier, "Concentration of Stress Around Spherical and Cylindrical Inclusions and Flaws," Journal of Applied Mechanics, Vol. 1, Trans. ASME, Vol. 55 (1933), pp. 39-44.

Additional studies were made by Sternberg and Sadowsky[8] on an infinite solid containing a triaxial ellipsoidal cavity. Also for stress concentrations around notches, Neuber[9] has presented analytical and numerical results for many cases.

As stated earlier, the theory of stress wave propagation was developed during the last century. However, for nearly the first half of the twentieth century, the subject was neglected by physicists as reflected by the dearth of literature on the topic from that period.

## C. Elastic and Acoustic Waves in Circular, Spherical, and Parabolic Geometries

Under dynamic loading the effects of an externally applied force are not felt instantaneously at all points of an elastic solid. Actually, the deformations and the associated strains and stresses produced by the force are propagated through the material in the form of waves, the propagation velocity being a function of material properties. If an obstacle is present in the body, the waves are scattered by the obstacle with the result that stress magnification may occur in the region of the scatterer. Surprisingly, the rebirth of interest in stress wave phenomena was not stimulated primarily by considerations of dynamic stress concentrations. Most of the studies which were begun after the inactive period early in the century were undertaken to determine the attenuating and scattering effects of

---

[8] E. Sternberg and M. Sadowsky, Journal of Applied Mechanics, Trans. ASME, Vol. 14 (1949), p. 149.

[9] H. Neuber, Theory of Notch Stresses (Berlin, 1958).

various inclusions on acoustic waves. Thus most studies were restricted to points in the solid far from the scatterer itself.

In 1955, Ying and Truell[10] investigated the scattering of waves by a spherical obstacle in an elastic solid using a separation of variables technique in spherical coordinates. They undertook their study in order to compare the scattering by obstacles in solids with the older and well-known solutions for scattering by a fluid sphere in a fluid. Contemporary laboratory experiments had dealt with the attenuation of ultrasonic wave pulses by precipitates in polycrystals and crystalline alloys. The work of Ying and Truell was intended to serve as a first step toward the solution of the more complicated problem of scattering by a large number of scatterers in a homogeneous solid or the scattering by an inhomogeneous solid.[11] Their results included expressions for the scattered wave and the total scattered energy for long wave (Rayleigh) scattering.

White presented results for elastic wave scattering by a cylinder in 1958.[12] He considered the scattering of plane compressional and shear elastic waves incident obliquely upon an infinitely long non-dissipative cylindrical elastic discontinuity in an isotropic solid.

---

[10]C. F. Ying and Rohn Truell, "Scattering of a Plane Longitudinal Wave by a Spherical Obstacle in an Isotropically Elastic Solid," Journal of Applied Physics, Vol. 27, No. 9 (Sept., 1956), pp. 1086-1097.

[11]Ibid., p. 1086.

[12]R. M. White, "Elastic Wave Scattering at a Cylindrical Discontinuity in a Solid," Journal of Acoustical Society of America, Vol. 30 (1958), pp. 771-785.

His solution was obtained by separating the wave equation in cylindrical coordinates. White analyzed the mode conversion process with respect to the energy contained in each mode as well as scattering cross sections[13] and the far zone angular distribution of intensity both experimentally and analytically for cavities and fluid-filled cavities.

Another major contributor was Knopoff who in 1959, published results for the scattering of compressional and shear waves by spherical obstacles.[14, 15] Using the method of separation of variables in spherical coordinates, he examined scattering by a perfectly rigid and immovable sphere and evaluated the scattered compressional and shear waves in the far field.

In 1960, Einspruch, Witterholt, and Truell presented their analysis of the scattering of transverse elastic waves by spherical obstacles.[16] They included scattering by a fluid-filled sphere and by a

---

[13]The mode conversion process is a phenomenon in which a shear or compressional wave incident upon a boundary produces reflected and refracted waves of both types. The scattering cross section for elastic waves is defined as the ratio of the energy scattered per unit time by the obstacle to the energy per unit area carried per unit time by the incident wave.

[14]Leon Knopoff, "Scattering of Compression Waves by Spherical Obstacles," Geophysics, Vol. XXIV, No. 1 (Feb., 1959), pp. 30-39.

[15]Leon Knopoff, "Scattering of Shear Waves by Spherical Obstacles," Geophysics, Vol. XXIV, No. 2 (April, 1959), pp. 209-219.

[16]N. G. Einspruch, E. J. Whitterholt, and Rohn Truell, "Scattering of a Plane Transverse Wave by a Spherical Obstacle in an Elastic Medium," Journal of Applied Physics, Vol. 31, No. 5 (May, 1960), pp. 806-818.

layered sphere. Again the method of separation of variables was used and the Rayleigh case examined in detail for scattering cross sections.

Until the 1960's, the theoretical work on sound scattering was motivated by the development of laboratory and engineering tools employing ultrasonic techniques. As a result, far field effects were of paramount interest, and near field phenomena, i.e., stress concentrations, were largely ignored. However, in 1962, Pao[17] presented a paper which was one of the first to deal with dynamical stress concentrations on the boundary of the scatterer itself. Pao discussed stress concentrations around a circular cavity in an infinite elastic plate during the passage of plane compressional waves. This was the dynamic counterpart of Kirsh's problem. Employing the separation of variables technique in cylindrical coordinates, Pao found that the dynamic stress concentration factors depended on the incident wave frequency and Poisson's ratio for the plate. He discovered that at certain wave lengths, the dynamical stress concentrations were larger than those encountered under statical loading.

The problem of stress concentration in an elastic plate with a rigid circular inclusion was presented in 1962 by Pao and Mow.[18] The rigid inclusion was excited by the passage of plane compressional

---

[17]Yih-Hsing Pao, "Dynamical Stress Concentration in an Elastic Plate," Journal of Applied Mechanics, Trans. ASME (June, 1962), pp. 299-305.

[18]Y. H. Pao and C. C. Mow, "Dynamic Stress Concentration in an Elastic Plate with Rigid Circular Inclusion," Proc. of the 4th U. S. National Congress of Applied Mechanics, ASME (1962), pp. 335-344.

waves and the inclusion was either fixed in space or free to translate with the plate. Pao and Mow showed that the magnitude of the stress concentration factors depended upon the incident wave length, Poisson's ratio for the plate, and the density of the inclusion. As in the case of the circular cavity, the dynamical stress concentrations were found to be larger for certain wave lengths than those in static cases. Also it was shown that if the rigid inclusion were immovable as well, the stresses could become very large.

A variation of Pao and Mow's problem was treated by Mow and McCabe[19] in 1963. They investigated dynamic stresses in an arbitrarily thick elastic cylinder in an infinite elastic solid during the passage of plane compressional waves. It was demonstrated that the dynamical stresses in the cylinder at certain wave lengths are higher than those in static cases. Mow and McCabe also showed that an increase in the thickness of the cylindrical lining caused a reduction of the stresses there. They indicated that the stresses produced in the cylinder by harmonically varying waves represented an upper bound for a class of non-periodic pulses such as step pulses[20] and exponentially decaying waves, although they presented no proof.

Additional problems of a similar nature but with slight

---

[19]C. C. Mow and W. L. McCabe, "Dynamic Stresses in an Elastic Cylinder," Journal of the Engineering Mechanics Div., ASCE, Vol. 89, No. EM-3 (1963), pp. 21-41.

[20]J. Miklowitz, "Scattering of a Plane Elastic Compressional Pulse by a Cylindrical Cavity," Proc. of the 11th International Congress of Applied Mechanics.

modifications were treated by Mow and Mente in 1963 and by Mow and Workman in 1966. Mow and Mente[21] studied dynamic stresses and displacements around cylindrical cavities and rigid inclusions excited by plane harmonic shear waves. Of principal interest was the close coupling observed between the stresses and the rigid body motion of the rigid discontinuity.

Mow and Workman[22] treated dynamic stresses around a fluid-filled cavity. They found that at critical wave numbers, the intensity of the stresses on the boundary is considerably higher than that under static loading. This phenomenon was caused by resonance in the fluid, and Mow and Workman discovered that they could predict the resonance conditions once the properties of the fluid and the elastic medium were specified.

The problems discussed thus far have dealt with circular or spherical geometries exclusively. In 1966, Thau presented results for the diffraction of elastic waves by a parabolic cylinder and the resultant stress concentrations.[23] His numerical results included the cases of a parabolic rigid cylinder with a semi-infinite line

---

[21]C. C. Mow and L. J. Mente, "Dynamic Stresses and Displacements Around Cylindrical Discontinuities Due to Plane Harmonic Shear Waves," Journal of Applied Mechanics, Vol. 30, Trans. ASME, Vol. 85, Series E (1963), pp. 598-604.

[22]C. C. Mow and J. W. Workman, "Dynamic Stresses Around a Fluid-Filled Cavity," Journal of Applied Mechanics, Trans. ASME (1966), pp. 793-799.

[23]S. A. Thau, "Diffraction of Elastic Waves by a Parabolic Cylinder and Dynamic Stress Concentrations," Ph.D. Thesis, Cornell Univ. (1966).

crack and a semi-infinite rigid ribbon as two special cases. Thau also established the singular behavior of the stresses near the tip of the crack or the rigid ribbon. He showed that the stresses near the tip were inversely proportional to the square root of the distance from the tip.[24]

Cheng and Jahanshahi[25] studied the redistribution of dynamic stresses about a circular discontinuity when the source of excitation was located a finite distance from the scatterer. In particular, they explored the effects of source location on the concentration of energy around a rigid insert and a cavity. Their results indicated that the source location was not a significant parameter in determining energy concentrations about rigid inclusions when the source was more than two or three scatterer diameters away. However, for cavity scatterers the source location had a pronounced influence on the energy concentrations. They concluded that the latter effect must be caused by the propagation of generalized Rayleigh waves on the free cylindrical surface of the cavity. Also the energy concentrations were not in general maximized on the illuminated side of the cavity, an effect also discovered by Pao.

In 1969, Cheng published results for the multiple scattering of

---

[24] S. A. Thau and Y. H. Pao, "Diffractions of Horizontal Shear Waves by a Parabolic Cylinder and Dynamic Stress Concentrations," Journal of Applied Mechanics, Trans. ASME (1966), pp. 785-792.

[25] S. L. Cheng and A. Jahanshahi, "On Dynamic Stress Concentration Around a Discontinuity," Journal of Applied Mechanics, Trans. ASME (1967), pp. 385-391.

elastic waves by parallel cylinders.[26] This work represented a second step toward the solution of the multiple acoustical scattering problem originally suggested by Ying and Truell, although results were confined to the near field of the scatterers. Cheng's solution was based on a method of multiple scattering originally developed for the electromagnetic case and used an iteration process based on systematically improving the results of a single scattering approximation. He showed that depending upon the propagation direction of the incident plane wave, the presence of more than one scatterer could significantly increase the stress magnitudes above the values existing for the single scatterer.

D. Electromagnetic and Acoustic Waves in Elliptical Geometries

Apparently, one of the first investigations to treat wave scattering by an elliptical discontinuity was that by Morse and Rubenstein.[27] Prior to this study the solutions to the elliptical scatterer had been discussed, but only a few numerical solutions had been completed. Morse and Rubinstein completed a table of the Mathieu functions (elliptic geometry eigenfunctions) which then allowed them to solve the problem of diffraction by a slit or ribbon by separating the wave equation in elliptic coordinates. Their numerical results were restricted to points in the far field, an elliptical scatterer of zero

---

[26] S. L. Cheng, "Multiple Scattering of Elastic Waves by Parallel Cylinders," Journal of Applied Mechanics, Trans. ASME (1969), pp. 523-527.

[27] P. M. Morse and P. J. Rubenstein, "The Diffraction of Waves by Ribbons and by Slits," Physical Review, Vol. 54 (1938), pp. 895-898.

thickness (slit or rigid ribbon), and treated only wave lengths on the order of the interfocal distance of the scatterer. Consequently, the range of parameters was generally useful for acoustics and for short radio waves, but was not too interesting for optics.[28]

To overcome some of the shortcomings of the solution of Morse and Rubenstein, Levy obtained a solution to the acoustic scattering problem by an elliptic cylinder that was valid for ultrasonic and optical frequencies.[29] He formulated the exact solution in terms of a series of the Mathieu functions. But the series solution converged well only at low frequencies, so Levy determined the asymptotic expansion of the diffracted field and showed that this solution agreed with that obtained by the methods of geometrical optics. Again the results were valid only for points in the far field, but the elliptical scatterer was not reduced to a slit or ribbon.

In 1962, Yeh obtained the solution for the scattering of electromagnetic waves by a dielectric ribbon[30] in contrast to the perfectly conducting ribbon treated by Morse and Rubenstein. Yeh's solution was given in terms of a series of the Mathieu functions, and he discovered that each of the expansion coefficients of the scattered wave was coupled to all of the coefficients of the series expansion for the

---

[28]Ibid., p. 898.

[29]Bertram R. Levy, "Diffraction by an Elliptic Cylinder," Journal of Mathematics and Mechanics, Vol. 9 (1960), p. 147.

[30]Cavour Yeh, "The Diffraction of Waves by a Penetrable Ribbon," Journal of Mathematical Physics, Vol. 4, No. 1 (Jan., 1963), pp. 65-71.

incident plane wave. This was entirely different from the circular scatterer case. Yeh's results were valid for the far zone and included not only infinitely thin ribbons but ribbons of finite thickness as well, excited by electromagnetic waves of various polarizations.

Barakat[31] presented results for the diffraction of plane waves by an elliptic cylinder nearly concurrently with Yeh's work. Barakat's solution was valid for both electromagnetic and acoustic problems in that he considered both the Dirichlet (soft) and the Neumann (hard) boundary conditions. However, his numerical results covered only the far field and the Rayleigh scattering region, but included discontinuity strips of finite thickness. Barakat's work represented the solutions to a wide range of scattering problems for cylindrical discontinuities from the infinitesimally thin strip, through the ellipse to the circular cylinder, for cases where at most one incident wave, one transmitted wave, and one reflected wave existed. This includes electromagnetic and acoustic waves of all polarizations but excludes incident elastic waves except for those polarized along the cylinder axis. As will be demonstrated shortly, the scattering of elastic waves is in general a considerably more difficult problem to solve than the problem of scattering of electromagnetic or acoustic waves. In addition, the scattering of elastic waves by elliptical discontinuities presents difficulties peculiar to the elliptical geometry.

---

[31]Richard Barakat, "Diffraction of Plane Waves by an Elliptic Cylinder," Journal of the Acoustical Society of America, Vol. 35, No. 12 (Dec., 1963), pp. 1990-1996.

E. Elastic Waves in the Elliptical Geometry

The problems of dynamic elasticity are in general quite complicated owing to the fact that in an elastic solid two waves (shear and compressional) may exist which have distinct characteristic velocities. Additionally, there is the phenomenon known as mode conversion whereby a single wave of either of the two types incident upon a discontinuity results in reflected and transmitted waves of both types. This must be true in order for the boundary conditions to be satisfied,[32] except when the incident wave is polarized in a certain direction determined by the geometry of the scatterer. When the scattered waves are expanded in a series of the eigenfunctions of the particular coordinate system, the wave numbers corresponding to the two separate wave types appear in the eigenfunction arguments. In spherical and cylindrical coordinates, the angular or periodic eigenfunctions are independent of the wave numbers, and the complete wave field can be represented by a simple series expansion. In any other coordinate system, this cannot be accomplished.[33] Thus it is not possible to invoke orthogonality properties of the functions in order to determine the coefficients of the scattered wave expansions. The elliptical scatterer problem is further complicated by the fact that the periodic functions and their derivatives do not have a simple relationship as is true for the trigonometric functions encountered in the cylindrical and spherical geometries. Therefore, even if the problem of the

---

[32]Kolsky, pp. 24-36.

[33]Thau, Ph.D. Thesis, p. 146.

different eigenfunction arguments could be removed according to some approximation or other technique, the difficulty with the derivatives would remain. Both problems are usually handled by one of two methods. First, it is possible to expand the eigenfunctions for either the shear or compressional wave in terms of the eigenfunctions of the other wave. Second, if the eigenfunctions have a periodicity property, a Fourier series representation for these functions may be obtained. Either method, where it is applicable, leads to the problem of solving an infinite set of equations with the result that for the elliptical scatterer no exact formal solution can be obtained by the separation of variables method. Nevertheless, very accurate approximate solutions may be developed for the elliptical scatterer which, when reduced to the special case of the circular cylinder, agree very closely with the results obtained for that case by Pao and others.

In 1961, Harumi published results for the scattering of plane compressional waves by a rigid and immovable ribbon in a solid.[34] Using the separation of variables method, Harumi obtained numerical results for the far field displacements about an elliptical cylindrical discontinuity of zero thickness and wave lengths in the Rayleigh region. In his solution he replaced the periodic eigenfunctions (Mathieu functions) by their Fourier series forms and then approximated the resulting infinite set of equations by a set of twenty.

---

[34]K. Harumi, "Scattering of Plane Waves by a Rigid Ribbon in a Solid," Journal of Applied Physics, Vol. 32, No. 8 (Aug., 1961), pp. 1488-1497.

Harumi's numerical results compared favorably with those obtained by Morse and Rubenstein for the acoustical wave. He showed that when the incident wave was a compressional wave, the scattered compressional wave was similar to the scattered sound wave but only when the incident wave propagated in the direction normal to the ribbon. Also when the wave length became shorter than the width of the ribbon, a sharp angular dependency of the scattered waves appeared.

A subsequent paper by Harumi treated the problem of a cavity ribbon discontinuity strip.[35] The boundary conditions for the vacuous cavity require the vanishing of normal and shear stresses on the cavity surface. In the elliptical geometry it becomes a very complex problem to make use of the available orthogonality conditions for the evaluation of the coefficients of the scattered wave expansions. This difficulty will be discussed in detail in Chapter V. Harumi considered an elliptical discontinuity of zero thickness and restricted his study to Rayleigh scattering and far zone points. Again his results compared favorably with those obtained by Morse and Rubenstein for acoustical scattering by a cavity.

Ang and Knopoff[36] treated a scattering problem very similar to that of Harumi but solved a singular integral equation (approximately)

---

[35]K. Harumi, "Scattering of Plane Waves by a Cavity Ribbon in a Solid," Journal of Applied Physics, Vol. 33, No. 12 (Dec., 1961), pp. 3588-3593.

[36]D. D. Ang and L. Knopoff, "Diffraction of Scalar Elastic Waves by a Clamped Finite Strip," Proc. of the National Academy of Sciences, Vol. 51, No. 3 (March, 1964), pp. 471-476.

for the scattered wave field rather than using separation of variables. Physically, their problem corresponded to the diffraction of acoustic waves by an infinitely massive rigid strip imbedded in a compressible fluid. Ang and Knopoff's results were valid for the far field zone and for long wave lengths.

The problem of crack development and propagation is of considerable interest in dynamic elasticity. Mathematically, these phenomena present great difficulty because it becomes necessary to find the solution near a geometrically induced singularity. While Ang and Knopoff treated this difficulty successfully for far field points, it is the near field that is of interest in elastodynamics from the point of view of stress concentrations. It is evident a priori that the stresses must be singular at a crack tip, but the character of the singularity must be determined analytically. Sih,[37] solving a set of two integral equations for the diffracted wave field in the region of the scatterer, found the singularity to be of the order of the inverse square root of the distance from the tip, thus substantiating the results of Thau for the parabolic crack.

## F. Object and Scope of Dissertation

It is evident from the historical development of wave scattering in elastodynamics summarized in the first five sections of this introduction that the geometrically simple scatterers have been quite

---

[37] G. C. Sih, "Singular Solution Near a Rigid Ribbon Excited by Plane Waves," Journal of the Franklin Institute, Vol. 286, No. 2 (Aug., 1968), pp. 152-157.

thoroughly treated. However, stress distributions on or near the scatterer, as well as the effects of source location have been nearly neglected for the elliptical discontinuity.

It is the purpose of this investigation to develop new solutions regarding the scattering of stress waves by elliptical discontinuities with emphasis on near field points. The formal solution is presented for an arbitrary elastic scatterer as well as a fluid-filled cavity scatterer, and the rigid immovable and the vacuous cavity discontinuities are studied in detail. Compressional and shear incident waves are studied and the effects of source location taken into account. Consequently, cylindrical as well as plane waves are considered. In addition, the eccentricity of the scatterer is allowed to vary. Also Rayleigh scattering is investigated in detail, and the high frequency limits and static limits are discussed.

Chapter II of this paper is devoted to a presentation of the elliptical coordinates and an introduction to the Mathieu functions which arise naturally in the solution to the scattering problem.

Chapter III covers the basic aspects of the problems to be examined including the governing dynamic equations and the boundary conditions.

Chapter IV includes a discussion of the incident wave types along with the appropriate high and low frequency approximations.

Chapter V presents the formal solution for the arbitrary elastic

scatterer. Then the derivation of the special cases of a fluid-filled cavity, a vacuous cavity, and a rigid and immovable inclusion from the general solution is indicated.

Chapter VI is a summary of the important results with suggestions for additional research.

The Appendix includes derivations of the elliptic metric, the Christoffel symbols, the Laplacian in elliptical coordinates, separation of the Helmholtz equation, as well as an explanation of the physical stress and displacement components, a discussion of shear and compressional wave potentials, numerical methods, and lastly, a comparison of the various methods of solution available for the analysis of the elliptical scatterer problem.

## II. ELLIPTICAL COORDINATES AND THE MATHIEU FUNCTIONS

### A. Elliptical Coordinates

The elliptical geometry of the discontinuity to be treated suggests the use of elliptic coordinates. All subsequent equations to be developed will be referred to elliptic coordinates for obvious reasons of convenience. The transformation to plane elliptic coordinates from the two-dimensional Cartesian coordinates is accomplished by the following transformation.[1]

$$x = \frac{a}{2}\cosh\xi\cos\eta\,, \quad y = \frac{a}{2}\sinh\xi\sin\eta \tag{2A.1}$$

where $a$ is a constant. The coordinate $\eta$ takes on values from $0$ to $2\pi$ and the coordinate $\xi$ varies from $0$ to $\infty$. When the coordinate $\xi$ is a constant $\xi_0$, the transformation (2A.1) yields a locus of points which is an ellipse because

$$\frac{x}{a/2\cosh\xi_0} = \cos\eta \quad \text{and} \quad \frac{y}{a/2\sinh\xi_0} = \sin\eta$$

and $\cos^2\eta + \sin^2\eta = 1$ which yields

$$\frac{x^2}{(a/2\cosh\xi_0)^2} + \frac{y^2}{(a/2\sinh\xi_0)^2} = 1 \tag{2A.2}$$

Then it may be shown that the semimajor axis of the ellipse is given by $\frac{a}{2}\cosh\xi_0$ and the semiminor axis by $\frac{a}{2}\sinh\xi_0$. The distance between the foci is given by[2]

---

[1]Kenneth S. Miller, Partial Differential Equations in Engineering Problems (Englewood Cliffs, N.J., 1964), pp. 180-182.

[2]P. Mainardi, C. Konove and E. G. Baker, A First Courst in Mathematics (Princeton, 1961), p. 274.

$$2\left[\left(\frac{a}{2}\cosh\xi_o\right)^2 - \left(\frac{a}{2}\sinh\xi_o\right)^2\right]^{1/2} = a \tag{2A.3}$$

Thus it may be concluded that the family of curves $\xi =$ constant represents a family of confocal ellipses. For the case $\xi_o = 0$, the ellipse degenerates to a straight line of length $a$ between $(-\frac{a}{2}, 0)$ and $(\frac{a}{2}, 0)$. When $\xi_o \to \infty$, the foci coalesce, and the elliptical boundary approaches a circle of infinite radius with center at the origin. If one considers the curves defined by $\eta =$ constant, one obtains

$$\frac{x}{a/2\cos\eta_o} = \cosh\xi \quad , \text{ and } \frac{y}{a/2\sin\eta_o} = \sinh\xi$$

and

$$\frac{x^2}{(a/2\cos\eta_o)^2} - \frac{y^2}{(a/2\sin\eta_o)^2} = \cosh^2\xi - \sinh^2\xi = 1 \tag{2A.4}$$

These curves define a family of hyperbolas whose principal axes coincide with the x-axis. Their interfocal distance is found to be[3]

$$2\left[(a/2\cos\eta_o)^2 + (a/2\sin\eta_o)^2\right]^{1/2} = a \tag{2A.5}$$

Therefore, the hyperbolas are confocal, and they share the foci with the family of ellipses.[4]

It may be shown that the family of ellipses is orthogonal to the family of hyperbolas with the following additional properties. For

---

[3]Mainardi, Konove and Baker, pp. 278-279.

[4]Miller, p. 181.

$\eta = 0$ , one finds that $x = \frac{a}{2}\cosh\xi$ , $y = 0$ indicating that the corresponding hyperbola degenerates to a straight line running from $x = \frac{a}{2}$ to $x = +\infty$ along the x-axis. For $\eta_0 = \pi$ , it is found that $x = -\frac{a}{2}\cosh\xi$ , $y = 0$ , and the hyperbola reduces to a line from $x = -a/2$ to $x = -\infty$ . For the case $\eta_0 = \pi/2$, one finds $x = 0$ , $y = \frac{a}{2}\sinh\xi$ which is the portion of the y-axis from $y = 0$ to $y = +\infty$. Similarly, for $\eta_0 = 3\pi/2$ , the hyperbola degenerates to the lower half of the x-axis. See Figure 1 for a graphical representation of the elliptical coordinate system.

B. Helmholtz Equation in Elliptical Coordinates

Dynamic elasticity problems can often be reduced to the solution of the wave equation for a set of potential functions. The derivation of the two-dimensional wave equation from the governing equations of elasticity is shown in Chapter III. The result of that derivation is

$$\left[\frac{\partial^2}{\partial x^2} + \frac{\partial^2}{\partial y^2} - \frac{1}{c^2}\frac{\partial^2}{\partial t^2}\right]\Phi = 0 \qquad (2B.1)$$

Equation (2B.1) is satisfied by each of the potential functions. Harmonic time dependence is prescribed for the potentials because it is believed that the stress concentrations caused by time harmonically varying waves represent an upper bound for stresses produced by a class of non-periodic incident pulses as reported by Mow and McCabe. Thus the time dependence is

$$\Phi(x,y,t) = \phi(x,y)\,e^{-i\omega t} \qquad (2B.2)$$

where $\omega$ is the angular frequency of the incident and diffracted waves.

Then the wave equation reduces to the scalar Helmholtz equation

$$\left[\frac{\partial^2}{\partial x^2} + \frac{\partial^2}{\partial y^2} + k^2\right]\phi = 0 \tag{2B.3}$$

for which $k = \omega/c = 2\pi/(\text{wave length})$ is the wave number. The transformation (2A.1) to elliptic coordinates changes (2B.3) to (see Appendix C)

$$\frac{4}{a^2}\left[\cosh^2\xi - \cos^2\eta\right]^{-1}\left[\frac{\partial^2}{\partial\xi^2} + \frac{\partial^2}{\partial\eta^2}\right]\phi + k^2\phi = 0 \tag{2B.4}$$

A solution to (2B.4) is sought by separating the variables as follows

$$\phi(\xi,\eta) = S(\eta)Z(\xi) \tag{2B.5}$$

Substituting (2B.5) into (2B.4), the separated equations are obtained

$$\frac{d^2S}{d\eta^2} + \left(b' - \frac{k^2a^2}{4}\cos^2\eta\right)S = 0 \tag{2B.6}$$

$$\frac{d^2Z}{d\xi^2} - \left(b' - \frac{k^2a^2}{4}\cosh^2\xi\right)Z = 0 \tag{2B.7}$$

Equation (2B.6) is known as Mathieu's equation, and equation (2B.7) is known as Mathieu's modified equation. With the identities $\cos^2\eta = \frac{1}{2}(1+\cos 2\eta)$ and $\cosh^2\xi = \frac{1}{2}(1+\cosh 2\xi)$, equations (2B.6) and (2B.7) are recast into the more common forms

$$\frac{d^2S}{d\eta^2} + (b - 2q\cos 2\eta)S = 0 \tag{2B.8}$$

$$\frac{d^2Z}{d\xi^2} - (b - 2q\cosh 2\xi)Z = 0 \tag{2B.9}$$

where $b$ is the separation constant, and $q$ is the elliptical wave number given by

$$q = \frac{k^2 a^2}{16} = \left(\frac{\pi a}{2\lambda}\right)^2 \tag{2B.10}$$

and $\lambda$ is the wave length.

The solutions to (2B.8) and (2B.9) are called the periodic Mathieu functions and the radial Mathieu functions, respectively. A full description of these solutions is presented in the following section beginning with the Helmholtz equation in a general three-dimensional form and with emphasis on the mathematical properties of the functions.

C. Properties of Mathieu Functions

Canonical Forms. The material[5] of this section consists of those definitions and properties of the Mathieu functions which are employed in analyzing the problems investigated in the following chapters. While the specific reference will not be listed for each expression, it should be noted that each of the references on Mathieu functions cited in the bibliography contains essentially the same basic material, although different notations are used.

The general three-dimensional form of equation (2B.4) is considered for the purpose of describing the Mathieu functions and their properties.

---

[5]G. Blanche and D. S. Clemm, Tables Relating to the Radial Mathieu Functions, Vol. 1, Functions of the First Kind (Aeronautical Research Laboratories, U. S. Air Force).

The general form can be written as

$$\left(\frac{\partial^2 f}{\partial u^2} + \frac{\partial^2 f}{\partial v^2}\right)\frac{2}{M(\cosh 2u - \cos 2v)} + \frac{\partial^2 f}{\partial z^2} + k^2 f = 0 \tag{2C.1}$$

The wave equation is known to be separable in elliptic coordinates so that

$$f = f_1(v)\, f_2(u)\, f_3(z) \tag{2C.2}$$

Substituting (2C.2) into (2C.1) and simplifying, the following is obtained

$$\left(\frac{1}{f_2}\frac{d^2 f_2}{du^2} + \frac{k^2 M \cosh 2u}{2}\right) + \left(\frac{1}{f_1}\frac{d^2 f_1}{dv^2} - \frac{k^2 M \cos 2v}{2}\right)$$

$$+ \frac{1}{f_3}\frac{d^2 f_3}{dz^2}\,\frac{M}{2}(\cosh 2u - \cos 2v) = 0 \tag{2C.3}$$

Then the following three equations are implied

$$\frac{d^2 f_3}{dz^2} + \alpha_1 f_3 = 0 \tag{2C.4}$$

$$\left(\frac{1}{f_2}\frac{d^2 f_2}{du^2} + \frac{k^2 M \cosh 2u}{2}\right) - \frac{\alpha_1 M \cosh 2u}{2} = b \tag{2C.5}$$

$$-\left(\frac{1}{f_1}\frac{d^2 f_1}{dv^2} - \frac{k^2 M \cos 2v}{2}\right) + \frac{\alpha_1 M \cos 2v}{2} = b \tag{2C.6}$$

where $b$ and $\alpha_1$ are the separation constants. Letting $\frac{M}{2}(k^2 - \alpha_1) = 2q$ and substituting into (2C.5) and (2C.6), the following results are obtained

$$\frac{d^2 f_1}{dv^2} + (b - 2q\cos 2v) f_1 = 0 \tag{2C.7}$$

$$\frac{d^2 f_2}{du^2} - (b - 2q\cosh 2u) f_2 = 0 \qquad (2C.8)$$

Equations (2C.7) and (2C.8) are Mathieu's equation and Mathieu's modified equation, respectively. It can be shown that the transformation $V = iu$ reduces (2C.7) to (2C.8). For many applications, the parameters $b$ and $q$ are not related. However, for solutions to the wave equation, the function $f_1$ must be periodic with period $\pi$ or $2\pi$. This arises from physical arguments which are presented by McLachlan.[6] It is found that for $f_1$ to be periodic, $b$ is restricted to a set of values $b(q)$ for each value of $q$. These special values are known as the characteristic values. It can further be proved that if $b$ takes on values such that $f_1$ is periodic of period $\pi$ or $2\pi$, then a second independent solution of (2C.7) cannot be periodic unless $q = 0$. For this reason in physical problems involving the solutions to the wave equation, the second solution to (2C.7) does not appear. The solutions to (2C.8) for the same $b$ and $q$ must be determined. There will be two independent solutions of (2C.8) both of which are required in a great number of physical problems.

The characteristic values $b(q)$ for $q$ real are tabulated in several references.[7]

The Periodic Solutions. Rewrite equation (2C.7) as follows

---

[6] N. W. McLachlan, Theory and Application of Mathieu Functions (London, 1951).

[7] Cf., NBS, Tables Relating to the Mathieu Functions (Columbia University Press, New York, 1951).

$$\frac{d^2f}{dz^2} + (b - 2q\cos 2z)f = 0 \qquad (2C.9)$$

The characteristic values $b$ which yield even periodic solutions are to be represented by $a_k$, $k = 0, 1, 2 \ldots$ The characteristic values yielding odd periodic solutions are designated by $b_k$, $k = 1, 2 \ldots$ The zero order odd solution is zero identically. Equation (2C.9) has four distinct types of periodic solutions. They are either odd or even functions of period $\pi$ or $2\pi$. The even and odd solutions are given respectively by (2C.10) and (2C.11).

$$ce_r(z,q) = \sum_{k=0}^{\infty} A_{2k+p}^{r} \cos(2k+p)z \qquad p = 0 \text{ or } 1$$

associated with $a_r$ (2C.10)

$$se_r(z,q) = \sum_{k=0}^{\infty} B_{2k+p}^{r} \sin(2k+p)z \qquad p = 0 \text{ or } 1$$

associated with $b_r$ (2C.11)

For $p = 0$ the periodic solutions have period $\pi$, and for $p = 1$ they have period $2\pi$. A given characteristic value $b$ is associated with one and only one of the four types of periodic solutions given by (2C.10) and (2C.11).

Power Series. For sufficiently small $|q|$ the following power series in $q$ may be used to calculate the periodic functions

$$ce_0(z,q) = 2^{-1/2}\left[1 - \frac{q}{2}\cos 2z + q^2\left(\frac{\cos 4z}{32} - \frac{1}{16}\right)\right] + \cdots \qquad (2C.12)$$

$$ce_1(z,q) = \cos z - \frac{q}{8}\cos 3z + q^2\left[\frac{\cos 5z}{192} - \frac{\cos 3z}{64} - \frac{\cos z}{128}\right]$$

$$- q^3\left[\frac{\cos 7z}{9216} - \frac{\cos 5z}{1152} - \frac{\cos 3z}{3072} + \frac{\cos z}{512}\right] + \cdots \qquad (2C.13)$$

$$se_1(z,q) = \sin z - \frac{q}{8}\sin 3z + q^2\left[\frac{\sin 5z}{192} + \frac{\sin 3z}{64} - \frac{\sin z}{128}\right]$$

$$- q^3\left[\frac{\sin 7z}{9216} + \frac{\sin 5z}{1152} - \frac{\sin 3z}{3072} - \frac{\sin z}{512}\right] + \cdots \qquad (2C.14)$$

$$ce_2(z,q) = \cos 2z - q\left(\frac{\cos 4z}{12} - \frac{1}{4}\right) + q^2\left(\frac{\cos 6z}{384} - \frac{19\cos 2z}{288}\right) \qquad (2C.15)$$

$$se_2(z,q) = \sin 2z - q\frac{\sin 4z}{12} + q^2\left(\frac{\sin 6z}{384} - \frac{\sin 2z}{288}\right) + \cdots \qquad (2C.16)$$

$$\begin{matrix} ce_r(z,q) \\ se_r(z,q) \end{matrix} = \cos(rz - p(\pi/2)) - q\left\{\frac{\cos[(r+2)z - p\pi/2]}{4(r+1)}\right.$$

$$\left. - \frac{\cos[(r-2)z - p\pi/2]}{4(r-1)}\right\} + q^2\left\{\frac{\cos[(r+4)z - p\pi/2]}{32(r+1)(r+2)}\right.$$

$$\left. + \frac{\cos[(r-4)z - p\pi/2]}{32(r-1)(r-2)} - \frac{\cos[rz - p\pi/2]}{32}\left[\frac{2(r^2+1)}{(r^2-1)^2}\right]\right\} + \cdots \qquad (2C.17)$$

with $p=0$ for $ce_r(z,q)$ and $p=1$ for $se_r(z,q)$, $r \geq 3$.

Normalization. The periodic solutions associated with the characteristic values $a_r$, $b_r$ can be normalized in a number of

ways. A normalization defined by Ince[8] is as follows

$$\int_0^{\pi} [ce_r(z,q)]^2 dz = \int_0^{\pi} [se_r(z,q)]^2 dz = \pi/2 \qquad (2C.18)$$

where $ce_r$ and $se_r$ have been defined in (2C.10) and (2C.11), respectively.

With another commonly used notation[9] the periodic functions are defined as

$$Se_{2m+p}(q,z) = \sum_{m=0}^{\infty} De_{2m+p}(q) \cos(2m+p)z \qquad a = a_r \qquad (2C.19)$$

$$So_{2m+p}(q,z) = \sum_{m=0}^{\infty} Do_{2m+p}(q) \sin(2m+p)z \qquad b = b_r \qquad (2C.20)$$

where $Se$ and $So$ are the even and odd periodic functions, respectively. The normalization often used in this case is defined such that

$$Se_r(q,0) = 1 \quad \text{and} \quad \left[\frac{d}{dz} So_r(q,z)\right] = 1 \quad \text{for } z = 0 \qquad (2C.21)$$

The Ince normalization will be used for the periodic functions. It should be noted that in general

$$\frac{d}{dz} se_r(z,q) \neq ce_r(z,q) \qquad (2C.22)$$

This fact considerably complicates the analysis in the exact analytical

---

[8]E. L. Ince, Tables of the Elliptic Cylinder Functions (Edin., 1932).

[9]Stratton, Morse, Chu and Hutner, Elliptic Cylinder and Spheroidal Wave Functions (New York, 1941).

solution to the wave scattering problem and in addition, leads to difficulties in the approximate average wave number perturbation solution discussed in the Appendix.

The Radial Solutions. For convenience, equation (2C.8) is rewritten as follows

$$\frac{d^2f}{dz^2} - (b - 2q\cosh 2z)f = 0 \tag{2C.23}$$

If $z$ is replaced by $iz$ in the periodic solutions (2C.10) and (2C.11), the first solutions of the modified Mathieu equation (2C.23) are obtained.

$$Ce_{2r+p}(z,q) = ce_{2r+p}(iz,q) = \sum_{k=0}^{\infty} A_{2k+p}^{2r+p}(q)\cosh(2k+p)z$$

associated with $a_r$ (2C.24)

$$Se_{2r+p}(z,q) = -ise_{2r+p}(iz,q) = \sum_{k=0}^{\infty} B_{2k+p}^{2r+p}(q)\sinh(2k+p)z$$

associated with $b_r$ (2C.25)

The first solutions to the Mathieu modified equation are known as the "radial" solutions of the first kind. From the nature of the elliptical geometry and the behavior of the modified Mathieu equation (2C.8) as the parameter $z$ grows large, one would expect the solutions of (2C.8) to be related to Bessel functions. It can be shown that for arbitrary $a$ and $q$, the solutions of the modified Mathieu equation can be written in terms of a series of Bessel functions. Following the notation of Blanche and Clemm, the following conventions

are adopted for specifying the various Bessel functions

$$J_\rho(z) = Z_\rho^{(1)}(z) \qquad Y_\rho(z) = Z_\rho^{(2)}(z)$$

$$H_\rho^{(1)}(z) = J_\rho(z) + i\,Y_\rho(z) = Z_\rho^{(3)}(z)$$

$$H_\rho^{2}(z) = J_\rho(z) - i\,Y_\rho(z) = Z_\rho^{(4)}(z)$$

With these definitions the following functions can be demonstrated to satisfy the modified Mathieu equation (2C.8) if $a$ is a characteristic value yielding solutions of the Mathieu equation (2C.9) having period $\pi$ or $2\pi$.

$$M_{C_{2n+\rho}}^{(j)}(z,q) = \sum_{k=0}^{\infty} A_{2k+\rho}(-1)^{k+n}\left[J_{k-s}(u_1)Z_{k+\rho+s}^{(j)}(u_2) + J_{k+s+\rho}(u_1)Z_{k-s}^{(j)}(u_2)\right] / A_{2s+\rho}\,\varepsilon_{2s+\rho} \tag{2C.26}$$

$$M_{S_{2n+\rho}}^{(j)}(z,q) = \sum_{k=0}^{\infty} B_{2k+\rho}(-1)^{k+n}\left[J_{k-s}(u_1)Z_{k+\rho+s}^{(j)}(u_2) - J_{k+\rho+s}(u_1)Z_{k-s}^{(j)}(u_2)\right] / B_{2s+\rho} \tag{2C.27}$$

where

$$u_1 = q^{1/2}e^{-z}, \quad u_2 = q^{1/2}e^{z} \quad ; \quad \rho = 0, 1$$

$\varepsilon_{2s+\rho} = 2$ if $2s+\rho = 0$ and $\varepsilon_{2s+\rho} = 1$ otherwise.

In (2C.26) and (2C.27) above, the choice of $s$ is arbitrary so long as $A_{2s+\rho}$ or $B_{2s+\rho}$ do not vanish. For numerical computations

$A_{2s+p}$ or $B_{2s+p}$ is generally taken as the largest coefficient of the set. Also in (2C.26) and (2C.27) with $j=1$, the radial solutions of the first kind are obtained in terms of Bessel functions of the first kind. If $j=2$, the radial solutions of the second kind are obtained in terms of products $J_n(u_1)Y_k(u_2)$. The first and second solutions are linearly independent, and with $j=3$ or $j=4$, one obtains the so-called Mathieu-Hankel solutions which are analogous to the Hankel functions of circular geometries.

The series solutions (2C.26) and (2C.27) converge rapidly for real positive $z$.[10] For numerical computations these Bessel function product solutions are the most advantageous to use owing to rapid convergence and simplicity. In the notation of (2C.23) the parameter $z$ represents the radial coordinate in the elliptical geometry. The ellipse eccentricity is specified by $1/\cosh z$. As $z \to \infty$ ($z$ real), the ellipse tends to a circle, and the eccentricity of the ellipse approaches zero. In this case the solutions to (2C.23) are known to be the Bessel functions. Thus the normalizations imposed on the radial solutions given by (2C.26) and (2C.27) are defined such that the radial solutions degenerate to the appropriate Bessel functions when $z \to \infty$.

---

[10] G. Blanche and D. S. Clemm, Vol. 1, p. xii.

# III. PROBLEM DEFINITION

## A. Physical Aspects of the Medium

The medium which contains the elliptical discontinuity is prescribed to be isotropic, homogeneous, and infinite in extent in all directions. The nature of the material is therefore such that it permits the propagation of both shear (transverse) and compressional (longitudinal) waves. The discontinuity scatterer is taken to be an infinitely long cylinder with elliptical cross section. The cylinder may be empty, or it may consist of a material different from that of the elastic matrix.

The principal elliptical axes at any section of the cylinder coincide with the x- and y-axes of a Cartesian coordinate system, while the foci at any section lie on lines parallel to the z-axis of the Cartesian system as shown in Figure 1. The boundary of the discontinuity coincides with the coordinate line $\xi = \xi_b$. Then the entire scatterer boundary surface is specified by a single number $\xi_b$. It is possible to allow the elliptical cylinder to degenerate to an infinite ribbon of width equal to the interfocal distance $a$ by letting $\xi_b \to 0$. Also the circular cylindrical scatterer may be obtained by prescribing $\xi_b \to \infty$.

The source of the incident waves is a line disturbance parallel to the cylinder axis and located at an arbitrary distance from the scatterer boundary. To generate plane incident waves of finite amplitude, the line source is caused to recede to infinity while its intensity becomes infinitely great. The line source is of uniform

intensity along its length so that each section of the elliptical scatterer will receive the same disturbance. This means that the displacements, strains, and stresses will be independent of the z-coordinate and uniform in that direction. The equations of the linear elasticity theory are assumed to govern the response of the medium which implies that the displacement gradients and the particle velocities are small.[1]

The principal purpose of this work is to determine the influence of the elliptical scatterer on the stress field with particular regard to stress concentrations in the near field.

B. Plane Strain and Plane Stress

The general three-dimensional problem is reduced to one of plane strain by prescribing that the propagation vector of the incident waves be normal to the cylinder axis and by disallowing any particle motion in the axial direction. Then the displacements are of the form

$$u = u(x, y, t) \; ; \; v = v(x, y, t) \; ; \; w = 0 \tag{3B.1}$$

Also

$$\sigma_{zz} = \nu(\sigma_{xx} + \sigma_{yy}) \tag{3B.2}$$

The state of stress in a thin flat plate containing an elliptical inclusion may be obtained from the plane strain problem by replacing Poisson's ratio $\nu$ by $\nu/(1+\nu)$ in the field equations (3C.5).[2]

---

[1] Y. C. Fung, Foundations of Solid Mechanics (Englewood Cliffs, N. J., 1965), pp. 154-155.

[2] Y. C. Fung, pp. 234-235.

For plane strain the compressional wave speed $C_1$ is related to the shear wave speed $C_2$ by the following expression (see equation 3D.12)

$$C_1^2/C_2^2 = 2(1-\nu)/(1-2\nu) \tag{3B.3}$$

For plane stress the relationship is[3]

$$C_1^2/C_2^2 = 2/(1-\nu) \tag{3B.4}$$

From (3D.11)

$$C_1^2/C_2^2 = k_2^2/k_1^2 \tag{3B.5}$$

where $k_1$ and $k_2$ are the wave numbers for the compressional and shear waves, respectively. However, from (2B.10), it is seen that

$$C_1^2/C_2^2 = \beta_2/\beta_1 \tag{3B.6}$$

where $\beta_1$ and $\beta_2$ are the elliptical wave numbers. Thus for plane strain

$$\beta_2/\beta_1 = 2(1-\nu)/(1-2\nu) \tag{3B.7}$$

and for plane stress

$$\beta_2/\beta_1 = 2/(1-\nu) \tag{3B.8}$$

It should be noted that the plane strain solution represents an exact solution to the long cylindrical scatterer problem, whereas the plane stress solution gives only an approximate solution to the thin plate problem since the stresses and displacements are average

---

[3]Y. H. Pao and C. C. Mow, p. 338.

values over the plate thickness.[4]

C. The Governing Equations of Elastodynamics

In the absence of body forces the equations of motion of a continuum in the Cartesian coordinates can be written

$$\tau_{ij,j} = \rho \frac{\partial^2 u_i}{\partial t^2} \tag{3C.1}$$

where $\rho$ is the mass density, $\tau_{ij}$ are the stresses and $u_i$ are the displacements. An explanation of the Cartesian tensor notation may be found in the monograph by Jeffreys.[5]

The linearized strains are given by

$$\varepsilon_{ij} = \frac{1}{2} (u_{i,j} + u_{j,i}) \tag{3C.2}$$

and the constitutive relations between the stresses and strains are

$$\tau_{ij} = 2\mu \left(\varepsilon_{ij} + \frac{\nu}{1-2\nu} \delta_{ij} \varepsilon_{kk}\right) \tag{3C.3}$$

where $\mu$ is the shear modulus of elasticity and $\nu$ is Poisson's ratio for the material. $\delta_{ij}$ is the Kronecker delta and $\varepsilon_{kk}$ is the dilatation defined by

$$\varepsilon_{kk} = u_{k,k} \tag{3C.4}$$

If (3C.2) is substituted into (3C.3), and the resulting equation substituted into (3C.1), the displacement equations of motion are

---

[4]Cf., Fung, pp. 234-235 or Timoshenko and Goodier, pp. 241-244.

[5]Harold Jeffreys, Cartesian Tensors (Cambridge, 1963).

obtained

$$u_{i,jj} + \frac{1}{1-2\nu} u_{k,ki} = \frac{\rho}{\mu} \frac{\partial^2 u_i}{\partial t^2} \tag{3C.5}$$

Henceforth, it will be assumed that $u_z \equiv 0$, thereby reducing the problem to one of plane strain and thus eliminating the $u_z$ displacement from (3C.5). It is possible to prescribe an alternate simplified problem by $u_x = u_y = 0$, and $u_z = w(x,y,t)$ which is known as the anti-plane strain case. However, this problem is mathematically analogous to the electromagnetic and the acoustic wave cases and will not be considered here.

D. The Governing Equations in Elliptical Coordinates

For plane strain in elliptical coordinates, the displacements are

$$u_\xi = u_\xi(\xi,\eta,t) \; ; \; u_\eta = u_\eta(\xi,\eta,t) \; ; \; u_z = 0 \tag{3D.1}$$

According to the Helmholtz theorem, any analytic vector field can be derived from two potential functions. Then the analytic displacement field $u_i$ may be derived as follows

$$u_i = \bar{\Phi}_{,i} + e_{ijk} \bar{\Psi}_{k,j} \tag{3D.2}$$

where $\bar{\Phi}$ is the scalar potential, and $\bar{\Psi}_k$ is the vector potential which in the plane strain case reduces to a single component $\bar{\Psi}$ in the z-direction. In elliptical coordinates (3D.2) leads to the physical displacement components[6]

---

[6]See Appendix E for a discussion of the physical components.

$$u_\xi = \frac{1}{\sqrt{g}}\left(\frac{\partial \Phi}{\partial \xi} + \frac{\partial \Psi}{\partial \eta}\right) \tag{3D.3}$$

$$u_\eta = \frac{1}{\sqrt{g}}\left(\frac{\partial \Phi}{\partial \eta} - \frac{\partial \Psi}{\partial \xi}\right) \tag{3D.4}$$

Substitution of (3D.3) or (3D.4) into the displacement equations of motion (3C.5) shows that $\Phi$ and $\Psi$ both satisfy wave equations

$$\frac{4}{a^2}(\cosh^2\xi - \cos^2\eta)^{-1}\left(\frac{\partial^2 \Phi}{\partial \xi^2} + \frac{\partial^2 \Phi}{\partial \eta^2}\right) = \frac{1}{c_1^2}\frac{\partial^2 \Phi}{\partial t^2} \tag{3D.5}$$

$$\frac{4}{a^2}(\cosh^2\xi - \cos^2\eta)^{-1}\left(\frac{\partial^2 \Psi}{\partial \xi^2} + \frac{\partial^2 \Psi}{\partial \eta^2}\right) = \frac{1}{c_2^2}\frac{\partial^2 \Psi}{\partial t^2} \tag{3D.6}$$

For harmonic time dependence

$$\Phi(\xi, \eta, t) = \phi(\xi, \eta)\, e^{-i\omega t} \tag{3D.7}$$

and

$$\Psi(\xi, \eta, t) = \psi(\xi, \eta)\, e^{-i\omega t} \tag{3D.8}$$

equations (3D.5) and (3D.6) reduce to scalar Helmholtz equations

$$\frac{4}{a^2}(\cosh^2\xi - \cos^2\eta)^{-1}\left(\frac{\partial^2 \phi}{\partial \xi^2} + \frac{\partial^2 \phi}{\partial \eta^2}\right) + k_1^2 \phi = 0 \tag{3D.9}$$

$$\frac{4}{a^2}(\cosh^2\xi - \cos^2\eta)^{-1}\left(\frac{\partial^2 \psi}{\partial \xi^2} + \frac{\partial^2 \psi}{\partial \eta^2}\right) + k_2^2 \psi = 0 \tag{3D.10}$$

where $k_1$ is the compressional wave number, and $k_2$ is the shear wave number given by

$$k_1 = \frac{\omega}{c_1} \quad ; \quad k_2 = \frac{\omega}{c_2} \tag{3D.11}$$

where $\omega$ is the circular frequency, and $c_1$ and $c_2$ are the compressional wave speed and the shear wave speed, respectively, given in terms of the material parameters as follows[7]

$$c_1 = \left(\frac{2\mu(1-\nu)}{(1-2\nu)\rho}\right)^{1/2} \quad ; \quad c_2 = c_1\left(\frac{1-2\nu}{2(1-\nu)}\right)^{1/2} = \left(\frac{2\mu}{\rho}\right)^{1/2} \tag{3D.12}$$

From (3D.3), (3D.4), (3C.2), and (3C.3), the stresses may be found in terms of the reduced potentials $\phi$ and $\psi$

$$\tau_{\xi\xi} = \frac{2\mu}{g}\left[\left(\frac{1-\nu}{1-2\nu}\right)\left(\frac{\partial^2\phi}{\partial\xi^2} + \frac{\partial^2\psi}{\partial\xi\partial\eta}\right) - \frac{\cosh\xi\sinh\xi}{\cosh^2\xi - \cos^2\eta}\left(\frac{\partial\phi}{\partial\xi} + \frac{\partial\psi}{\partial\eta}\right)\right.$$
$$\left. + \frac{\cos\eta\sin\eta}{\cosh^2\xi - \cos^2\eta}\left(\frac{\partial\phi}{\partial\eta} - \frac{\partial\psi}{\partial\xi}\right) + \frac{\nu}{1-2\nu}\left(\frac{\partial^2\phi}{\partial\eta^2} - \frac{\partial^2\psi}{\partial\xi\partial\eta}\right)\right] \tag{3D.13}$$

$$\tau_{\xi\eta} = \frac{2\mu}{g}\left[\frac{1}{2}\left(2\frac{\partial^2\phi}{\partial\xi\partial\eta} + \frac{\partial^2\psi}{\partial\eta^2} - \frac{\partial^2\psi}{\partial\xi^2}\right) - \frac{\cos\eta\sin\eta}{\cosh^2\xi - \cos^2\eta}\left(\frac{\partial\phi}{\partial\xi} + \frac{\partial\psi}{\partial\eta}\right)\right.$$
$$\left. - \frac{\cosh\xi\sinh\xi}{\cosh^2\xi - \cos^2\eta}\left(\frac{\partial\phi}{\partial\eta} - \frac{\partial\psi}{\partial\xi}\right)\right] \tag{3D.14}$$

$$\tau_{\eta\eta} = \frac{2\mu}{g}\left[\left(\frac{1-\nu}{1-2\nu}\right)\left(\frac{\partial^2\psi}{\partial\eta^2} - \frac{\partial^2\psi}{\partial\eta\partial\xi}\right) + \frac{\cosh\xi\sinh\xi}{\cosh^2\xi - \cos^2\eta}\left(\frac{\partial\phi}{\partial\xi} + \frac{\partial\phi}{\partial\eta}\right)\right.$$
$$\left. - \frac{\cos\eta\sin\eta}{\cosh^2\xi - \cos^2\eta}\left(\frac{\partial\phi}{\partial\eta} - \frac{\partial\psi}{\partial\xi}\right) + \frac{\nu}{1-2\nu}\left(\frac{\partial^2\phi}{\partial\xi^2} + \frac{\partial^2\psi}{\partial\xi\partial\eta}\right)\right] \tag{3D.15}$$

---

[7]Fung, p. 177.

$$\tau_{zz} = \nu(\tau_{\xi\xi} + \tau_{\eta\eta}) \tag{3D.16}$$

Thus the elastodynamic wave scattering problem is diminished to the solution of two scalar Helmholtz equations with the appropriate boundary conditions.

As was shown in Chapter II, the Helmholtz equation is separable in elliptic coordinates, the separated solutions being the periodic and radial Mathieu functions. Then the reflected and transmitted wave potentials are

$$\phi^S = \sum_{m=0}^{\infty} B_m ce_m(\eta, q_c) M_{c_m}^{(3)}(\xi, q_c) + \sum_{m=1}^{\infty} C_m se_m(\eta, q_c) M_{s_m}^{(3)}(\xi, q_c)$$

$$\psi^S = \sum_{m=0}^{\infty} D_m ce_m(\eta, q_s) M_{c_m}^{(3)}(\xi, q_s) + \sum_{m=1}^{\infty} E_m se_m(\eta, q_s) M_{s_m}^{(3)}(\xi, q_s)$$

(3D.17)

and

$$\phi^T = \sum_{m=0}^{\infty} F_m ce_m(\eta, q_c') M_{c_m}^{(4)}(\xi, q_c') + \sum_{m=1}^{\infty} G_m se_m(\eta, q_c') M_{s_m}^{(4)}(\xi, q_c')$$

$$\psi^T = \sum_{m=0}^{\infty} H_m ce_m(\eta, q_s') M_{c_m}^{(4)}(\xi, q_s') + \sum_{m=1}^{\infty} I_m se_m(\eta, q_s') M_{s_m}^{(4)}(\xi, q_s')$$

(3D.18)

where $B_m$, $C_m$, $D_m$, $E_m$, $F_m$, $G_m$, $H_m$, and $I_m$ are expansion coefficients to be determined by application of the appropriate boundary conditions.

E. SH-, SV-, and P-Waves

In general two distinct types of waves may propagate through an

ideal elastic solid. These are the compressional (P) wave, for which the particle motion is parallel to the propagation vector, and the shear (S) wave, for which the particle motion is perpendicular to the propagation vector.

When a P-wave impinges upon an interface between two media, both P- and S-waves are refracted and reflected. This must be the case in order that the boundary conditions be satisfied. It can be shown that Huygen's principle can be applied to the reflected and refracted waves and that these waves satisfy an "elastic Snell's law."[8]

The shear (S) waves can be classified in two subgroups. The first is known as the SH-wave and derives its name from seismology where the resultant displacement is parallel to the earth's surface.[9] In the present problem the displacements for the SH-wave would be parallel to the cylinder axis, and it can be proved that for this polarization only SH-waves would be reflected and refracted. The elastic SH-wave case is analogous to the electromagnetic or the acoustic wave case where only a single type of wave is reflected and refracted. The second type of shear wave is the SV-wave. For the present problem, the displacements for the SV-wave would lie in planes normal to the cylinder axis. Also when an SV-wave impinges upon a boundary, both P- and SV-waves are reflected and refracted. These waves also satisfy the Huygen's principle and the "elastic

---

[8]Kolsky, pp. 27-32.

[9]Thau, Ph.D. Thesis, p. 43.

Snell's law." From the relationships (3D.12) it is seen that the P-wave velocity is always greater than the S-wave velocity because for real materials $0 < \gamma < \frac{1}{2}$. For this reason the compressional wave is called the Primary or P-wave, and the shear wave is called the Secondary or S-wave. Both P- and SV-incident waves are treated in this investigation.

F. Boundary Conditions

The solution to the elastodynamic stress concentration problem will appear as a series of Mathieu function products (2B.5) when referred to the elliptical coordinates. Having satisfied the governing differential equations, the solution must be made to satisfy the boundary conditions for the particular type of elliptical inclusion.

The simplest case to treat is that of the rigid and immovable inclusion whose density is infinite. The boundary condition may be written

$$\left.\begin{aligned} u_{\xi}^{inc.} + u_{\xi}^{ref.} &= 0 \\ u_{\eta}^{inc.} + u_{\eta}^{ref.} &= 0 \end{aligned}\right\} \quad \text{on } \xi = \xi_b \tag{3F.1}$$

Thus no motion whatsoever is permitted at the boundary of the discontinuity. Summing the stress components which are parallel to the incident wave vector over the elliptical cylindrical surface, the resultant force, which equals the externally applied restraining force, is obtained. This force must be applied to the scatterer to

hold it stationary in space. The immovability condition becomes a severe condition only as the static limit is approached where the stresses become infinite. If the cylinder is allowed to move freely with the surrounding elastic material, the zero frequency limit reduces to the static case which is a rigid body translation of the whole matrix. Only the rigid and immovable cylinder is treated in this work. Note however that the displacement $U$ of the movable rigid inclusion in the propagation direction can be found from

$$\text{area} \times \rho \times \ddot{U} = \int_0^{2\pi} (\tau_{\xi\xi} \cos\theta - \tau_{\xi\eta} \sin\theta)\, ds$$

where $\rho$ is the inclusion density, $ds$ is an element of boundary arc, and $\theta$ is measured with respect to the propagation direction.

The next problem considered is known as the vacuous cavity inclusion. The boundary condition is

$$\left.\begin{aligned} \tau_{\xi\xi}^{inc.} + \tau_{\xi\xi}^{ref.} &= 0 \\ \tau_{\xi\eta}^{inc.} + \tau_{\xi\eta}^{ref.} &= 0 \end{aligned}\right\} \quad \text{on} \quad \xi = \xi_b \tag{3F.2}$$

The limiting case of a thin crack is obtained in the limit $\xi_b \to 0$. It should be noted that the boundary conditions for the cavity do not guarantee that the top and bottom surfaces of the crack will not come into contact. Therefore, only cracks with a finite gap are treated numerically.

For both the rigid and immovable cylinder and the cavity cylinder, no waves exist within the cylinder, and therefore, only the incident and reflected waves need to be considered.

The third problem treated is that of the fluid-filled cavity. The fluid is compressible, but it cannot support shear. The boundary condition for the fluid-filled cavity is

$$\left.\begin{aligned} \tau_{\xi\xi}^{inc.} + \tau_{\xi\xi}^{ref.} &= \tau_{\xi\xi}^{trans.} \\ \tau_{\xi\eta}^{inc.} + \tau_{\xi\eta}^{ref.} &= 0 \\ u_{\xi}^{inc.} + u_{\xi}^{ref.} &= u_{\xi}^{trans.} \end{aligned}\right\} \quad \text{on } \xi = \xi_b \tag{3F.3}$$

The last and most general problem is that of the arbitrary elastic discontinuity for which the boundary condition is

$$\left.\begin{aligned} \tau_{\xi\xi}^{inc.} + \tau_{\xi\xi}^{ref.} &= \tau_{\xi\xi}^{trans.} \\ \tau_{\xi\eta}^{inc.} + \tau_{\xi\eta}^{ref.} &= \tau_{\xi\eta}^{trans.} \\ u_{\xi}^{inc.} + u_{\xi}^{ref.} &= u_{\xi}^{trans.} \\ u_{\eta}^{inc.} + u_{\eta}^{ref.} &= u_{\eta}^{trans.} \end{aligned}\right\} \quad \text{on } \xi = \xi_b \tag{3F.4}$$

The stresses and displacements are continuous at the interface between the surrounding elastic matrix and the elastic discontinuity.

The stresses and displacements appearing in the boundary condition equations must be expressed in terms of the potentials as in (3D.3), (3D.4), (3D.13), and (3D.14). Then the Mathieu function

product representations for the potentials must be substituted and the expansion coefficients determined.

# IV. INCIDENT WAVES

## A. Cylindrical P- and SV-Waves

It is assumed that the source of the incident waves has been present and varying harmonically in time for an infinite length of time such that at the instant the stress field is examined, no transient effects are present. For cylindrical wave fronts to exist, $i\pi H_0^{(1)}(k_c R)$ the source is located a finite distance away from the cylinder axis. The P-wave potential $\phi^i$ is given by[1]

$$\phi^i = -2\pi^2 \left\{ \sum_{m=0}^{\infty} ce_m(\eta_0, q_c)\, ce_m(\eta, q_c)\, Mc_m^{(1)}(\xi, q_c)\, Mc_m^{(3)}(\xi_0, q_c)/N_m \right.$$

$$\left. + \sum_{m=1}^{\infty} se_m(\eta_0, q_c)\, se_m(\eta, q_c)\, Ms_m^{(1)}(\xi, q_c)\, Ms_m^{(3)}(\xi_0, q_c)/N_m' \right\} \quad \text{(4A.1)}$$

where $(\eta_0$

where $(\eta_0, \xi_0)$ are the coordinates of the source point and $q_c$ is the compressional wave number. Also

$$N_m = \int_0^{2\pi} ce_m^2(\eta, q_c)\, d\eta$$

and

$$N_m' = \int_0^{2\pi} se_m^2(\eta, q_c)\, d\eta \quad \text{(4A.2)}$$

By the Ince normalization, $N_m = N_m' = \pi$ . The above cylindrical wave expansion is the Mathieu function expansion of $i\pi H_0^{(1)}(k_c R)$ where $H_0^{(1)}$ is the Hankel function of the first kind of order zero.[2]

---

[1] P. M. Morse and H. Feshbach, Methods of Theoretical Physics (New York, 1953), Vol. II, p. 1421.

[2] Ibid.

This function, together with the harmonic time dependence represents the propagation of cylindrical wave fronts. The cylindrical SV-wave potential $\psi^i$ is obtained from the $\phi^i$ expansion by replacing $q_c$ with $q_s$, the shear wave number.

For the cylindrical P-wave, the displacement is normal to the wave fronts, while for the SV-wave the displacement is parallel to the cylindrical wave fronts.

B. Plane P- and SV-Waves

Plane waves result when the source location is removed to infinity while the magnitude of the source becomes infinite. This is accomplished as follows:[3] set the source point a large distance from the origin in a direction $\theta_0 + \pi$ to the positive x-axis, then

$$\lim_{\xi_0 \to \infty} i\pi H_0^{(1)}(kR) \to (2\pi i/2q^{1/2}\cosh\xi_0)^{1/2} \exp[2iq^{1/2}\cosh\xi_0 + ik(x\cos\theta_0 + y\sin\theta_0)] \tag{4B.1}$$

Also take the asymptotic form of the Mathieu-Hankel functions

$$\lim_{\xi_0 \to \infty} \begin{bmatrix} Mc_m^{(3)}(\xi_0, q) \\ Ms_m^{(3)}(\xi_0, q) \end{bmatrix} = \left(\frac{2}{\pi}\right)^{1/2} (2q\cosh\xi_0)^{-1/2} \exp\left[2iq^{1/2}\cosh\xi_0 - \frac{i\pi}{2}\left(m + \tfrac{1}{2}\right)\right] \tag{4B.2}$$

From (4B.1), (4B.2), and (4A.1), the plane incident wave potential is found to be

$$\phi^i = \exp[ik_c(x\cos\theta_0 + y\sin\theta_0)] \tag{4B.3}$$

where

---

[3] Ibid., pp. 1421-1422.

$$\phi^i = 2\left\{\sum_{m=0}^{\infty} i^{m+1} ce_m(\theta_0, q_c)\, ce_m(\eta, q_c)\, Mc_m^{(1)}(\xi, q_c)\right.$$

$$\left. + \sum_{m=1}^{\infty} i^{m+1} se_m(\theta_0, q_c)\, se_m(\eta, q_c)\, Ms_m^{(1)}(\xi, q_c)\right\} \tag{4B.4}$$

with $k_c = 4q_c^{1/2}/a$ , and similarly for $\psi^i$ . (4B.4) represents a plane incident wave of unit amplitude. It is important to note that the forms of the reflected and transmitted waves are the same for both cylindrical and plane incident waves. Also in the static limit, the stresses of the incident plane wave are caused by tractions over one infinite plane boundary of the elastic matrix at infinity, the resultant of which is an infinite force.

C. High Frequency Limit

At frequencies where the wave length is much shorter than any radius of curvature of the boundary of the scatterer, the incident wave fronts "see" each element of boundary arc as a plane element. For this reason, at high frequencies the stresses and displacements become insensitive to changes in frequency, and they attain the values which result at a plane interface between two media. Therefore, the stresses and displacements at high frequencies are of little interest for the elliptical inclusion provided that the series solution (3D.17) and (3D.18) yields the limiting values which the stresses and displacements reach as the frequency becomes large. Fortunately, this is the case for the series solution although this solution converges rapidly only at low frequencies.

D. Low Frequency Limit

The series solution (3D.17) and (3D.18) converges well at low frequencies and yields accurate results in that region. For small values of the wave numbers $\gamma_c$ and $\gamma_s$, the expressions (2C.12) through (2C.17) are used for the calculation of the periodic Mathieu functions. An exact solution to the plane strain problem cannot be determined so that it is not possible to derive a power series expansion in $\gamma_c$ or $\gamma_s$ for the stresses and displacements at low frequency. The approximate solution method discussed in Chapter V must be used even at low frequencies. It is not the purpose of this investigation to derive the static solutions from the dynamic solutions since no exact dynamic solution is possible. Nevertheless, it is shown in Chapter V that the low frequency results approach the corresponding static limits for the cases where such a comparison is feasible.

It is of interest to observe that the largest stresses occur at frequencies where the series solution converges well. This is also true for discontinuities of other geometries as indicated by the results reported by other investigators.[4] Therefore, the series solution yields stress information at the frequencies of most interest for elastic waves.

---

[4]Cf., Pao, Pao and Mow, Thau, et. al.

# V. PLANE STRAIN PROBLEMS

## A. Arbitrary Elastic Inclusion

The primary difference between electromagnetic waves or acoustic waves and elastic wave propagation is that for the latter case, two distinct types of waves, characterized by the potentials $\phi$ (compressional waves) and $\psi$ (shear waves), are needed to fully describe the motion of an elastic solid. Moreover, these two wave motions propagate at different speeds and may exist simultaneously but independently of each other. When a wave of either type strikes a discontinuity boundary, both types of waves are, in general, reflected and refracted. This coupling of the two wave types has no counterpart in electromagnic problems.

The particular problems to be numerically investigated in this chapter are of the plane strain classification. That is, the elliptical discontinuity is infinite in length and is excited such that all cross sections receive the same loading. Furthermore, no motion is permitted in the direction of the elliptical cylinder axis. The corresponding plane stress problems can be easily obtained by replacing Poisson's ratio $\nu$ by $\nu/(1+\nu)$ .

The relevant equations developed in Chapter III are repeated here.

$$u_\xi = \frac{1}{\sqrt{g}}\left(\frac{\partial \phi}{\partial \xi} + \frac{\partial \psi}{\partial \eta}\right) \tag{5A.1}$$

$$u_\eta = \frac{1}{\sqrt{g}}\left(\frac{\partial \phi}{\partial \eta} - \frac{\partial \psi}{\partial \xi}\right) \tag{5A.2}$$

$$\tau_{\xi\xi} = \frac{2\mu}{g}\left[\left(\frac{1-\nu}{1-2\nu}\right)\left(\frac{\partial^2\phi}{\partial\xi^2} + \frac{\partial^2\psi}{\partial\xi\partial\eta}\right) - \frac{\cosh\xi\sinh\xi}{\cosh^2\xi - \cos^2\eta}\left(\frac{\partial\phi}{\partial\xi} + \frac{\partial\psi}{\partial\eta}\right)\right.$$

$$\left. + \frac{\cos\eta\sin\eta}{\cosh^2\xi - \cos^2\eta}\left(\frac{\partial\phi}{\partial\eta} - \frac{\partial\psi}{\partial\xi}\right) + \frac{\nu}{1-2\nu}\left(\frac{\partial^2\phi}{\partial\eta^2} - \frac{\partial^2\psi}{\partial\xi\partial\eta}\right)\right] \tag{5A.3}$$

$$\tau_{\xi\eta} = \frac{2\mu}{g}\left[\frac{1}{2}\left(2\frac{\partial^2\phi}{\partial\xi\partial\eta} + \frac{\partial^2\psi}{\partial\eta^2} - \frac{\partial^2\psi}{\partial\xi^2}\right) - \frac{\cos\eta\sin\eta}{\cosh^2\xi - \cos^2\eta}\left(\frac{\partial\phi}{\partial\xi} + \frac{\partial\psi}{\partial\eta}\right)\right.$$

$$\left. - \frac{\cosh\xi\sinh\xi}{\cosh^2\xi - \cos^2\eta}\left(\frac{\partial\phi}{\partial\eta} - \frac{\partial\psi}{\partial\xi}\right)\right] \tag{5A.4}$$

$$\tau_{\eta\eta} = \frac{2\mu}{g}\left[\left(\frac{1-\nu}{1-2\nu}\right)\left(\frac{\partial^2\phi}{\partial\eta^2} - \frac{\partial^2\psi}{\partial\xi\partial\eta}\right) + \frac{\cosh\xi\sinh\xi}{\cosh^2\xi - \cos^2\eta}\left(\frac{\partial\phi}{\partial\xi} + \frac{\partial\psi}{\partial\eta}\right)\right.$$

$$\left. - \frac{\cos\eta\sin\eta}{\cosh^2\xi - \cos^2\eta}\left(\frac{\partial\phi}{\partial\eta} - \frac{\partial\psi}{\partial\xi}\right) + \frac{\nu}{1-2\nu}\left(\frac{\partial^2\phi}{\partial\xi^2} + \frac{\partial^2\psi}{\partial\xi\partial\eta}\right)\right] \tag{5A.5}$$

The Six Wave Potentials. The potential functions $\phi$ and $\psi$ which appear in the stress and displacement expressions above were given in terms of infinite series of Mathieu function products (3D.17), (3D.18), and (4A.1), a form which satisfies the Helmholtz equations in elliptical coordinates. If the periodic Mathieu functions are replaced by their Fourier series representations, the potentials take the following form

$$\phi^i = -2\pi\left[\sum_m \sum_n ce_m(\eta_0, q_c) A_n^m(q_c) \cos n\eta \, Mc_m^{(1)}(\xi, q_c) \, Mc_m^{(3)}(\xi_0, q_c)\right.$$

$$\left. + \sum_m \sum_n se_m(\eta_0, q_c) B_n^m(q_c) \sin n\eta \, Ms_m^{(1)}(\xi, q_c) \, Ms_m^{(3)}(\xi_0, q_c)\right] \tag{5A.6}$$

$$\psi^i = -2\pi\left[\sum_m \sum_n ce_m(\eta_0, q_s) A_n^m(q_s) \cos n\eta \, Mc_m^{(1)}(\xi, q_s) \, Mc_m^{(3)}(\xi_0, q_s)\right.$$

$$\left. + \sum_m \sum_n se_m(\eta_0, q_s) B_n^m(q_s) \sin n\eta \, Ms_m^{(1)}(\xi, q_s) \, Ms_m^{(3)}(\xi_0, q_s)\right] \tag{5A.7}$$

$$\phi^s = \sum_m \sum_n B_m A_n^m(q_c) \cos n\eta \, Mc_m^{(3)}(\xi, q_c) + \sum_m \sum_n C_m B_n^m(q_c) \sin n\eta \, Ms_m^{(3)}(\xi, q_c) \tag{5A.8}$$

$$\psi^s = \sum_m \sum_n D_m A_n^m(q_s) \cos n\eta \, Mc_m^{(3)}(\xi, q_s) + \sum_m \sum_n E_m B_n^m(q_s) \sin n\eta \, Ms_m^{(3)}(\xi, q_s) \tag{5A.9}$$

$$\phi^T = \sum_m \sum_n F_m A_n^m(q_c') \cos n\eta \, Mc_m^{(4)}(\xi, q_c') + \sum_m \sum_n G_m B_n^m(q_c') \sin n\eta \, Ms_m^{(4)}(\xi, q_c') \tag{5A.10}$$

$$\psi^T = \sum_m \sum_n H_m A_n^m(q_s') \cos n\eta \, Mc_m^{(4)}(\xi, q_s') + \sum_m \sum_n I_m B_n^m(q_s') \sin n\eta \, Ms_m^{(4)}(\xi, q_s') \tag{5A.11}$$

where $B_m \rightarrow I_m$ are the expansion coefficients to be determined by

the application of the boundary conditions. Superscripts $i$ , $s$ , $T$ correspond to the incident, reflected and transmitted waves, respectively. Also $q_c'$ and $q_s'$ are the compressional and shear wave numbers, respectively, for the material within the elliptical cylinder which will in general differ from the surrounding elastic matrix.

Partial Potentials. When the boundary conditions are specified, $\xi \to \xi_b$ and the angular coordinate $\eta$ is eliminated by employing the orthogonality of the trigonometric functions. To facilitate the implementation of the boundary conditions, certain simplifying manipulations are performed. In the expressions for the displacement potentials, the order of summation is reversed and "partial potentials" are defined

$$e\phi_n^i = -2\pi \sum_m ce_m(\eta_0, q_c) A_n^m(q_c) Mc_m^{(1)}(\xi, q_c) Mc_m^{(3)}(\xi_0, q_c) \tag{5A.12}$$

$$o\phi_n^i = -2\pi \sum_m se_m(\eta_0, q_c) B_n^m(q_c) Ms_m^{(1)}(\xi, q_c) Ms_m^{(3)}(\xi_0, q_c) \tag{5A.13}$$

$$e\psi_n^i = -2\pi \sum_m ce_m(\eta_0, q_s) A_n^m(q_s) Mc_m^{(1)}(\xi, q_s) Mc_m^{(3)}(\xi_0, q_s) \tag{5A.14}$$

$$o\psi_n^i = -2\pi \sum_m se_m(\eta_0, q_s) B_n^m(q_s) Ms_m^{(1)}(\xi, q_s) Ms_m^{(3)}(\xi_0, q_s) \tag{5A.15}$$

$$e\phi_n^s = \sum_m B_m A_n^m(q_c) Mc_m^{(3)}(\xi, q_c) \tag{5A.16}$$

$$ {}^{e}\phi_n^s = \sum_m C_m B_n^m(\beta_c) M_{s_m}^{(3)}(\xi, \beta_c) $$

(5A.17)

$$ {}^{e}\psi_n^s = \sum_m D_m A_n^m(\beta_s) M_{c_m}^{(3)}(\xi, \beta_s) $$

(5A.18)

$$ {}^{o}\psi_n^s = \sum_m E_m B_n^m(\beta_s) M_{s_m}^{(3)}(\xi, \beta_s) $$

(5A.19)

$$ {}^{e}\phi_n^T = \sum_m F_m A_n^m(\beta_c') M_{c_m}^{(4)}(\xi, \beta_c') $$

(5A.20)

$$ {}^{o}\phi_n^T = \sum_m G_m B_n^m(\beta_c') M_{s_m}^{(4)}(\xi, \beta_c') $$

(5A.21)

$$ {}^{e}\psi_n^T = \sum_m H_m A_n^m(\beta_s') M_{c_m}^{(4)}(\xi, \beta_s') $$

(5A.22)

$$ {}^{o}\psi_n^T = \sum_m I_m B_n^m(\beta_s') M_{s_m}^{(4)}(\xi, \beta_s') $$

(5A.23)

Then the potentials have the forms

$$ \phi^k = \sum_n {}^{e}\phi_n^k \cos n\eta + \sum_n {}^{o}\phi_n^k \sin n\eta $$

(5A.24)

$$ \psi^k = \sum_n {}^{e}\psi_n^k \cos n\eta + \sum_n {}^{o}\psi_n^k \sin n\eta $$

(5A.25)

where $k = c$ , $s$ , $T$ . The derivatives of the potentials are obtained by differentiating the expressions (5A.24) and (5A.25) termwise. Single or double primes over the partial potentials will indicate $\frac{\partial}{\partial \xi}$ and $\frac{\partial^2}{\partial \xi^2}$ , respectively, of that partial potential.

Stresses and Displacements. The stresses and displacements are now given in terms of the partial potentials and their derivatives

$$u_\xi^k = \frac{1}{\sqrt{g}}\left[\sum_n \left({}^{e}\phi_n'^{k} + n\,{}^{o}\psi_n^{k}\right)\cos n\eta + \sum_n \left({}^{o}\phi_n'^{k} - n\,{}^{e}\psi_n^{k}\right)\sin n\eta\right] \tag{5A.26}$$

$$u_\eta^k = \frac{1}{\sqrt{g}}\left[\sum_n \left(n\,{}^{o}\phi_n^{k} - {}^{e}\psi_n'^{k}\right)\cos n\eta - \sum_n \left(n\,{}^{e}\phi_n^{k} + {}^{o}\psi_n'^{k}\right)\sin n\eta\right] \tag{5A.27}$$

$$\begin{aligned}
\tau_{\xi\xi}^k = \frac{2\mu^k}{g}\Big\{&(\cosh^2\xi - \cos^2\eta)\left(\frac{1-\nu^k}{1-2\nu^k}\right)\Big[\sum_n \left({}^{e}\phi_n''^{k} + n\,{}^{o}\psi_n'^{k}\right)\cos n\eta \\
&+ \sum_n \left({}^{o}\psi_n''^{k} - n\,{}^{e}\psi_n'^{k}\right)\sin n\eta\Big] - \cosh\xi\sinh\xi\Big[\sum_n \left({}^{e}\phi_n'^{k} + n\,{}^{o}\psi_n^{k}\right)\cos n\eta \\
&+ \sum_n \left({}^{o}\phi_n'^{k} - n\,{}^{e}\psi_n^{k}\right)\sin n\eta\Big] + \cos\eta\sin\eta\Big[\sum_n \left(n\,{}^{o}\phi_n^{k} - {}^{e}\psi_n'^{k}\right)\cos n\eta \\
&- \sum_n \left(n\,{}^{e}\phi_n^{k} + {}^{o}\psi_n'^{k}\right)\sin n\eta\Big] + (\cosh^2\xi - \cos^2\eta)\frac{\nu^k}{1-2\nu^k}\Big[-\sum_n \left(n^2\,{}^{e}\phi_n^{k}\right. \\
&\left. + n\,{}^{o}\psi_n'^{k}\right)\cos n\eta + \sum_n \left(n\,{}^{e}\psi_n'^{k} - n^2\,{}^{o}\phi_n^{k}\right)\sin n\eta\Big]\Big\}
\end{aligned} \tag{5A.28}$$

$$\tau_{\xi\eta}^{k} = \frac{2\mu^{k}}{g}\left\{\frac{1}{2}(\cosh^2\xi - \cos^2\eta)\left[\sum_n (2n\,{}^{o}\phi_n^{\prime k} - n^2\,{}^{e}\psi_n^{k} - {}^{e}\psi_n^{\prime\prime k})\cos n\eta \right.\right.$$

$$- \sum_n (2n\,{}^{e}\phi_n^{\prime k} + n^2\,{}^{o}\psi_n^{k} + {}^{o}\psi_n^{\prime\prime k})\sin n\eta\Big] - \cos\eta\sin\eta\Big[\sum_n ({}^{e}\phi_n^{\prime k} + n\,{}^{o}\psi_n^{k})\cos n\eta$$

$$+ \sum_n ({}^{o}\phi_n^{\prime k} - n\,{}^{e}\psi_n^{k})\sin n\eta\Big] - \cosh\xi\sinh\xi\Big[\sum_n (n\,{}^{o}\phi_n^{k} - {}^{e}\psi_n^{\prime k})\cos n\eta$$

$$\left. - \sum_n (n\,{}^{e}\phi_n^{k} + {}^{o}\psi_n^{\prime\prime k})\sin n\eta\Big]\right\} \tag{5A.29}$$

where $g = \frac{a^2}{4}(\cosh^2\xi - \cos^2\eta)$ . The stress boundary conditions are handled first. Expressions (5A.28) and (5A.29) indicate that the normal stress $\tau_{\xi\xi}$ and the shear stress $\tau_{\xi\eta}$ for the incident, reflected, and transmitted waves may be represented by two general terms $\tau_{\xi\xi}^{k}$ and $\tau_{\xi\eta}^{k}$ which isolate the $\xi$ and $\eta$ dependent factors separately. It is the $\xi$ dependent factors which have special forms for the incident, reflected, and transmitted waves while the $\eta$ dependent factors are identical for all three wave fields. Since the boundary conditions must be satisfied at all boundary points regardless of the angular coordinate, it is the $\eta$ dependent factors which must be manipulated in order to ultimately eliminate the $\eta$ parameter from the boundary condition expressions. The stress conditions at the boundary of the elastic inclusion are

$$\tau_{\xi\xi}^{inc.} + \tau_{\xi\xi}^{ref.} = \tau_{\xi\xi}^{trans.} \tag{5A.30}$$

$$\tau_{\xi\eta}^{inc.} + \tau_{\xi\eta}^{ref.} = \tau_{\xi\eta}^{trans.} \tag{5A.31}$$

The stress expressions (5A.28) and (5A.29) must be substituted into (5A.30) and (5A.31) and the results brought into a form where the orthogonality of the trigonometric functions may be used to remove the $\eta$ parameter from the equations. The details of eliminating the $\eta$ dependence from the boundary condition equations are included in Appendix I; only the final results are given here in abbreviated form. It is found that the stress conditions reduce to the following

$$\phi^{e}\bar{\tau}^{T}_{\xi\xi} + \psi^{e}\bar{\tau}^{T}_{\xi\xi} - \phi^{e}\bar{\tau}^{S}_{\xi\xi} - \psi^{e}\bar{\tau}^{S}_{\xi\xi} = \phi^{e}\bar{\tau}^{i}_{\xi\xi} + \psi^{e}\bar{\tau}^{i}_{\xi\xi} \tag{5A.32}$$

$$\phi^{o}\bar{\tau}^{T}_{\xi\eta} + \psi^{o}\bar{\tau}^{T}_{\xi\eta} - \phi^{o}\bar{\tau}^{S}_{\xi\eta} - \psi^{o}\bar{\tau}^{S}_{\xi\eta} = \phi^{o}\bar{\tau}^{i}_{\xi\eta} + \psi^{o}\bar{\tau}^{i}_{\xi\eta} \tag{5A.33}$$

and

$$\phi^{o}\bar{\tau}^{T}_{\xi\xi} + \psi^{o}\bar{\tau}^{T}_{\xi\xi} - \phi^{o}\bar{\tau}^{S}_{\xi\xi} - \psi^{o}\bar{\tau}^{S}_{\xi\xi} = \phi^{o}\bar{\tau}^{i}_{\xi\xi} + \psi^{o}\bar{\tau}^{i}_{\xi\xi} \tag{5A.34}$$

$$\phi^{e}\bar{\tau}^{T}_{\xi\eta} + \psi^{e}\bar{\tau}^{T}_{\xi\eta} - \phi^{e}\bar{\tau}^{S}_{\xi\eta} - \psi^{e}\bar{\tau}^{S}_{\xi\eta} = \phi^{e}\bar{\tau}^{i}_{\xi\eta} + \psi^{e}\bar{\tau}^{i}_{\xi\eta} \tag{5A.35}$$

Equations (5A.32) and (5A.33) contain the expansion coefficients $B_m$, $E_m$, $F_m$, $I_m$ while (5A.34) and (5A.35) contain $C_m$, $D_m$, $G_m$, and $H_m$. The displacement boundary conditions provide four additional

equations for these expansion coefficients.

The displacement boundary conditions are

$$u_\xi^{inc.} + u_\xi^{ref.} = u_\xi^{trans.} \tag{5A.36}$$

$$u_\eta^{inc.} + u_\eta^{ref.} = u_\eta^{trans.} \tag{5A.37}$$

These conditions yield relationships analogous to (5A.32) through (5A.35). They are

$$\phi^{e}u_\xi^{T} + \psi^{e}u_\xi^{T} - \phi^{e}u_\xi^{S} - \psi^{e}u_\xi^{S} = \phi^{e}u_\xi^{i} + \psi^{e}u_\xi^{i} \tag{5A.38}$$

$$\phi^{o}u_\eta^{T} + \psi^{o}u_\eta^{T} - \phi^{o}u_\eta^{S} - \psi^{o}u_\eta^{S} = \phi^{o}u_\eta^{i} + \psi^{o}u_\eta^{i} \tag{5A.39}$$

and

$$\phi^{o}u_\xi^{T} + \psi^{o}u_\xi^{T} - \phi^{o}u_\xi^{S} - \psi^{o}u_\xi^{S} = \phi^{o}u_\xi^{i} + \psi^{o}u_\xi^{i} \tag{5A.40}$$

$$\phi^{e}u_\eta^{T} + \psi^{e}u_\eta^{T} - \phi^{e}u_\eta^{S} - \psi^{e}u_\eta^{S} = \phi^{e}u_\eta^{i} + \psi^{e}u_\eta^{i} \tag{5A.41}$$

Each of the equations (5A.32) through (5A.35) and (5A.38) through

(5A.41) actually represents an infinite number of equations, each with an infinite number of terms. The only simplification is the fact that $B_m$, $E_m$, $F_m$, and $I_m$ occur together and $C_m$, $D_m$, $G_m$, and $H_m$ occur together. The explicit forms for the terms in the above eight equations are extremely lengthy and are given in Appendix I. These equations are linear algebraic equations which lend themselves to a computer solution, the details of which are left to Appendix G.

Therefore, the formal solution to the elastic discontinuity problem has been obtained, although not in closed form. This most general case will not be treated further except for a brief discussion of a certain special problem.

When electromagnetic energy such as visible light, propagating in the form of waves, passes through a thin lens, a focusing effect may take place whereby energy is concentrated in a very small area behind the lens. It would appear that a similar focusing phenomenon may occur when elastic waves are refracted by two surfaces corresponding to the boundary surfaces of a discontinuity within an elastic matrix. Since the optically refracting thin lens consists of two spherical surfaces, it may be possible in the elastic wave case to simulate an effective focusing discontinuity by the use of an elastic elliptical inclusion of the proper eccentricity. It is recognized of course that certain aberrations will occur because the refracting surfaces are elliptical rather than circular. Nevertheless, a region of energy (stress) concentration may be produced behind the discontinuity.

B. Rigid Immovable Inclusion

The boundary conditions for the rigid immovable inclusion are the vanishing of the displacements on $\xi = \xi_b$ . Thus the stress expressions do not enter into the solution for the expansion coefficients. In addition, for this case, no waves exist within the discontinuity so that the $F_m$ , $G_m$ , $H_m$ , $I_m$ expansion coefficients are zero at the outset.

Incident P-Wave. When the incident wave is compressional in nature, the incident shear wave potential is identically zero and the boundary condition equations are

$$ {}^{e}_{\phi}u^{s}_{\xi} + {}^{e}_{\psi}u^{s}_{\xi} = -{}^{e}_{\phi}u^{i}_{\xi} \tag{5B.1} $$

$$ {}^{o}_{\phi}u^{s}_{\eta} + {}^{o}_{\psi}u^{s}_{\eta} = -{}^{o}_{\phi}u^{i}_{\eta} \tag{5B.2} $$

and

$$ {}^{o}_{\phi}u^{s}_{\xi} + {}^{o}_{\psi}u^{s}_{\xi} = -{}^{o}_{\phi}u^{i}_{\xi} \tag{5B.3} $$

$$ {}^{e}_{\phi}u^{s}_{\eta} + {}^{e}_{\psi}u^{s}_{\eta} = -{}^{e}_{\phi}u^{i}_{\eta} \tag{5B.4} $$

The terms in the above equations are given explicitly in Appendix I. (5B.1) and (5B.2) contain $B_m$ and $E_m$ only while (5B.3) and (5B.4) contain $C_m$ and $D_m$ only (see Appendix I).

Incident SV-Wave. The incident SV-wave case yields expressions similar to (5B.1) through (5B.4) with the $\phi$ subscripted displacement terms on the right-hand side replaced by $\psi$ subscripted displacement terms. Again, only $B_m$, $C_m$, $D_m$, and $E_m$ are non-zero.

Numerical Results. Some important numerical results for the rigid immovable inclusion with an incident compressional wave are presented in Figures 2 through 8. The series in (5A.6) through (5A.11) were summed with truncation after satisfactory convergence was achieved. For small eccentricity ( $B/A \geq 0.46$ ) and for source points relatively far from the scatterer boundary ( $(R_o - R_b)/\lambda \geq 0.63$ ), it was found that fifteen terms were sufficient. For $B/A < 0.46$ up to twenty-five terms were needed for proper convergence. Appendix G contains further details on numerical methods.

All stresses are normalized by the maximum stress in the incident wave field. For the incident compressional wave, the normalizing factor is the stress normal to the incident wave fronts. Thus all stresses are normalized by $\tau_o = |\tau^{inc.}_{max.}|$ computed in the direction of propagation. The normalized stresses may be considered to be dynamic stress concentration factors.

The wave number $\gamma_c$ is normalized by $4\sinh^2 \xi_b$ . With this normalization, when the ellipse approaches a circle, $4\gamma_c \sinh^2 \xi_b$ approaches $kr$ for the circular case where $r$ is the circle radius and $k$ is the wave number in the circular geometry. Then the abscissa $4\gamma_c \sinh^2 \xi_b$ may be interpreted as the wave number for a fixed

elliptical boundary $\xi_b$ or as $4\sinh^2\xi_b$ for a fixed wave number. Note that when $\xi_b$ is large and the ellipse approaches a circle, the radius is given by $r = \frac{a}{2}\sinh\xi_b$ where $a$ is the interfocal distance.

Poisson's ratio $\nu$ was chosen to be 0.25 for all computations except for Figures 9 and 18.

Figure 2 shows the angular distribution of normalized stress versus ellipse eccentricity for an incident plane P-wave on the major axis. It is apparent that the curvature of the boundary begins to play a role as the eccentricity increases. For low eccentricities the radial stress is maximized at the point of first contact while the shear stress is greater at points between $45^o$ and $60^o$ away. At higher eccentricities the radial stress is not maximized at the point of first contact.

In Figure 3 the plane P-wave is incident along the minor axis. For all values of eccentricity examined, the radial stress is maximized at the point of first contact and has the value of 2.0. Contrary to the results of the preceding case, the more eccentric ellipses yield the smaller stresses. The point of maximum curvature does not exhibit the largest radial stress because the radial stress of the incident wave field is zero at this point.

Figure 4 shows the angular distribution of the normalized stress at the boundary of the rigid immovable inclusion as a function of

P-wave source location on the major axis. The radial stress concentration is largest at the point of first contact. The value of 2.0 equals the normal stress concentration value at the plane interface between a rigid immovable half space and an elastic half space for a plane P-wave at normal incidence. Also this result agrees with the work of Pao and Mow, et. al., for the circular case at comparable frequencies. The fact that the largest radial stress occurs at the point of greatest curvature is of no significance in this case.

The magnitude of the shear stress does not vary significantly with changes in source location. However, the point of greatest shear stress on the boundary tends to move closer to the point of first contact as the source moves closer.

In Figure 5 the source is located on the minor axis. Again a stress concentration value of 2.0 is obtained at the point of first contact which also happens to be the point of least curvature.

Figure 6 presents the angular distribution of the normalized radial and shear stresses for an incident plane P-wave on the major axis and $B/A = 0.29$. The curvature of the ellipse plays a significant role in the magnitudes of both stresses. The wave numbers considered are such that the incident waves no longer "see" the discontinuity boundary as a plane boundary. It is of considerable interest to note that the maximum shear and radial stresses occur at about $75^{o}$ away from the point of first contact. However, the shear stress is zero at the point of first contact and $180^{o}$ away as would be expected. In the

case of the rigid circular scatterer, Pao and Mow found that the maximum radial stress occurred at the point of first contact and that the maximum shear stress did not occur at a point $90^{o}$ away from the point of first contact as might be expected.

Figure 7 shows the low frequency results for the normalized radial stress at the point of first contact for various eccentricities. The abscissa is the parameter $4q_c \sinh^2 \beta b$ and the graphs have two different interpretations. For a given elliptical boundary the frequency may be regarded as approaching zero or the static limit. In the static limit the incident stress field is produced by a uniform normal stress at infinity over one infinite plane boundary of the elastic matrix. The resultant of this uniform stress distribution is an infinite force. An equal and opposite force must be applied to the insert to satisfy the zero-displacement boundary conditions. Therefore, infinite stresses result. An alternate interpretation is that for a given frequency, the boundary of the inclusion reduces to a crack with a tip of infinite curvature or zero area. Thus infinite stresses must exist at the crack tip. Note that at finite frequencies the more eccentric ellipses exhibit the larger stresses at the point of first contact and that as the frequency increases, the curves asymptotically approach the value of 2.0.

Figure 8 presents the distribution of normalized radial stress along a line in front of the ellipse with a plane P-wave incident along the same line. On the boundary the stress concentration value is 2.0. As the distance from the boundary increases, the stress magnitude

decays in an oscillating manner to the value of 1.0. The oscillation of the stress is a reflection of the incident stress wave behavior. The fact that the stress value decays to 1.0 indicates that at great distances from the inclusion, the inclusion does not appreciably alter the stress field, as would be expected.

Figure 9 shows the normalized radial stress on the rigid inclusion versus Poisson's ratio for an incident plane P-wave on the major axis. It is observed that the larger values of Poisson's ratio lead to the larger stresses.

Figure 10 shows the distribution of normalized stress versus ellipse eccentricity for a plane shear wave incident along the major axis of the rigid cylinder. In comparison with the incident compressional wave, it is seen that the shear wave generally produces larger stress concentrations for the same values of wave number and eccentricity.

In Figure 11 the plane shear wave arrives along the minor axis and yields stress intensities which are less severe than in the previous case.

Figure 12 presents the distribution of normalized stress on the rigid cylinder as a function of SV-wave source location on the major axis. The location of the source does not significantly alter the magnitude of the stresses for a wide range of source positions. However, the angular distribution varies greatly as the source proximity changes.

In Figure 13 the SV-wave is incident along the minor axis. Both the angular distribution and the intensity of the stresses change considerably with variations in source position.

Figure 14 presents the distribution of normalized radial stress $90^{o}$ away from the point of first contact on the rigid inclusion with a plane SV-wave incident along the major axis. In comparison with the incident P-wave, the stress concentrations are larger for the same wave number and eccentricity.

C. Cavity Inclusion

The cavity inclusion is a vacuous elliptical cylindrical space contained within the infinite elastic matrix. At the boundary surface of the vacuous cavity, the normal and shear stresses must vanish and the coefficients for the transmitted waves are zero as in the rigid immovable case.

Incident P-Wave. For the incident compressional (P) wave, the boundary condition equations become

$$ {}^{e}_{\phi}\tau^{s}_{\xi\xi} + {}^{e}_{\psi}\tau^{s}_{\xi\xi} = -{}^{e}_{\phi}\tau^{i}_{\xi\xi} \tag{5C.1} $$

$$ {}^{o}_{\phi}\tau^{s}_{\xi\eta} + {}^{o}_{\psi}\tau^{s}_{\xi\eta} = -{}^{o}_{\phi}\tau^{i}_{\xi\eta} \tag{5C.2} $$

and

$$ {}^{o}_{\phi}\tau^{s}_{\xi\xi} + {}^{o}_{\psi}\tau^{s}_{\xi\xi} = -{}^{o}_{\phi}\tau^{i}_{\xi\xi} \tag{5C.3} $$

$$\phi^{e}\tau^{s}_{\xi\eta} + \psi^{e}\tau^{s}_{\xi\eta} = -\phi^{e}\tau^{i}_{\xi\eta}$$

(5C.4)

The explicit forms of the terms above are given in Appendix I. The first two equations contain $B_m$ and $E_m$ only while the second two contain $C_m$ and $D_m$ only.

Incident SV-Wave. If the right-hand side terms in equations (5C.1) through (5C.4) are replaced by their $\psi$ wave counterparts, the boundary condition equations for the incident SV-wave are obtained. The left-hand side terms are unchanged. Notice that in both cases, the displacements need not be considered in the determination of the expansion coefficients.

Numerical Results. Figure 15 shows the distribution of normalized hoop stress versus ellipse eccentricity for an incident plane P-wave. The largest stresses occur when the wave arrives on the major axis as was true in the rigid case. The hoop stress is maximized at points approximately $75^{o}$ away from the point of first contact. In the case of the vacuous cavity, the possibility exists that Rayleigh-type waves may propagate on the concave free surface of the cavity. These waves could not propagate at the interface between a rigid inclusion and an elastic matrix. Therefore, in the cavity case the surface waves can transport energy from the illuminated side to the shadow side which may explain the large stress intensities on the shadow side.

Figure 16 presents the distribution of normalized hoop stress on

the cavity versus normalized source location. As the source point moves closer, the point of maximum stress tends to move toward the point of first contact.

Figure 17 presents the distribution of normalized hoop stress $90^{o}$ away from the point of first contact on the cavity with a plane P-wave incident on the major axis. The plot for the circular case is in excellent agreement with the results of Pao. As the eccentricity increases, the hoop stress grows larger for the same frequencies.

Figure 18 shows the normalized hoop stress on the cavity versus Poisson's ratio for an incident plane P-wave on the major axis. The smaller values of Poisson's ratio yield the larger stresses. Also as the value of Poisson's ratio reaches its upper limit, the shape of the stress distribution changes.

Figure 19 shows the distribution of normalized hoop stress versus ellipse eccentricity for an incident plane SV-wave. The largest stresses are obtained when the wave arrives on the major axis. It is of interest to note that the hoop stress intensity is not in general maximized on the illuminated side owing to the transport of energy by waves on the concave cavity surface. Also the stress intensities obtained are greater than those which occur in the rigid case.

Figure 20 presents the distribution of normalized hoop stress as a function of source location. As the source moves closer to the cavity, the point of maximum stress moves from the shadow side to the illuminated side, although the magnitude of the maximum stress tends

to decrease.

Figure 21 is a plot of normalized hoop stress $90^{o}$ away from the point of first contact on the cavity with a plane shear wave incident on the major axis. The parameter $4/\gamma_c \sinh^2 \xi_b$ plotted on the abscissa contains both the wave number $\gamma_c$ and the elliptical boundary coordinate number $\xi_b$ . Therefore, two interpretations are possible for the curves of Figure 21. On the one hand, it may be considered that the boundary is fixed while the frequency decreases. When the static limit is reached, the hoop stress at $\eta = \pi/2$ reaches zero owing to the static shear forces at infinity on the elastic matrix. For the second interpretation, the frequency remains finite while the elliptical cavity thickness approaches zero. When the limiting case of the crack is reached, the hoop stress at $\pi/2$ is again zero since the material elements are loaded in pure shear.

D. Fluid-Filled Cavity Inclusion

If the vacuous cavity is filled with a compressible but inviscid fluid, the result is that the normal stress and displacement must be continuous across the fluid-solid interface. The shear stress is still required to vanish at the boundary. Thus the boundary condition equations for the incident P-wave are

$$\phi^{e}\tau^{T}_{\xi\xi} - \phi^{e}\tau^{s}_{\xi\xi} - \psi^{e}\tau^{s}_{\xi\xi} = \phi^{e}\tau^{i}_{\xi\xi} \qquad (5D.1)$$

$$\phi^{o}\tau^{s}_{\xi\eta} + \psi^{o}\tau^{s}_{\xi\eta} = -\phi^{o}\tau^{i}_{\xi\eta} \qquad (5D.2)$$

$$\phi^{e}u_{\xi}^{T} - \phi^{e}u_{\xi}^{S} - \psi^{e}u_{\xi}^{S} = \phi^{e}u_{\xi}^{i} \tag{5D.3}$$

and

$$\phi^{o}\tau_{\xi\xi}^{T} - \phi^{o}\tau_{\xi\xi}^{S} - \psi^{o}\tau_{\xi\xi}^{S} = \phi^{o}\tau_{\xi\xi}^{i} \tag{5D.4}$$

$$\phi^{e}\tau_{\xi\eta}^{S} + \psi^{e}\tau_{\xi\eta}^{S} = -\phi^{e}\tau_{\xi\eta}^{i} \tag{5D.5}$$

$$\phi^{o}u_{\xi}^{T} - \phi^{o}u_{\xi}^{S} - \psi^{o}u_{\xi}^{S} = \phi^{o}u_{\xi}^{i} \tag{5D.6}$$

The first three equations contain $F_m$, $B_m$, $E_m$ only while the second three equations contain only $G_m$, $C_m$, and $D_m$. The incident SV-wave is treated in a similar way.

# VI. CONCLUSIONS AND RECOMMENDATIONS

It was the purpose of this investigation to study the influence of an elliptical discontinuity on the stress distribution in an otherwise uninterrupted unbounded elastic medium. The special cases of the rigid immovable inclusion and the cavity inclusion were examined in detail. The motivations were both academic and practical at the same time. Academically, the problem is of interest because it eliminates one more gap in the theory of elastodynamics while verifying the results of previous investigators. From a practical point of view, the solution to the elliptical wave scatterer problem for the elastic medium provides valuable insights into phenomena such as crack development and growth as well as material failure and its prevention.

In the majority of cases examined, including both the rigid immovable inclusion and the cavity inclusion, the least severe stresses occurred when the wave arrived along the minor axis. In structural design problems it is conceivable that for certain known dynamic loading conditions, a properly oriented fastener of elliptical cross section could produce stress levels lower than those for a circular fastener.

It was found in most cases that the incident shear wave caused higher stresses than did the compressional wave with all other parameters being equal. An additional finding was that the vacuous cavity yielded higher stresses than did the rigid inclusion except in the static limit. It would appear that the absence of material in the cavity leads to a decreased resistance to stress. Also of interest

was the fact that for the cavity the stresses were not always largest on the illuminated side probably owing to the transport of energy to the shadow side by surface waves.

For both the rigid immovable inclusion and the cavity inclusion, it was found that the location of the wave source was not a significant parameter as far as the stress magnitude is concerned. However, the angular distribution changed with the result that the point of highest stress tended to move toward the point of first contact as the wave source point moved closer to the scatterer.

With the incident wave arriving on the major axis, the stresses tended to increase markedly as the eccentricity of the inclusion increased. This phenomenon is apparently attributable to the increase in curvature of the scatterer boundary. With the incident wave on the minor axis, the more eccentric discontinuities produced smaller stresses. As the limiting case of the zero thickness rigid ribbon is reached, it is seen that for an incident P-wave on the minor axis, the shear stress becomes zero on the boundary, and for an incident SV-wave on the minor axis, the normal stress becomes zero. When the vacuous cavity goes to a zero thickness crack, the hoop stress vanishes on the boundary for both incident P- and SV-waves on the minor axis. Thus in these cases the crack tip does not produce singularities as might be expected.

Variations in Poisson's ratio produced relatively minor variations in the stress levels. However, it is interesting to note that

for the rigid inclusion the largest Poisson's ratio produced the largest stresses, while for the cavity the smallest Poisson's ratio caused the largest stresses in addition to causing a change in the shape of the stress distribution.

The present paper contains the formal solution for the general cases of the fluid-filled discontinuity as well as for the arbitrary elastic inclusion, although no numerical results are presented for these cases. It would be of great interest to investigate numerically the effects of resonance within the discontinuity on the stress intensity. For the circular case, it was found that the resonance conditions caused very large stresses and that these conditions could be predicted once all the material parameters were specified. An additional problem of interest is that of the so-called "stress lens" mentioned in the introduction. Further extensions of this problem would include multiple scatterers, scattering in the presence of boundaries, layered scatterers, and perhaps scattering by a discontinuity in an inelastic matrix.

# APPENDIX

## A. Elliptic Metric Tensor

The defining expression is

$$ds^2 = dx^i dx^i = x^i_{,j} x^i_{,k} d\bar{x}^j d\bar{x}^k = g_{jk} d\bar{x}^j d\bar{x}^k$$

$$x = a/2 \cosh\xi \cos\eta \; ; \quad y = a/2 \sinh\xi \sin\eta \tag{AA.1}$$

Then

$$g_{jk} = x^i_{,j} x^i_{,k} = a^2/4 (\cosh^2\xi - \cos^2\eta)\delta_{jk} = g\,\delta_{jk} \tag{AA.2}$$

(except $g_{33} = 1$ )

Also

$$g^{jk} = \frac{1}{g}\delta^{jk}$$

(except $g^{33} = 1$ )

## B. Christoffel Symbols

The defining expression is

$$\Gamma^i_{jk} = \tfrac{1}{2} g^{il}\left[g_{lj,k} + g_{lk,j} - g_{jk,l}\right] \tag{AB.1}$$

Then

$$\Gamma^1_{11} = a^2/4 \,\frac{\cosh\xi \sinh\xi}{g}$$

$$\Gamma^1_{12} = a^2/4 \,\frac{\cos\eta \sin\eta}{g} = \Gamma^1_{21}$$

$$\Gamma^1_{22} = -\Gamma^1_{11} \; ; \quad \Gamma^2_{11} = -\Gamma^1_{12}$$

$$\Gamma^2_{12} = \Gamma^1_{11} \; ; \quad \Gamma^2_{22} = \Gamma^1_{12}$$

all others zero. (AB.2)

C. Laplacian Operator in Elliptic Coordinates

The tensor definition of the Laplacian operator in any coordinate system is

$$\nabla^2\phi = \frac{1}{g}\frac{\partial}{\partial x^k}\left(g g^{kl}\frac{\partial \phi}{\partial x^l}\right) \tag{AC.1}$$

Using the definition of $g$ and $g^{kl}$ given in (AA.3), and performing the indicated differentiation, the following is obtained

$$\nabla^2\phi = g^{11}\frac{\partial^2\phi}{\partial \xi^2} + g^{22}\frac{\partial^2\phi}{\partial \eta^2} + \frac{\partial^2\phi}{\partial z^2} \tag{AC.2}$$

This reduces to

$$\nabla^2\phi = \frac{1}{g}\left(\frac{\partial^2\phi}{\partial \xi^2} + \frac{\partial^2\phi}{\partial \eta^2}\right) + \frac{\partial^2\phi}{\partial z^2} \tag{AC.3}$$

D. Separation of the Helmholtz Equation

The Helmholtz equation in elliptic coordinates is

$$\frac{1}{g}\left(\frac{\partial^2\phi}{\partial \xi^2} + \frac{\partial^2\phi}{\partial \eta^2}\right) + \frac{\partial^2\phi}{\partial z^2} + k_j^2\phi = 0 \tag{AD.1}$$

Look for a solution of the form

$$\phi(\xi,\eta,z) = S(\eta)Z(\xi)e^{-ikz} \tag{AD.2}$$

Then the separated solutions are found to satisfy

$$\frac{d^2Z}{d\xi^2} - \left(b - \frac{k_j'^2 a^2}{4}\cosh^2\xi\right)Z = 0$$

Modified Mathieu Eqn. (AD.3)

$$\frac{d^2S}{d\eta^2} + \left(b - \frac{k_j'^2 a^2}{4}\cos^2\eta\right)S = 0$$

Mathieu Eqn. (AD.4)

where $k_j'^2 = k_j^2 - k^2$ .

E. Physical Stress and Displacement Components

Vectors or tensors which represent physical quantities consist of a magnitude multiplied by one or more unit vectors. In the Cartesian coordinate system this magnitude or physical component is the same as the tensor component, that is, the tensor component has the correct physical units of the quantity represented. In other coordinate systems the tensor components may not have the correct units. This arises from the fact that the basis vectors of the coordinate system are not generally unit vectors. Thus, for example, an arbitrary first order tensor may be written as

$$\bar{V} = v^k \bar{g}_k \tag{AE.1}$$

where the $v^k$ are the vector components and $\bar{g}_k$ are the basis vectors. $\bar{g}_k$ becomes a unit vector when it is divided by its magnitude given by $|\bar{g}_k| = \sqrt{g_{\underline{k}\underline{k}}}$ , underlined repeated indices not summed. Then

$$\bar{V} = \sum_k v^k \sqrt{g_{\underline{k}\underline{k}}}\ \bar{g}_k / \sqrt{g_{\underline{k}\underline{k}}} \tag{AE.2}$$

where $\bar{g}_k / \sqrt{g_{\underline{k}\underline{k}}}$ is a unit vector and $v^k \sqrt{g_{\underline{k}\underline{k}}}$ is called the physical component. The physical stress and displacement components will be denoted by using the coordinate labels as subscripts. Then in general

$$\tau_{ij}{}_{\text{physical}} = \left( g_{\underline{i}\underline{i}} / g^{\underline{j}\underline{j}} \right)^{1/2} \tau^{ij} \tag{AE.3}$$

and

$$\tau_{\xi\xi} = g\,\tau^{11} \;;\; \tau_{\xi\eta} = \tau_{\eta\xi} = g\,\tau^{12}$$

$$\tau_{\xi z} = \tau_{z\xi} = g^{1/2}\,\tau^{13} \;;\; \tau_{\eta\eta} = g\,\tau^{22}$$

$$\tau_{\eta z} = \tau_{z\eta} = g^{1/2}\,\tau^{23} \;;\; \tau_{zz} = \tau^{33}$$

$$u_\xi = g^{-1/2}\,u_1 \quad ; \quad u_\eta = g^{-1/2}\,u_2$$

$$u_z = u_3 \qquad \text{(AE.4)}$$

F. Shear and Compressional Wave Potentials

It can be demonstrated that the compressional wave potential $\phi$ is associated with the dilatation, i.e., volumetric effects, and that the shear wave potential $\psi$ is associated with the rotation, i.e., shape change effects.

$$u_i = \phi_{,i} + e_{ijk}\,\psi_{k,j} \qquad \text{(AF.1)}$$

Then

$$u_{i,i} = \phi_{,ii} + e_{ijk}\,\psi_{k,ji} \qquad \text{(AF.2)}$$

The last term of (AF.2) vanishes so that

$$u_{i,i} \equiv e = \phi_{,ii} \qquad \text{the dilatation} \qquad \text{(AF.3)}$$

Also

$$e_{ijk}\,u_{k,j} = e_{ijk}\,\phi_{,kj} + e_{ijk}\,e_{klm}\,\psi_{m,lj} \qquad \text{(AF.4)}$$

The first term of (AF.4) vanishes, and the result is

$$e_{ijk} u_{k,j} \equiv 2\omega_i = -\psi_{i,jj} \qquad \text{the rotation} \tag{AF.5}$$

where the condition $\psi_{j,j} = 0$ has been imposed.

The displacement equations of motion are

$$\rho \frac{\partial^2 u_i}{\partial t^2} = \mu u_{i,jj} + (\lambda+\mu) u_{j,ji} \tag{AF.6}$$

If $u$, $v$, $w$ are the $x$, $y$, $z$ displacement components, respectively, then for the case $v = w = 0$, (AF.6) is satisfied by the motion

$$u = A \sin \frac{2\pi}{\ell}(x \pm c_L t) \tag{AF.7}$$

if $c_L = \left(\frac{\lambda+2\mu}{\rho}\right)^{1/2}$. Also the particle motion is in the direction of propagation. Next, for the case $u = w = 0$, (AF.6) is satisfied by

$$v = A \sin \frac{2\pi}{\ell}(x \pm c_T t) \tag{AF.8}$$

if $c_T = \left(\frac{\mu}{\rho}\right)^{1/2}$. The particle motion here is transverse to the direction of propagation. Substituting

$$u_i = \frac{\partial \phi}{\partial x_i} + e_{ijk} \frac{\partial \psi_k}{\partial x_j}$$

into (AF.6), it is found that (AF.6) will be satisfied if

$$\nabla^2 \phi = \frac{1}{c_L^2} \frac{\partial^2 \phi}{\partial t^2}$$

and

$$\nabla^2 \psi_k = \frac{1}{c_T^2} \frac{\partial^2 \psi_k}{\partial t^2} \tag{AF.9}$$

where $C_L = \left(\frac{\lambda+2\mu}{\rho}\right)^{1/2}$; $C_T = \left(\frac{\mu}{\rho}\right)^{1/2}$. Substitute $e = \phi_{,ii}$ and $\psi_{i,jj} = -2\omega_i$ into (AF.9) to obtain

$$\nabla^2 e = \frac{1}{C_L^2}\frac{\partial^2 e}{\partial t^2} \; ; \; \nabla^2 \omega_i = \frac{1}{C_T^2}\frac{\partial^2 \omega_i}{\partial t^2} \qquad \text{(AF.10)}$$

Therefore, it has been shown that $\phi$ is associated with the dilatation $e$ which propagates as a longitudinal wave, and that $\psi$ is associated with the rotation $\omega$ which propagates as a transverse wave.

G. Numerical Methods

The primary purpose of this research is to present numerical results regarding stresses and displacements in the vicinity of the elliptical discontinuity. To accomplish this task, two basic numerical problems had to be overcome:

(a) calculation of the Mathieu functions, their derivatives, characteristic values, and Fourier expansions of the periodic functions

(b) approximate solution of an infinite set of linear algebraic equations with complex coefficients.

The first problem was essentially eliminated by obtaining a computer routine from Gertrude Blanche and Donald Clemm of the Wright Patterson Air Force Base, which would compute the periodic and radial functions and their first derivatives. Also included was the calculation of the characteristic values and the Fourier coefficients. The second derivatives of the functions were found from the differential equations, i.e.,

$$\text{(radial)}\quad \frac{d^2 Z}{d\xi^2} = (b - 2q\cosh 2\xi)Z$$

and

$$\text{(periodic)}\quad \frac{d^2 S}{d\eta^2} = -(b - 2q\cos 2\eta)S \qquad \text{(AG.1)}$$

The solution to the infinite set of simultaneous algebraic equations was treated as follows. In matrix notation, the equations can be written as

$$AX = B \qquad \text{(AG.2)}$$

where $A$ is the matrix of the coefficients, $X$ is the solution vector consisting of the unknown expansion coefficients and $B$ consists of known terms from the incident wave. Then

$$A^{-1}AX = A^{-1}B \qquad \text{(AG.3)}$$

and

$$IX = A^{-1}B \qquad \text{(AG.4)}$$

Thus the problem became one of inverting the matrix of the coefficients. The inversion routine for a matrix with complex elements consisted of a Gauss-Jordan elimination method which inverted the matrix in place with complete pivoting. A back substitution check on a (30 x 30) inversion produced agreement to six significant figures for all parameters treated where the solution converged satisfactorily. For cases where the elliptical discontinuity had eccentricity of 0.958, i.e., $B/A \simeq 0.3$, it was necessary to invert a (50 x 50) matrix in order to obtain satisfactory convergence of the stress and displacement

series. In most cases convergence was such that the last term of the series was less than one percent of the sum. However, for $B/A \simeq 0.3$ and $\zeta$ very small, the last term retained from a (50 x 50) inversion was on the order of five percent of the sum. Owing to storage limitations within the computer, it was not feasible to invert matrices larger than (50 x 50). Also the larger matrices were very poorly behaved because their complex elements varied by as much as thirty or forty orders of magnitude in some cases. This behavior arose from the fact that the radial functions and their derivatives vary greatly with the order of the function at certain frequencies. It was decided that the application of an error correction technique to the matrix inversion routine would prove unnecessarily complicated, and would in fact cause the storage capacity of the computer to be exceeded.

## H. Some Alternate Methods of Solution

The technique of separating the wave equation in the elliptical coordinates was employed primarily because it was the method used in similar problems involving dynamic stresses and because it leads to a solution that approaches the exact analytical solution in its generality. Some of the other solution techniques which were considered are now discussed briefly.

Average Wave Number Perturbation Method. The basic difficulty encountered in analyzing dynamic elasticity problems is that the stresses and displacements are each composed of two wave motions which travel at distinct characteristic speeds. When these stress and displacement waves are expanded in a series of the eigenfunctions of the

coordinate system being considered, the two wave numbers are contained in the eigenfunction arguments. In order to satisfy the boundary conditions of the problem at hand, it is necessary to evaluate the coefficients of the wave expansions which in turn requires the employment of the orthogonality properties of the characteristic functions. However, the presence of the two distinct wave numbers in the eigenfunction arguments prevents the use of orthogonality relations. In the present method of solution, this problem is overcome by writing the periodic Mathieu functions in terms of their Fourier series forms which introduces the orthogonal trigonometric functions. However, the solution is then represented by a doubly infinite series, and only an approximate solution may be obtained.

As pointed out by Thau,[1] if the two wave numbers were equal, no difficulty would arise, and an exact formal solution could be obtained. Unfortunately, the two wave speeds are never equal for real materials. Thau developed a perturbation method which used a function of the average wave number as the wave number of the unperturbed or zero order solution. Then the difference between each of the wave numbers and the average wave number can be related to a perturbation parameter. If $k_1$ is the compressional wave number and $k_2$ is the shear wave number, then

$$k_1 = \bar{k}\,(1-\varepsilon)$$
$$k_2 = \bar{k}\,(1+\varepsilon) \qquad \text{(AH.1)}$$

---

[1] S. A. Thau, Ph.D. Thesis, p. 146.

where $\bar{k} = (k_1 + k_2)/2$ and $\varepsilon = \frac{k_2 - k_1}{k_2 + k_1}$ . Substituting into the Helmholtz equations for $\phi$ and $\psi$ ,

$$[\nabla^2 + \bar{k}^2(1 - 2\varepsilon + \varepsilon^2)]\,\phi = 0$$

$$[\nabla^2 + \bar{k}^2(1 + 2\varepsilon + \varepsilon^2)]\,\psi = 0 \qquad \text{(AH.2)}$$

Define

$$\tilde{k} = (1+\varepsilon^2)^{1/2} \quad ; \quad \tilde{\varepsilon} = \frac{\varepsilon}{1+\varepsilon^2}$$

Then

$$[\nabla^2 + \tilde{k}^2(1 - 2\tilde{\varepsilon})]\,\phi = 0$$

$$[\nabla^2 + \tilde{k}^2(1 + 2\tilde{\varepsilon})]\,\psi = 0 \qquad \text{(AH.3)}$$

For real materials it can be shown that $0.167 < \tilde{\varepsilon}^2 < 0.5$ , the upper and lower limits corresponding to $\nu = 0.5$ and $\nu = 0.0$ , respectively. Then it is assumed that $\phi$ , $\psi$ stresses and displacements can be expanded in a power series of $\varepsilon$ or $\tilde{\varepsilon}$ . Consider a plane wave expansion in $\varepsilon$ .

$$e^{ikx} = e^{i\bar{k}(1-\varepsilon)x} = e^{i\bar{k}x}(1 - i\varepsilon\bar{k}x + \cdots) \qquad \text{(AH.4)}$$

It may be concluded that near field low frequency results will be most accurate. It must be noted at this point that the same conclusion applies to the separation of variables, doubly infinite series approximate solution employed in the present paper. Therefore, the average wave number perturbation method could not be expected to yield new or better results. It will be shown that the average wave

number perturbation method cannot be applied to dynamic stress problems in elliptical coordinates. Consider

$$\phi = \phi^0 + \tilde{\varepsilon}\phi^1 + \tilde{\varepsilon}^2\phi^2 + \cdots$$

$$\psi = \psi^0 + \tilde{\varepsilon}\psi^1 + \tilde{\varepsilon}^2\psi^2 + \cdots \qquad \text{(AH.5)}$$

Then the zero order potentials satisfy

$$(\nabla^2 + \tilde{k}^2)\phi^0 = 0 \quad ; \quad (\nabla^2 + \tilde{k}^2)\psi^0 = 0 \qquad \text{(AH.6)}$$

The governing equations for the higher order perturbations will not be derived since the perturbation method fails already with the zero order solution.

The solutions to (AH.6) are Mathieu function products. For a rigid immovable inclusion with an incident shear wave

$$\overset{inc.}{\psi^0} = -2\pi\Big[\sum_m ce_m(\eta_0,\tilde{q})\,ce_m(\eta,\tilde{q})\,Mc_m^{(1)}(\xi,\tilde{q})\,Mc_m^{(3)}(\xi_0,\tilde{q}) + \sum_m se_m(\eta_0,\tilde{q})\,se_m(\eta,\tilde{q})\,Ms_m^{(1)}(\xi,\tilde{q})\,Ms_m^{(3)}(\xi_0,\tilde{q})\Big]$$

$$\overset{ref.}{\phi^0} = \sum_m B_m\,ce_m(\eta,\tilde{q})\,Mc_m^{(3)}(\xi,\tilde{q}) + \sum_m C_m\,se_m(\eta,\tilde{q})\,Ms_m^{(3)}(\xi,\tilde{q})$$

$$\overset{ref.}{\psi^0} = \sum_m D_m\,ce_m(\eta,\tilde{q})\,Mc_m^{(3)}(\xi,\tilde{q}) + \sum_m E_m\,se_m(\eta,\tilde{q})\,Ms_m^{(3)}(\xi,\tilde{q}) \qquad \text{(AH.7)}$$

The displacements are

$$ {}^{inc.}U_{\xi}^{o} = \frac{-2\pi}{\sqrt{g}}\left[\sum_m ce_m(\eta_0,\tilde{q})\,ce_m'(\eta,\tilde{q})\,Mc_m^{(1)}(\xi,\tilde{q})\,Mc_m^{(3)}(\xi_0,\tilde{q})\right.$$

$$\left. + \sum_m se_m(\eta_0,\tilde{q})\,se_m'(\eta,\tilde{q})\,Ms_m^{(1)}(\xi,\tilde{q})\,Ms_m^{(3)}(\xi_0,\tilde{q})\right] \qquad \text{(AH.8)}$$

$$ {}^{ref.}U_{\xi}^{o} = \frac{1}{\sqrt{g}}\left[\sum_m B_m\,ce_m(\eta,\tilde{q})\,Mc_m^{(3)\prime}(\xi,\tilde{q}) + \sum_m C_m\,se_m(\eta,\tilde{q})\,Ms_m^{(3)\prime}(\xi,\tilde{q})\right.$$

$$\left. + \sum_m D_m\,ce_m'(\eta,\tilde{q})\,Mc_m^{(3)}(\xi,\tilde{q}) + \sum_m E_m\,se_m'(\eta,\tilde{q})\,Ms_m^{(3)}(\xi,\tilde{q})\right] \qquad \text{(AH.9)}$$

and similarly for ${}^{inc.}U_{\eta}^{o}$ and ${}^{ref.}U_{\eta}^{o}$. The boundary conditions are

$$ {}^{inc.}U_{\xi}^{o} + {}^{ref.}U_{\xi}^{o} = 0$$

$$ {}^{inc.}U_{\eta}^{o} + {}^{ref.}U_{\eta}^{o} = 0 \qquad \text{(AH.10)}$$

(AH.10) represents essentially two equations for $B_m$, $C_m$, $D_m$, and $E_m$. At this point it would be desirable to employ the orthogonality properties of the periodic Mathieu functions to obtain four equations. Even though the arguments are now identical, the method fails because

$$se'(\eta,\tilde{q}) \propto ce(\eta,\tilde{q})$$

and

$$ce'(\eta,\tilde{q}) \propto se(\eta,\tilde{q})$$

do not hold. In fact there is no simple relationship between the derivative of one function and the other function except at zero wave number which is the static limit of the dynamic case. Therefore, while the perturbation method proved to be a fruitful technique in the parabolic geometry treated by Thau, the method fails in the present problem.

Characteristics. In general, problems involving the propagation of stress waves in solids are presented as problems of partial differential equations which describe disturbances in ideal continua obeying the mass, energy, and momentum conservation laws. Boundary value problems of systems of hyperbolic quasi-linear partial differential equations involving only two independent variables can be solved using the method of characteristics. Physically, the independent variables are either two space coordinates or one space coordinate and time. In the present plane elasticity problem, the introduction of harmonic time dependence reduces the number of independent variables to two space coordinates, and it would appear at first glance that the method of characteristics might apply, although the time reduced equations might present some difficulties. In the absence of discontinuity boundaries, the dynamic stress problem could be treated by this method. However, the presence of a discontinuity introduces the phenomenon of mode conversion whereby both P- and SV-waves are reflected and refracted from an incident wave of either type. As late as 1968, the method of characteristics as applied to elastic waves was generally restricted to propagation in the absence of boundaries,

and it appears that the mode conversion problem has not been treated. Therefore, the method of characteristics does not readily lend itself to the solution of the present problem.

Integral Transforms. The primary difficulty encountered in the use of transform techniques lies in carrying out the inversion of the transformed solution. Generally, the inversion entails the evaluation of integrals in the complex plane. For the present problem, the transformed solution would contain the Mathieu functions which means that the integrands in the inversion would contain them as well. Integrals involving the Mathieu functions have not been well treated in the literature, and while a numerical integration procedure might prove feasible for carrying out the inversions, the numerical problems encountered would be formidable. Therefore, the integral transform methods were not considered for the present problem.

Direct Numerical Integration. Another alternative approach might be to directly integrate the Navier's equation for the displacements after transforming to elliptical coordinates. The difficulties inherent in this method include

(a) divergent paths of integration caused by the nature of the elliptical coordinate system

(b) governing equations in terms of displacements and boundary conditions in terms of stresses or vice-versa

(c) mode conversion phenomenon

(d) convergence of solution.

Also the method itself is undesirable since it eliminates all parametric generality at the outset. For the reasons above, this method was not used.

## I. Derivation of the Boundary Condition Expressions

The aim of the following derivation is to reduce the stress and displacement relations such that only one trigonometric function appears in each term, i.e., all products of trigonometric functions must be eliminated through the use of certain identities. When this is accomplished, the orthogonality properties of the functions may be used.

Define partial potentials as in (5A.12) through (5A.23); also define $P = \frac{1-\nu}{1-2\nu}$ ; $Q = \frac{\nu}{1-2\nu}$ and introduce

$$I = \sum_n A_1^n \cos n\eta + \sum_n A_2^n \sin n\eta$$

$$II = \sum_n A_3^n \cos n\eta + \sum_n A_4^n \sin n\eta$$

$$III = \sum_n A_5^n \cos n\eta + \sum_n A_6^n \sin n\eta$$

$$IV = \sum_n A_7^n \cos n\eta + \sum_n A_8^n \sin n\eta$$

$$V = \sum_n A_9^n \cos n\eta + \sum_n A_{10}^n \sin n\eta$$

$$VI = \sum_n A_{11}^n \cos n\eta + \sum_n A_{12}^n \sin n\eta$$

$$VII = \sum_n A_{13}^n \cos n\eta + \sum_n A_{14}^n \sin n\eta$$

(AI.1)

where

$$A_1^n = ({}^{e}\phi_n^{''k} + n\,{}^{o}\psi_n^{'k}) \quad ; \quad A_2^n = ({}^{o}\phi_n^{''k} - n\,{}^{e}\psi_n^{'k})$$

$$A_3^n = ({}^{e}\phi_n^{'k} + n\,{}^{o}\psi_n^{k}) \quad ; \quad A_4^n = ({}^{o}\phi_n^{'k} - n\,{}^{e}\psi_n^{k})$$

$$A_5^n = (n\,{}^{o}\phi_n^{k} - {}^{e}\psi_n^{'k}) \quad ; \quad A_6^n = -(n\,{}^{e}\phi_n^{k} + {}^{o}\psi_n^{'k})$$

$$A_7^n = -(n^2\,{}^{e}\phi_n^{k} + n\,{}^{o}\psi_n^{'k}) \quad ; \quad A_8^n = -(n^2\,{}^{o}\phi_n^{k} - n\,{}^{e}\psi_n^{'k})$$

$$A_9^n = \tfrac{+}{2}(2n\,{}^{o}\phi_n^{'k} - n^2\,{}^{e}\psi_n^{k} - {}^{e}\psi_n^{''k}) \quad ; \quad A_{10}^n = -\tfrac{+}{2}(2n\,{}^{e}\phi_n^{'k} + n^2\,{}^{o}\psi_n^{k} + {}^{o}\psi_n^{''k})$$

$$A_{11}^n = ({}^{e}\phi_n^{'k} + n\,{}^{o}\psi_n^{k}) \quad ; \quad A_{12}^n = ({}^{o}\phi_n^{'k} - n\,{}^{e}\psi_n^{k})$$

$$A_{13}^n = (n\,{}^{o}\phi_n^{k} - {}^{e}\psi_n^{'k}) \quad ; \quad A_{14}^n = -(n\,{}^{e}\phi_n^{k} + {}^{o}\psi_n^{'k}) \qquad \text{(AI.2)}$$

Then if $k = i, s, T$ for the incident, scattered, and transmitted wave fields, respectively, the stresses can be written as

$$\tau_{\xi\xi}^{k} \to P(\cosh^2\xi - \cos^2\eta)\,\underline{\mathrm{I}} - \cosh\xi\sinh\xi\,\underline{\mathrm{II}} + \cos\eta\sin\eta\,\underline{\mathrm{III}}$$

$$+ Q(\cosh^2\xi - \cos^2\eta)\,\underline{\mathrm{IV}}$$

$$\tau_{\xi\eta}^{k} \to (\cosh^2\xi - \cos^2\eta)\,\underline{\mathrm{V}} - \cos\eta\sin\eta\,\underline{\mathrm{VI}} - \cosh\xi\sinh\xi\,\underline{\mathrm{VII}} \qquad \text{(AI.3)}$$

These may be reduced by means of trigonometric identities to

$$\tau^{k}_{\xi\xi} \to \cosh^2\xi\,(P\mathrm{I} + Q\mathrm{IV}) - \tfrac{1}{2}(P\mathrm{I} - Q\mathrm{IV}) - \tfrac{1}{2}\cos 2\eta\,(P\mathrm{I} + Q\mathrm{IV})$$

$$- \cosh\xi \sinh\xi\,\mathrm{II} + \tfrac{1}{2}\sin 2\eta\,\mathrm{III}$$

$$\tau^{k}_{\xi\eta} \to \cosh^2\xi\,\mathrm{V} - \tfrac{1}{2}\mathrm{V} - \tfrac{1}{2}\cos^2\eta\,\mathrm{V} - \tfrac{1}{2}\sin^2\eta\,\mathrm{VI} - \cosh\xi\sinh\xi\,\mathrm{VII} \qquad \text{(AI.4)}$$

In terms of the $A^n$'s these become

$$\tau^{k}_{\xi\xi} \to \sum_n \Big\{\Big[(\cosh^2\xi - \tfrac{1}{2})(PA^n_1 + QA^n_7) - \cosh\xi\sinh\xi\,A^n_3\Big]\cos n\eta$$

$$+\Big[(\cosh^2\xi - \tfrac{1}{2})(PA^n_2 + QA^n_8) - \cosh\xi\sinh\xi\,A^n_4\Big]\sin n\eta$$

$$-\tfrac{1}{2}\Big[(PA^n_1 + QA^n_9)\cos^2\eta\cos n\eta + (PA^n_2 + QA^n_8)\cos^2\eta\sin n\eta\Big]$$

$$+\tfrac{1}{2}A^n_5\sin^2\eta\cos n\eta + \tfrac{1}{2}A^n_6\sin^2\eta\sin n\eta\Big\}$$

$$\tau^{k}_{\xi\eta} \to \sum_n \Big\{\Big[(\cosh^2\xi - \tfrac{1}{2})A^n_9 - \cosh\xi\sinh\xi\,A^n_{13}\Big]\cos n\eta$$

$$+\Big[(\cosh^2\xi - \tfrac{1}{2})A^n_{10} - \cosh\xi\sinh\xi\,A^n_{14}\Big]\sin n\eta$$

$$-\tfrac{1}{2}A^n_9\cos 2\eta\cos n\eta - \tfrac{1}{2}A^n_{10}\cos 2\eta\sin n\eta$$

$$-\tfrac{1}{2}A^n_{11}\sin^2\eta\cos n\eta - \tfrac{1}{2}A^n_{12}\sin^2\eta\sin n\eta\Big\} \qquad \text{(AI.5)}$$

Expand using trigonometric identities to obtain

$$\tau^k_{\xi\xi} \to \sum_n \Big\{ \Big[ (\cosh^2\xi - \tfrac{1}{2})(PA_1^n + QA_7^n) - \cosh\xi \sinh\xi A_3^n \Big] \cos n\eta$$

$$- \tfrac{1}{4}(PA_1^n + QA_7^n)(\cos(n+2)\eta + \cos(n-2)\eta)$$

$$+ \tfrac{1}{4} A_6^n \big[\cos(n-2)\eta - \cos(n+2)\eta\big] + \Big[(\cosh^2\xi - \tfrac{1}{2})(PA_2^n + QA_8^n)$$

$$- \cosh\xi \sinh\xi A_4^n \Big] \sin n\eta - \tfrac{1}{4}(PA_2^n + QA_8^n)\big[\sin(n+2)\eta$$

$$+ \sin(n-2)\eta\big] + \tfrac{1}{4} A_5^n \big[\sin(n+2)\eta - \sin(n-2)\eta\big] \Big\}$$

$$\tau^k_{\xi\eta} \to \sum_n \Big\{ \Big[ (\cosh^2\xi - \tfrac{1}{2}) A_9^n - \cosh\xi \sinh\xi A_{13}^n \Big] \cos n\eta$$

$$- \tfrac{1}{4} A_9^n \big[\cos(n+2)\eta + \cos(n-2)\eta\big] - \tfrac{1}{4} A_{12}^n \big[\cos(n-2)\eta - \cos(n+2)\eta\big]$$

$$+ \Big[ (\cosh^2\xi - \tfrac{1}{2}) A_{10}^n - \cosh\xi \sinh\xi A_{14}^n \Big] \sin n\eta$$

$$- \tfrac{1}{4} A_{10}^n \big[\sin(n+2)\eta + \sin(n-2)\eta\big] - \tfrac{1}{4} A_{11}^n \big[\sin(n+2)\eta - \sin(n-2)\eta\big] \Big\} \quad \text{(AI.6)}$$

Introduce the orthogonality properties of the trigonometric functions and reduce (AI.6) to the following four expressions

e $$\tau^k_{\xi\xi} \to \sum_n \Big\{ \tfrac{1}{4}(A_6^n - PA_1^n - QA_7^n)\cos(n-2)\eta + \Big[(\cosh^2\xi - \tfrac{1}{2})(PA_1^n + QA_7^n)$$

$$- \cosh\xi \sinh\xi A_3^n \Big] \cos n\eta - \tfrac{1}{4}(A_6^n + PA_1^n + QA_7^n)\cos(n+2)\eta \Big\}$$

o. $$\tau^k_{\xi\xi} \to \sum_n \Big\{ -\tfrac{1}{4}(A_5^n + PA_2^n + QA_8^n)\sin(n-2)\eta + \Big[(\cosh^2\xi - \tfrac{1}{2})(PA_2^n + QA_8^n)$$

$$- \cosh\xi \sinh\xi A_4^n \Big] \sin n\eta + \tfrac{1}{4}(A_5^n - PA_2^n - QA_8^n)\sin(n+2)\eta \Big\}$$

cont.

$$e\hat{\tau}^{k}_{\xi\eta} \rightarrow \sum_n \Big\{ -\tfrac{1}{4}(A^n_{12}+A^n_9)\cos(n-2)\eta + \big[(\cosh^2\xi - \tfrac{1}{2})A^n_9 - \cosh\xi\sinh\xi A^n_{13}\big]\cos n\eta$$

$$+ \tfrac{1}{4}(A^n_{12} - A^n_9)\cos(n+2)\eta \Big\}$$

$$o\hat{\tau}^{k}_{\xi\eta} \rightarrow \sum_n \Big\{ \tfrac{1}{4}(A^n_{11} - A^n_{10})\sin(n-2)\eta + \big[(\cosh^2\xi - \tfrac{1}{2})A^n_{10} - \cosh\xi\sinh\xi A^n_{14}\big]\sin n\eta$$

$$- \tfrac{1}{4}(A^n_{10} + A^n_{11})\sin(n+2)\eta \Big\} \qquad \text{(AI.7)}$$

Now define the following

$$B^n_1 = \tfrac{1}{4}(A^n_6 - PA^n_1 - QA^n_7) \; ; \; B^n_2 = \big[(\cosh^2\xi - \tfrac{1}{2})(PA^n_1 + QA^n_7) - \cosh\xi\sinh\xi A^n_3\big]$$

$$B^n_3 = -\tfrac{1}{4}(A^n_6 + PA^n_1 - QA^n_7) \; ; \; B^n_4 = -\tfrac{1}{4}(A^n_5 + PA^n_2 + QA^n_8)$$

$$B^n_5 = \big[(\cosh^2\xi - \tfrac{1}{2})(PA^n_2 + QA^n_8) - \cosh\xi\sinh\xi A^n_4\big] \; ; \; B^n_6 = \tfrac{1}{4}(A^n_5 - PA^n_2 - QA^n_8]$$

$$B^n_7 = -\tfrac{1}{4}(A^n_{12} + A^n_9) \; ; \; B^n_8 = \big[(\cosh^2\xi - \tfrac{1}{2})A^n_9 - \cosh\xi\sinh\xi A^n_{13}\big]$$

$$B^n_9 = \tfrac{1}{4}(A^n_{12} - A^n_9) \; ; \; B^n_{10} = \tfrac{1}{4}(A^n_{11} - A^n_{10})$$

$$B^n_{11} = \big[(\cosh^2\xi - \tfrac{1}{2})A^n_{10} - \cosh\xi\sinh\xi A^n_{14}\big] \; ; \; B^n_{12} = -\tfrac{1}{4}(A^n_{10} + A^n_{11})$$

(AI.8)

Write out the first six terms of each series for the four separated stress expressions

$$e\hat{\tau}^{k}_{\xi\xi} \rightarrow B^0_1\cos 2\eta + B^0_2 + B^0_3\cos 2\eta \qquad n=0$$

$$+ B^1_1\cos\eta + B^1_2\cos\eta + B^1_3\cos 3\eta \qquad n=1 \qquad \text{cont.}$$

$$+ B_1^2 + B_2^2 \cos 2\eta + B_3^2 \cos 4\eta \qquad n=2$$

$$+ B_1^3 \cos\eta + B_2^3 \cos 3\eta + B_3^3 \cos 5\eta \qquad n=3$$

$$+ B_1^4 \cos 2\eta + B_2^4 \cos 4\eta + B_3^4 \cos 6\eta \qquad n=4$$

$$+ B_1^5 \cos 3\eta + B_2^5 \cos 5\eta + B_3^5 \cos 7\eta \qquad n=5$$

$$+ \sum_{n=6}^{\infty} [\quad] \qquad \text{(AI.9)}$$

Collect like terms to obtain

$$e^k_{\xi\xi\xi} \rightarrow (B_2^0 + B_1^2) + (B_1^1 + B_2^1 + B_1^3)\cos\eta + (B_1^0 + B_3^0 + B_2^2 + B_1^4)\cos 2\eta + \sum_{n=3}^{\infty} (B_3^{n-2} + B_2^n + B_1^{n+2})\cos n\eta$$

Similarly

$$o^k_{\xi\xi\xi} \rightarrow (-B_4^1 + B_5^1 + B_4^3)\sin\eta + (-B_4^0 + B_6^0 + B_5^2 + B_4^4)\sin 2\eta + \sum_{n=3}^{\infty} (B_6^{n-2} + B_5^n + B_4^{n+2})\sin n\eta \qquad \text{(AI.10)}$$

Also

$$e^k_{\xi\eta} \rightarrow (B_8^0 + B_7^2) + (B_7^1 + B_8^1 + B_7^3)\cos\eta + (B_7^0 + B_9^0 + B_8^2 + B_7^4)\cos 2\eta + \sum_{n=3}^{\infty} (B_9^{n-2} + B_8^n + B_7^{n+2})\cos n\eta$$

cont.

$$\overset{o\ k}{\mathcal{L}}_{\xi\eta} \rightarrow (-B^{1}_{10} + B^{1}_{11} + B^{3}_{10})\sin\eta + (-B^{0}_{10} + B^{0}_{12} + B^{2}_{11} + B^{4}_{10})\sin 2\eta$$

$$+\sum_{n=3}^{\infty}(B^{n-2}_{12} + B^{n}_{11} + B^{n+2}_{10})\sin n\eta \qquad \text{(AI.11)}$$

Next replace the $B$'s by the $A$ terms; then replace the $A$'s by the potential terms; and finally, replace the partial potentials by the Mathieu function expressions. Then simplify the resulting expressions and define

$$[b^{e}_{m}(q_c) - 2q_c\cosh 2\xi] = G_m$$

$$[b^{o}_{m}(q_c) - 2q_c\cosh 2\xi] = H_m$$

$$[b^{e}_{m}(q_s) - 2q_s\cosh 2\xi] = T_m$$

$$[b^{o}_{m}(q_s) - 2q_s\cosh 2\xi] = U_m \qquad \text{(AI.12)}$$

Also separate the $\phi$ and $\psi$ terms. Then for the reflected waves the explicit forms of the coefficients of the trigonometric functions in (AI.10) and (AI.11) are

$$\phi\overset{e\ s}{\mathcal{L}}_{\xi\xi} \; n=0 \sum_{m} B_m\Big\{M^{(3)}_{c_m}(\xi,q_c)\Big[\Big(\tfrac{1-\nu}{1-2\nu}\Big)\Big(\cosh^2\xi - \tfrac{1}{2}\Big)A^{m}_{0}(q_c)G_m$$

$$+\tfrac{1}{4}\Big[2\Big(\tfrac{4\nu-1}{1-2\nu}\Big)A^{m}_{2}(q_c) - \Big(\tfrac{1-\nu}{1-2\nu}\Big)A^{m}_{2}(q_c)G_m\Big]\Big] - \cosh\tfrac{\xi}{2}\sinh\tfrac{\xi}{2}\times$$

$$A^{m}_{0}(q_c)M^{(3)'}_{c_m}(\xi,q_c)\Big\}$$

cont.

$$n=1 \sum_m B_m \Big\{ M_{c_m}^{(3)}(\xi,\eta_c)\Big[-\Big[\Big(\cosh^2\xi-\tfrac{3}{4}\Big)\Big(\tfrac{\nu}{1-2\nu}\Big)+\tfrac{1}{4}\Big]A_1^m(\eta_c)+\Big(\cosh^2\xi-\tfrac{3}{4}\Big)\Big(\tfrac{1-\nu}{1-2\nu}\Big)A_1^m(\eta_c)G_m$$

$$+\tfrac{1}{4}\Big[3\Big(\tfrac{5\nu-1}{1-2\nu}\Big)A_3^m(\eta_c)-\Big(\tfrac{1-\nu}{1-2\nu}\Big)A_3^m(\eta_c)G_m\Big]\Big]-\cosh\xi\sinh\xi A_1^m(\eta_c)M_{c_m}^{(3)\prime}(\xi,\eta_c)\Big\}$$

$$n=2 \sum_m B_m \Big\{ M_{c_m}^{(3)}(\xi,\eta_c)\Big[-\tfrac{1}{2}\Big(\tfrac{1-\nu}{1-2\nu}\Big)A_0^m(\eta_c)G_m+\Big(\cosh^2\xi-\tfrac{1}{2}\Big)\Big[\Big(\tfrac{1-\nu}{1-2\nu}\Big)A_2^m(\eta_c)G_m$$

$$-\Big(\tfrac{4\nu}{1-2\nu}\Big)A_2^m(\eta_c)\Big]+\tfrac{1}{4}\Big[4\Big(\tfrac{6\nu-1}{1-2\nu}\Big)A_4^m(\eta_c)-\Big(\tfrac{1-\nu}{1-2\nu}\Big)A_4^m(\eta_c)G_m\Big]\Big]-\cosh\xi\sinh\xi A_2^m(\eta_c)M_{c_m}^{(3)\prime}(\xi,\eta_c)\Big\}$$

$$n\geq 3 \sum_m B_m \Big\{ M_{c_m}^{(3)}(\xi,\eta_c)\Big[-\tfrac{1}{4}\Big[-(n-2)\Big(\Big(\tfrac{\nu}{1-2\nu}\Big)(n-2)+1\Big)A_{n-2}^m(\eta_c)+\Big(\tfrac{1-\nu}{1-2\nu}\Big)A_{n-2}^m(\eta_c)G_m\Big]$$

$$+\Big(\cosh^2\xi-\tfrac{1}{2}\Big)\Big[\Big(\tfrac{1-\nu}{1-2\nu}\Big)A_n^m(\eta_c)G_m-\tfrac{n^2\nu}{1-2\nu}A_n^m(\eta_c)\Big]+\tfrac{1}{4}\Big[(n+2)\Big(\tfrac{\nu}{1-2\nu}\Big)(n+2)-1\Big)A_{n+2}^m(\eta_c)$$

$$-\Big(\tfrac{1-\nu}{1-2\nu}\Big)A_{n+2}^m(\eta_c)G_m\Big]\Big]-\cosh\xi\sinh\xi A_n^m(\eta_c)M_{c_m}^{(3)\prime}(\xi,\eta_c)\Big\}$$

(AI.13)

$$4\,{}^{e}_{s}\Sigma_{\xi\xi}\ n=0\ -\tfrac{3}{4}\sum_m E_m B_2^m(\eta_s)M_{s_m}^{(3)\prime}(\xi,\eta_s)$$

$$n=1 \sum_m E_m\Big\{M_{s_m}^{(3)\prime}(\xi,\eta_s)\Big[\big(\cosh^2\xi-1\big)B_1^m(\eta_s)-B_3^m(\eta_s)\Big]-\cosh\xi\sinh\xi B_1^m(\eta_s)M_{s_m}^{(3)}(\xi,\eta_s)\Big\}$$

$$n=2 \sum_m E_m\Big\{M_{s_m}^{(3)\prime}(\xi,\eta_s)\Big[2\Big(\cosh^2\xi-\tfrac{1}{2}\Big)B_2^m(\eta_s)-\tfrac{5}{4}B_4^m(\eta_s)\Big]-2\cosh\xi\sinh\xi B_2^m(\eta_s)M_{s_m}^{(3)}(\xi,\eta_s)\Big\}$$

$$n\geq 3 \sum_m E_m\Big\{M_{s_m}^{(3)\prime}(\xi,\eta_s)\Big[-\tfrac{1}{4}(n-3)B_{n-2}^m(\eta_s)+n\Big(\cosh^2\xi-\tfrac{1}{2}\Big)B_n^m(\eta_s)-\tfrac{1}{4}(n+3)B_{n+2}^m(\eta_s)\Big]$$

$$-n\cosh\xi\sinh\xi B_n^m(\eta_s)M_{s_m}^{(3)}(\xi,\eta_s)\Big\}$$

(AI.14)

$$\overset{o}{\phi}\overset{s}{\tau}_{\xi\xi}\; n=1 \sum_m C_m \Big\{ Ms_m^{(3)}(\xi,\eta_c)\Big[\Big[\Big(\tfrac{1}{4}-\Big(\tfrac{\nu}{1-2\nu}\Big)\Big(\cosh^2\xi-\tfrac{1}{4}\Big)\Big)+\Big(\tfrac{1-\nu}{1-2\nu}\Big)\Big(\cosh^2\xi-\tfrac{1}{4}\Big)H_m\Big]B_1^m(\eta_c)$$

$$-\tfrac{1}{4}\Big[3\Big(\tfrac{1-5\nu}{1-2\nu}\Big)+\Big(\tfrac{1-\nu}{1-2\nu}\Big)H_m\Big]B_3^m(\eta_c)\Big]-\cosh\xi\sinh\xi\, B_1^m(\eta_c)\,Ms_m^{(3)\prime}(\xi,\eta_c)\Big\}$$

$$n=2 \sum_m C_m \Big\{ Ms_m^{(3)}(\xi,\eta_c)\Big[\Big(\cosh^2\xi-\tfrac{1}{2}\Big)\Big[\Big(\tfrac{1-\nu}{1-2\nu}\Big)H_m-\tfrac{4\nu}{1-2\nu}\Big]B_2^m(\eta_c)$$

$$-\tfrac{1}{4}\Big[4\Big(\tfrac{1-6\nu}{1-2\nu}\Big)+\Big(\tfrac{1-\nu}{1-2\nu}\Big)H_m\Big]B_4^m(\eta_c)\Big]-\cosh\xi\sinh\xi\, B_2^m(\eta_c)\,Ms_m^{(3)\prime}(\xi,\eta_c)\Big\}$$

$$n\geq 3 \sum_m C_m \Big\{ Ms_m^{(3)}(\xi,\eta_c)\Big[\tfrac{1}{4}\Big[(n-2)\Big(1+\tfrac{\nu}{1-2\nu}(n-2)\Big)-\Big(\tfrac{1-\nu}{1-2\nu}\Big)H_m\Big]B_{n-2}^m(\eta_c)$$

$$+\Big(\cosh^2\xi-\tfrac{1}{2}\Big)\Big[\Big(\tfrac{1-\nu}{1-2\nu}\Big)H_m-\tfrac{n^2\nu}{1-2\nu}\Big]B_n^m(\eta_c)-\tfrac{1}{4}\Big[(n+2)\Big(1-\tfrac{\nu}{1-2\nu}(n+2)\Big)$$

$$+\Big(\tfrac{1-\nu}{1-2\nu}\Big)H_m\Big]B_{n+2}^m(\eta_c)\Big]-\cosh\xi\sinh\xi\, B_n^m(\eta_c)\,Ms_m^{(3)\prime}(\xi,\eta_c)\Big\}$$

(AI.15)

$$\overset{o}{\phi}\overset{s}{\tau}_{\xi\xi}\; n=1 \sum_m D_m \Big[ Mc_m^{(3)\prime}(\xi,\eta_s)\Big[-\cosh^2\xi\, A_1^m(\eta_s)+A_3^m(\eta_s)\Big]+\cosh\xi\sinh\xi\, A_1^m(\eta_s)\,Mc_m^{(3)}(\xi,\eta_s)\Big]$$

$$n=2 \sum_m D_m \Big\{ Mc_m^{(3)\prime}(\xi,\eta_s)\Big[-\tfrac{1}{2}A_0^m(\eta_s)-2\Big(\cosh^2\xi-\tfrac{1}{2}\Big)A_2^m(\eta_s)+\tfrac{5}{4}A_4^m(\eta_s)\Big]$$

$$+2\cosh\xi\sinh\xi\, A_2^m(\eta_s)\,Mc_m^{(3)}(\xi,\eta_s)\Big\}$$

$$n\geq 3 \sum_m D_m \Big\{ Mc_m^{(3)\prime}(\xi,\eta_s)\Big[\tfrac{1}{4}(n-3)A_{n-2}^m(\eta_s)-n\Big(\cosh^2\xi-\tfrac{1}{2}\Big)A_n^m(\eta_s)$$

$$+\tfrac{1}{4}(n+3)A_{n+2}^m(\eta_s)\Big]+n\cosh\xi\sinh\xi\, A_n^m(\eta_s)\,Mc_m^{(3)}(\xi,\eta_s)\Big\}$$

(AI.16)

$$\phi^{es}\hat{L}_{\xi\eta}\ n=0\quad -\tfrac{3}{4}\sum_m C_m B_2^m(\gamma_c) Ms_m^{(3)\prime}(\xi,\gamma_c)$$

$$n=1\quad \sum_m C_m\Big\{Ms_m^{(3)\prime}(\xi,\gamma_c)\Big[(\cosh^2\xi-1)B_1^m(\gamma_c)-B_3^m(\gamma_c)\Big]-\cosh\xi\sinh\xi\, B_1^m(\gamma_c)Ms_m^{(3)}(\xi,\gamma_c)\Big\}$$

$$n=2\quad \sum_m C_m\Big\{Ms_m^{(3)\prime}(\xi,\gamma_c)\Big[2(\cosh^2\xi-\tfrac{1}{2})B_2^m(\gamma_c)-\tfrac{5}{4}B_4^m(\gamma_c)\Big]-2\cosh\xi\sinh\xi\, B_2^m(\gamma_c)Ms_m^{(3)}(\xi,\gamma_c)\Big\}$$

$$n\geq 3\quad \sum_m C_m\Big\{Ms_m^{(3)\prime}(\xi,\gamma_c)\Big[-\tfrac{1}{4}(n-3)B_{n-2}^m(\gamma_c)+n(\cosh^2\xi-\tfrac{1}{2})B_n^m(\gamma_c)$$

$$-\tfrac{1}{4}(n+3)B_{n+2}^m(\gamma_c)\Big]-n\cosh\xi\sinh\xi\, B_n^m(\gamma_c)Ms_m^{(3)}(\xi,\gamma_c)\Big\}$$

(AI.17)

$$\phi^{es}\hat{L}_{\xi\eta}\ n=0\ \sum_m D_m\Big\{Mc_m^{(3)}(\xi,\gamma_s)\Big[-\tfrac{1}{2}(\cosh^2\xi-\tfrac{1}{2})A_0^m(\gamma_s)T_m+(1-\tfrac{1}{8}T_m)A_2^m(\gamma_s)\Big]$$

$$+\cosh\xi\sinh\xi\, A_0^m(\gamma_s)Mc_m^{(3)\prime}(\xi,\gamma_s)\Big\}$$

$$n=1\quad \sum_m D_m\Big\{Mc_m^{(3)}(\xi,\gamma_s)\Big[\Big(-\tfrac{1}{2}(\cosh^2\xi-5/4)-\tfrac{1}{2}(\cosh^2\xi-\tfrac{3}{4})T_m\Big)A_1^m(\gamma_s)$$

$$+\tfrac{1}{8}(15+T_m)A_3^m(\gamma_s)\Big]+\cosh\xi\sinh\xi\, A_1^m(\gamma_s)Mc_m^{(3)\prime}(\xi,\gamma_s)\Big\}$$

$$n=2\quad \sum_m D_m\Big\{Mc_m^{(3)}(\xi,\gamma_s)\Big[\tfrac{1}{4}A_0^m(\gamma_s)T_m-\tfrac{1}{2}(\cosh^2\xi-\tfrac{1}{2})(4+T_m)A_2^m(\gamma_s)$$

$$+(3+\tfrac{1}{8}T_m)A_4^m(\gamma_s)\Big]+\cosh\xi\sinh\xi\, A_2^m(\gamma_s)Mc_m^{(3)\prime}(\xi,\gamma_s)\Big\}$$

$$n\geq 3\quad \sum_m D_m\Big\{Mc_m^{(3)}(\xi,\gamma_s)\Big[\tfrac{1}{4}\Big[(n-2)\Big(\frac{(n-2)}{2}-1\Big)+\tfrac{1}{2}T_m\Big]A_{n-2}^m(\gamma_s)$$

$$-\tfrac{1}{2}(\cosh^2\xi-\tfrac{1}{2})(n^2+T_m)A_n^m(\gamma_s)+\tfrac{1}{4}\Big[(n+2)\Big(\frac{(n+2)}{2}+1\Big)+\tfrac{1}{2}T_m\Big]A_{n+2}^m(\gamma_s)\Big]$$

(AI.18)

$$+\cosh\xi\sinh\xi\, A_n^m(\gamma_s)Mc_m^{(3)\prime}(\xi,\gamma_s)\Big\}$$

$$\phi \hat{\tau}^{os}_{\xi\eta}\, n=1 \sum_m B_m \Big\{ Mc_m^{(3)'}(\xi,\eta_c)\Big[-\cosh^2\xi\, A_1^m(\eta_c) + A_3^m(\eta_c)\Big] + \cosh\xi\sinh\xi\, A_1^m(\eta_c)\, Mc_m^{(3)}(\xi,\eta_c)\Big\}$$

$$n=2 \sum_m B_m \Big\{ Mc_m^{(3)'}(\xi,\eta_c)\Big[-\tfrac{1}{2}A_0^m(\eta_c) - 2(\cosh^2\xi - \tfrac{1}{2})A_2^m(\eta_c) + \tfrac{5}{4}A_4^m(\eta_c)\Big]$$

$$+2\cosh\xi\sinh\xi\, A_2^m(\eta_c)\, Mc_m^{(3)}(\xi,\eta_c)\Big\}$$

$$n\geq 3 \sum_m B_m \Big\{ Mc_m^{(3)'}(\xi,\eta_c)\Big[\tfrac{1}{4}(n-3)A_{n-2}^m(\eta_c) - n(\cosh^2\xi - \tfrac{1}{2})A_n^m(\eta_c)$$

$$+\tfrac{1}{4}(n+3)A_{n+2}^m(\eta_c)\Big] + n\cosh\xi\sinh\xi\, A_n^m(\eta_c)\, Mc_m^{(3)}(\xi,\eta_c)\Big\}$$

(AI.19)

$$4\hat{\tau}^{os}_{\xi\eta}\, n=1 \sum_m E_m \Big\{ Ms_m^{(3)}(\xi,\eta_s)\Big[-\tfrac{1}{2}\big((\cosh^2\xi+\tfrac{1}{4})+(\cosh^2\xi-\tfrac{1}{4})U_m\big)B_1^m(\eta_s)$$

$$+\tfrac{1}{8}(15+U_m)B_3^m(\eta_s)\Big] + \cosh\xi\sinh\xi\, B_1^m(\eta_s)\, Ms_m^{(3)'}(\xi,\eta_s)\Big\}$$

$$n=2 \sum_m E_m \Big\{ M_{sm}^{(3)}(\xi,\eta_s)\Big[-\tfrac{1}{2}(\cosh^2\xi-\tfrac{1}{2})(4+U_m)B_2^m(\eta_s)$$

$$+(3+\tfrac{1}{8}U_m)B_4^m(\eta_s)\Big] + \cosh\xi\sinh\xi\, B_2^m(\eta_s)\, Ms_m^{(3)'}(\xi,\eta_s)\Big\}$$

$$n\geq 3 \sum_m E_m \Big\{ Ms_m^{(3)}(\xi,\eta_s)\Big[-\tfrac{1}{4}\Big[(n-2)\Big(1-\tfrac{(n-2)}{2}\Big)-\tfrac{1}{2}U_m\Big]B_{n-2}^m(\eta_s)$$

$$-\tfrac{1}{2}(\cosh^2\xi-\tfrac{1}{2})(n^2+U_m)B_n^m(\eta_s) + \tfrac{1}{4}\Big[(n+2)\Big(\tfrac{(n+2)}{2}+1\Big)$$

$$+\tfrac{1}{2}U_m\Big]B_{n+2}^m(\eta_s)\Big] + \cosh\xi\sinh\xi\, B_n^m(\eta_s)\, Ms_m^{(3)'}(\xi,\eta_s)\Big\}$$

(AI.20)

To obtain the incident wave stress expressions, make the following

substitutions into the expressions for the reflected waves

$$B_m Mc_m^{(3)}(\xi,q_c) \to -2\pi ce_m(\eta_0,q_c) Mc_m^{(1)}(\xi,q_c) Mc_m^{(3)}(\xi_0,q_c)$$

$$C_m Ms_m^{(3)}(\xi,q_c) \to -2\pi se_m(\eta_0,q_c) Ms_m^{(1)}(\xi,q_c) Ms_m^{(3)}(\xi_0,q_c)$$

$$D_m Mc_m^{(3)}(\xi,q_s) \to -2\pi ce_m(\eta_0,q_s) Mc_m^{(1)}(\xi,q_s) Mc_m^{(3)}(\xi_0,q_s)$$

$$E_m Ms_m^{(3)}(\xi,q_s) \to -2\pi se_m(\eta_0,q_s) Ms_m^{(1)}(\xi,q_s) Ms_m^{(3)}(\xi_0,q_s) \qquad \text{(AI.21)}$$

To obtain the transmitted wave stress expressions, substitute

$$B_m A_n^m(q_c) Mc_m^{(3)}(\xi,q_c) \to F_m A_n^m(q_c') Mc_m^{(4)}(\xi,q_c')$$

$$C_m B_n^m(q_c) Ms_m^{(3)}(\xi,q_c) \to G_m B_n^m(q_c') Ms_m^{(4)}(\xi,q_c')$$

$$D_m A_n^m(q_s) Mc_m^{(3)}(\xi,q_s) \to H_m A_n^m(q_s') Mc_m^{(4)}(\xi,q_s')$$

$$E_m B_n^m(q_s) Ms_m^{(3)}(\xi,q_s) \to I_m B_n^m(q_s') Ms_m^{(4)}(\xi,q_s') \qquad \text{(AI.22)}$$

This completes the derivation of the stress boundary condition expressions. The displacement boundary condition expressions are more easily determined as follows. In terms of the partial potentials, the displacements are written

$$u_\xi^k \to \left[\sum_n \left({}^{e}\phi_n^{\prime k} + n\,{}^{o}\psi_n^{k}\right)\cos n\eta + \sum_n \left({}^{o}\phi_n^{\prime k} - n\,{}^{e}\psi_n^{k}\right)\sin n\eta\right]$$

$$u_\eta^k \to \left[\sum_n \left(n\,{}^{o}\phi_n^{k} - {}^{e}\psi_n^{\prime k}\right)\cos n\eta + \sum_n \left(n\,{}^{e}\phi_n^{k} + {}^{o}\psi_n^{\prime k}\right)\sin n\eta\right] \qquad \text{(AI.23)}$$

Using the orthogonality of the trigonometric functions and separating the $\phi$ and $\psi$ terms, the expressions for the reflected wave displacements are obtained.

$$
\begin{aligned}
{}^{e}_{\phi}U^{s}_{\xi} &\rightarrow \sum_m B_m A_n^m(\xi_c) M_{c_m}^{(3)\prime}(\xi,\xi_c) \\
{}^{e}_{\psi}U^{s}_{\xi} &\rightarrow \sum_m n E_m B_n^m(\xi_s) M_{s_m}^{(3)}(\xi,\xi_s) \\
{}^{o}_{\phi}U^{s}_{\xi} &\rightarrow \sum_m C_m B_n^m(\xi_c) M_{s_m}^{(3)\prime}(\xi,\xi_c) \\
{}^{o}_{\psi}U^{s}_{\xi} &\rightarrow \sum_m -n D_m A_n^m(\xi_s) M_{c_m}^{(3)}(\xi,\xi_s) \\
{}^{e}_{\phi}U^{s}_{\eta} &\rightarrow \sum_m n C_m B_n^m(\xi_c) M_{s_m}^{(3)}(\xi,\xi_c) \\
{}^{e}_{\psi}U^{s}_{\eta} &\rightarrow \sum_m -D_m A_n^m(\xi_s) M_{c_m}^{(3)\prime}(\xi,\xi_s) \\
{}^{o}_{\phi}U^{s}_{\eta} &\rightarrow \sum_m -n B_m A_n^m(\xi_c) M_{c_m}^{(3)}(\xi,\xi_c) \\
{}^{o}_{\psi}U^{s}_{\eta} &\rightarrow \sum_m -E_m B_n^m(\xi_s) M_{s_m}^{(3)\prime}(\xi,\xi_s)
\end{aligned}
$$

(AI.24)

The incident and transmitted wave displacement expressions are obtained by making the substitutions (AI.21) and (AI.22), respectively.

## REFERENCES

Ang, D. D. and L. Knopoff, "Diffraction of Scalar Elastic Waves by a Clamped Finite Strip," Proceedings of the National Academy of Sciences, Vol. 51, No. 3, March, 1964, pp. 471-476.

Barakat, Richard, "Diffraction of Plane Waves by an Elliptic Cylinder," Journal of the Acoustical Society of America, Vol. 35, No. 12, Dec., 1963, pp. 1990-1996.

Blanche, G. and D. S. Clemm, Tables Relating to the Radial Mathieu Functions, Vol. 1, Functions of the First Kind, Aeronautical Research Labs, U. S. Air Force.

Blanche, G. and D. S. Clemm, Tables Relating to the Radial Mathieu Functions, Vol. 2, Functions of the Second Kind, Aeronautical Research Labs, U. S. Air Force.

Brillouin, Leon, Tensors in Mechanics and Elasticity, Academic Press, New York, 1964, pp. 124-125.

Cheng, S. L., "Multiple Scattering of Elastic Waves by Parallel Cylinders," Journal of Applied Mechanics, Trans. ASME, 1969, pp. 523-527.

Cheng, S. L. and A. Jahanshahi, "On Dynamic Stress Concentrations Around a Discontinuity," Journal of Applied Mechanics, Trans. ASME, 1967, pp. 385-391.

Einspruch, N. G., E. J. Witterhold and Rohn Truell, "Scattering of a Plane Transverse Wave by a Spherical Obstacle in an Elastic Medium," Journal of Applied Physics, Vol. 31, No. 5, May, 1960, pp. 806-818.

Fung, Y. C., Foundations of Solid Mechanics, Prentice-Hall, Inc., Englewood Cliffs, N. J., 1965, pp. 154-155.

Goodier, J. N., "Concentration of Stress Around Spherical and Cylindrical Inclusions and Flaws," Journal of Applied Mechanics, Vol. 1, Trans. ASME, Vol. 55, 1933, pp. 39-44.

Green, A. E. and W. Zerna, Theoretical Elasticity, Oxford University Press, London, 1954, p. 149.

Harumi, K., "Scattering of Plane Waves by a Rigid Ribbon in a Solid," Journal of Applied Physics, Vol. 32, No. 8, Aug., 1961, pp. 1488-1497.

Harumi, K., "Scattering of Plane Waves by a Cavity Ribbon in a Solid," Journal of Applied Physics, Vol. 33, No. 12, Dec., 1961, pp. 3588-3593.

Ince, E. L., "Tables of the Elliptic Cylinder Functions," Proc. of the Royal Society Edinburgh, 1932.

Jeffreys, Harold, Cartesian Tensors, Cambridge University Press, 1963.

Kirsh, G., V. D. I., Vol. 42, 1898.

Knopoff, Leon, "Scattering of Compression Waves by Spherical Obstacles," Geophysics, Vol. XXIV, No. 1, Feb., 1959, pp. 30-39.

Knopoff, Leon, "Scattering of Shear Waves by Spherical Obstacles," Geophysics, Vol. XXIV, No. 2, April, 1959, pp. 209-219.

Kolosoff, G., Z. Math. Physik., Vol. 62, 1914.

Kolsky, H., Stress Waves in Solids, Dover Publications, New York, 1963, pp. v-vi, 14, 24-36.

Levy, Bertram R., "Diffraction by an Elliptic Cylinder," Journal of Mathematics and Mechanics, Vol. 9, 1960, p. 147.

Mainardi, P., C. Konove and E. G. Baker, A First Course in Mathematics, D. Van Nostrand Co., Inc., Princeton, 1961, p. 274.

McLachlan, N. W., Theory and Application of Mathieu Functions, Oxford University Press, London, 1951.

Miklowitz, J., "Scattering of a Plane Elastic Compressional Pulse by a Cylindrical Cavity," Proc. of the Eleventh International Congress of Applied Mechanics.

Miller, Kenneth S., Partial Differential Equations in Engineering Problems, Prentice-Hall, Inc., Englewood Cliffs, N. J., 1964, pp. 180-182.

Morse, P. M. and H. Feshbach, Methods of Theoretical Physics, McGraw-Hill Book Co., Inc., New York, 1953, Vol. II, pp. 1421-1422.

Morse, P. M. and P. J. Rubenstein, "The Diffraction of Waves by Ribbons and by Slits," Physical Review, Vol. 54, 1938, pp. 895-898.

Mow, C. C. and W. L. McCabe, "Dynamic Stresses in an Elastic Cylinder," Journal of the Engineering Mechanics Division, ASCE, Vol. 89, No. EM-3, 1963, pp. 21-41.

Mow, C. C. and L. J. Mente, "Dynamic Stresses and Displacements Around Cylindrical Discontinuities due to Plane Harmonic Shear Waves," Journal of Applied Mechanics, Vol. 30, Trans. ASME, Vol. 85, Series E, 1963, pp. 598-604.

Mow, C. C. and J. W. Workman, "Dynamic Stresses Around a Fluid-Filled Cavity," Journal of Applied Mechanics, Trans. ASME, 1966, pp. 793-799.

National Bureau of Standards, Tables Relating to the Mathieu Functions, Columbia University Press, New York, 1951.

Neuber, H., Theory of Notch Stresses, Springer-Verlag, Berlin, 1958.

Pao, Y. H., "Dynamical Stress Concentration in an Elastic Plate," Journal of Applied Mechanics, Trans. ASME, June, 1962, pp. 299-305.

Pao, Y. H. and C. C. Mow, "Dynamic Stress Concentration in an Elastic Plate with Rigid Circular Inclusion," Proc. of the Fourth U. S. National Congress of Applied Mechanics, ASME, 1962, pp. 335-344.

Sih, G. C., "Singular Solution Near a Rigid Ribbon Excited by Plane Waves," Journal of the Franklin Institute, Vol. 286, No. 2, Aug., 1968, pp. 152-157.

Southwill, R. V. and H. J. Gough, Philosophical Magazine, Jan., 1926, p. 71.

Sternberg, E. and M. Sadowsky, Journal of Applied Mechanics, Trans. ASME, Vol. 16, 1949, p. 149.

Stratton, Morse, Chu and Hutner, Elliptic Cylinder and Spheriodal Wave Functions, Wiley, New York, 1941.

Thau, S. A., "Diffraction of Elastic Waves by a Parabolic Cylinder and Dynamic Stress Concentrations," Ph.D. Thesis, Cornell University, 1966.

Thau, S. A. and Y. H. Pao, "Diffraction of Horizontal Shear Waves by a Parabolic Cylinder and Dynamic Stress Concentrations," Journal of Applied Mechanics, Trans. ASME, 1966, pp. 785-792.

Timoshenko, S. and J. N. Goodier, Theory of Elasticity, McGraw-Hill Book Co., Inc., New York, 1951, pp. 78-81, 201-203, 359.

White, R. M., "Elastic Wave Scattering at a Cylindrical Discontinuity in a Solid," Journal of the Acoustical Society of America, Vol. 30, 1958, pp. 771-785.

Yeh, Cavour, "The Diffraction of Waves by a Penetrable Ribbon," Journal of Mathematical Physics, Vol. 4, No. 1, Jan., 1963, pp. 65-71.

Ying, C. F. and Rohn Truell, "Scattering of a Plane Longitudinal Wave by a Spherical Obstacle in an Isotropically Elastic Solid," Journal of Applied Physics, Vol. 27, No. 9, Sept., 1956, pp. 1086-1097.

# VITA

The author was born in , on . He received the B.S. in Mechanical Engineering (Cum Laude) from Newark College of Engineering in June, 1966, and the M.S. in Mechanical and Aerospace Sciences from the University of Rochester in June, 1967.

From September, 1967, to September, 1970, the author pursued doctoral studies at Newark College of Engineering in the Mechanical Engineering Department. During these years he held an N.C.E. Graduate Assistantship (1967-1969) and an N.D.E.A. Graduate Fellowship (1969-1970). The author is a member of Pi Tau Sigma and Tau Beta Pi honor societies and is an associate member of A.S.M.E.

The computational work carried out in the course of research was performed at the Courant Institute of Mathematical Sciences and at Newark College of Engineering.

The author will begin employment as a Member of Technical Staff at Bell Telephone Laboratories at Whippany, New Jersey, in September, 1970.

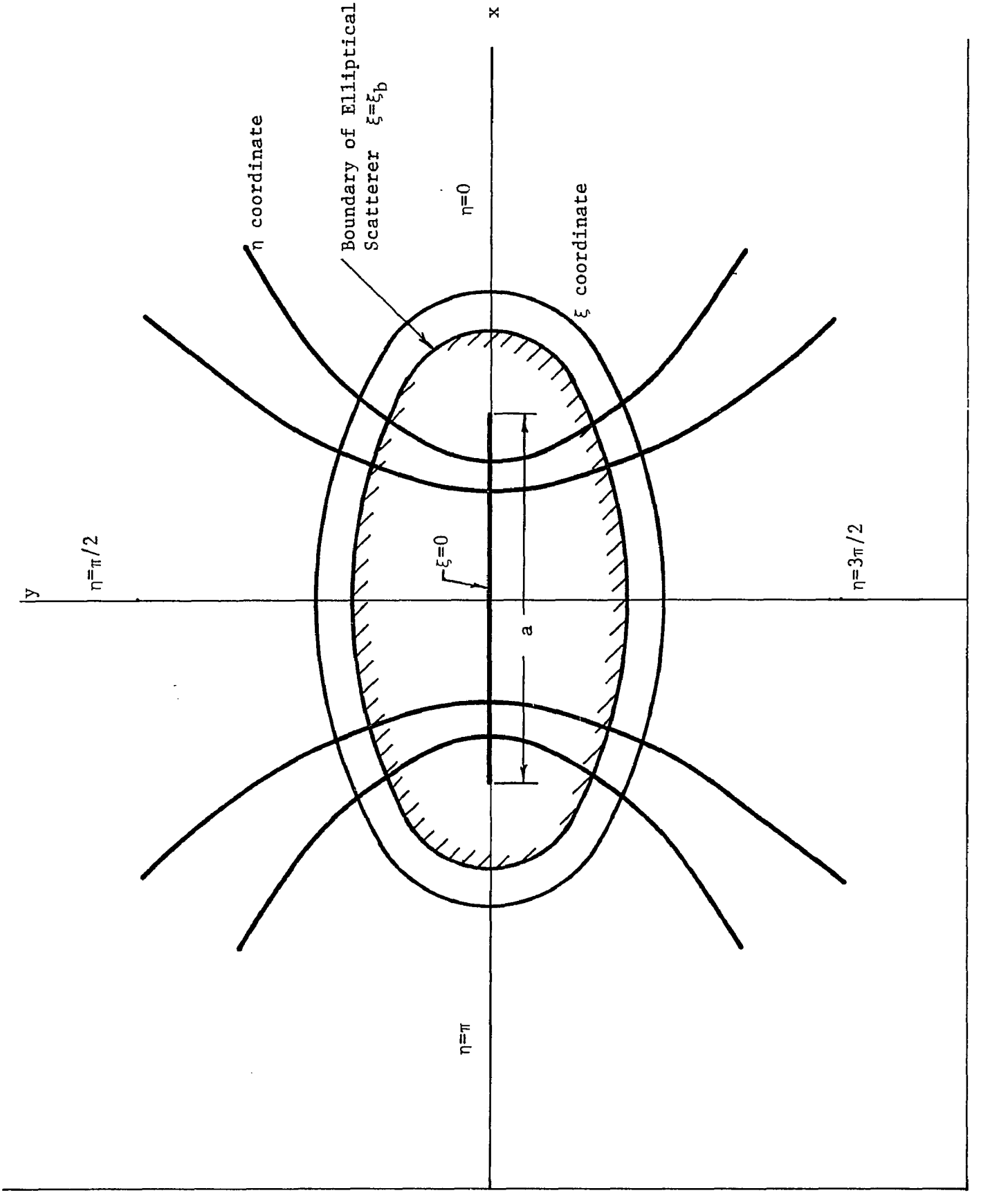


Fig. 1 Transverse Section of Elliptical Scatterer and Elliptical Coordinate System

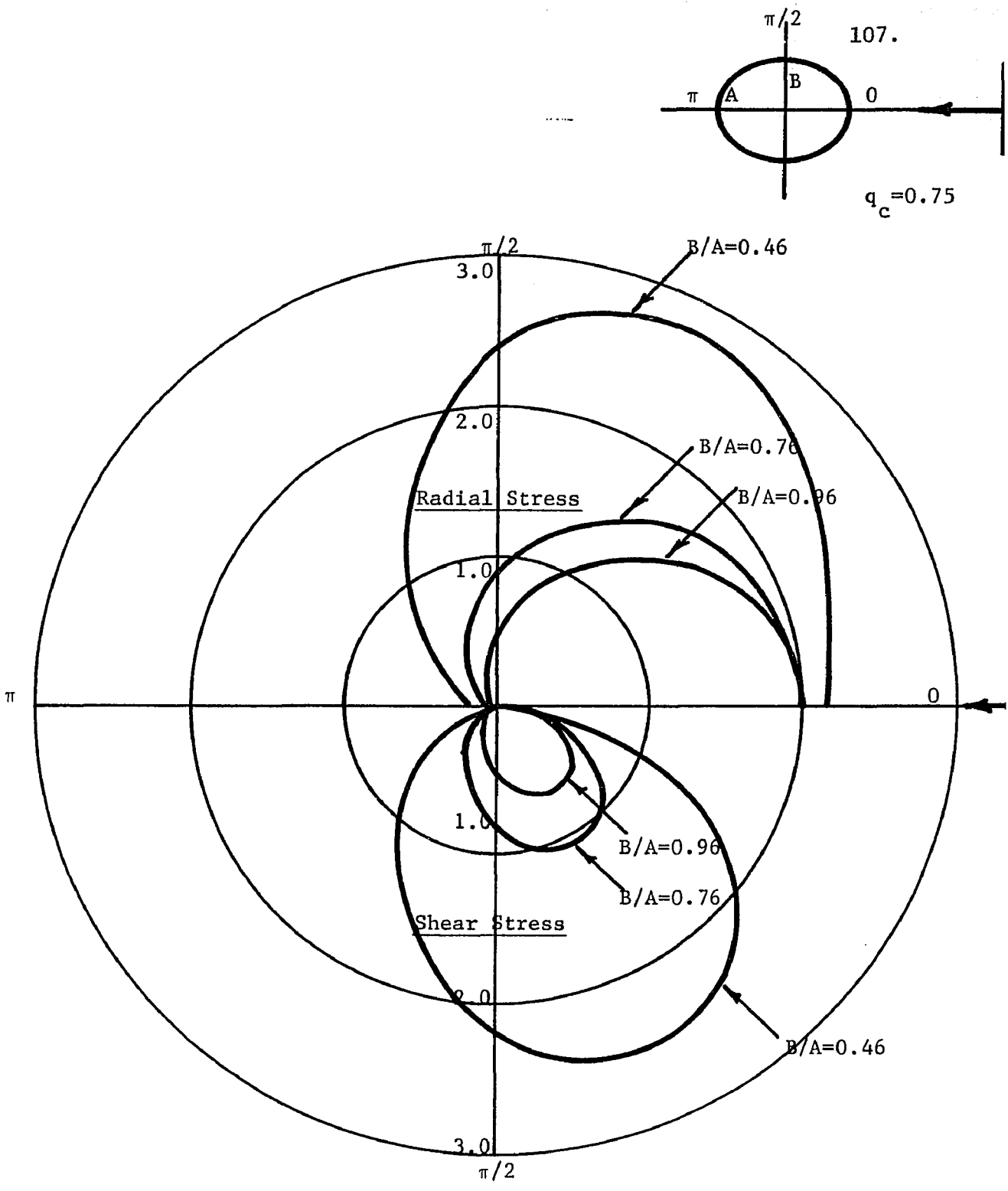


Fig. 2 Distribution of Normalized Stress vs. Ellipse Eccentricity for Incident Plane P-Wave on Major Axis of Rigid Cylinder.

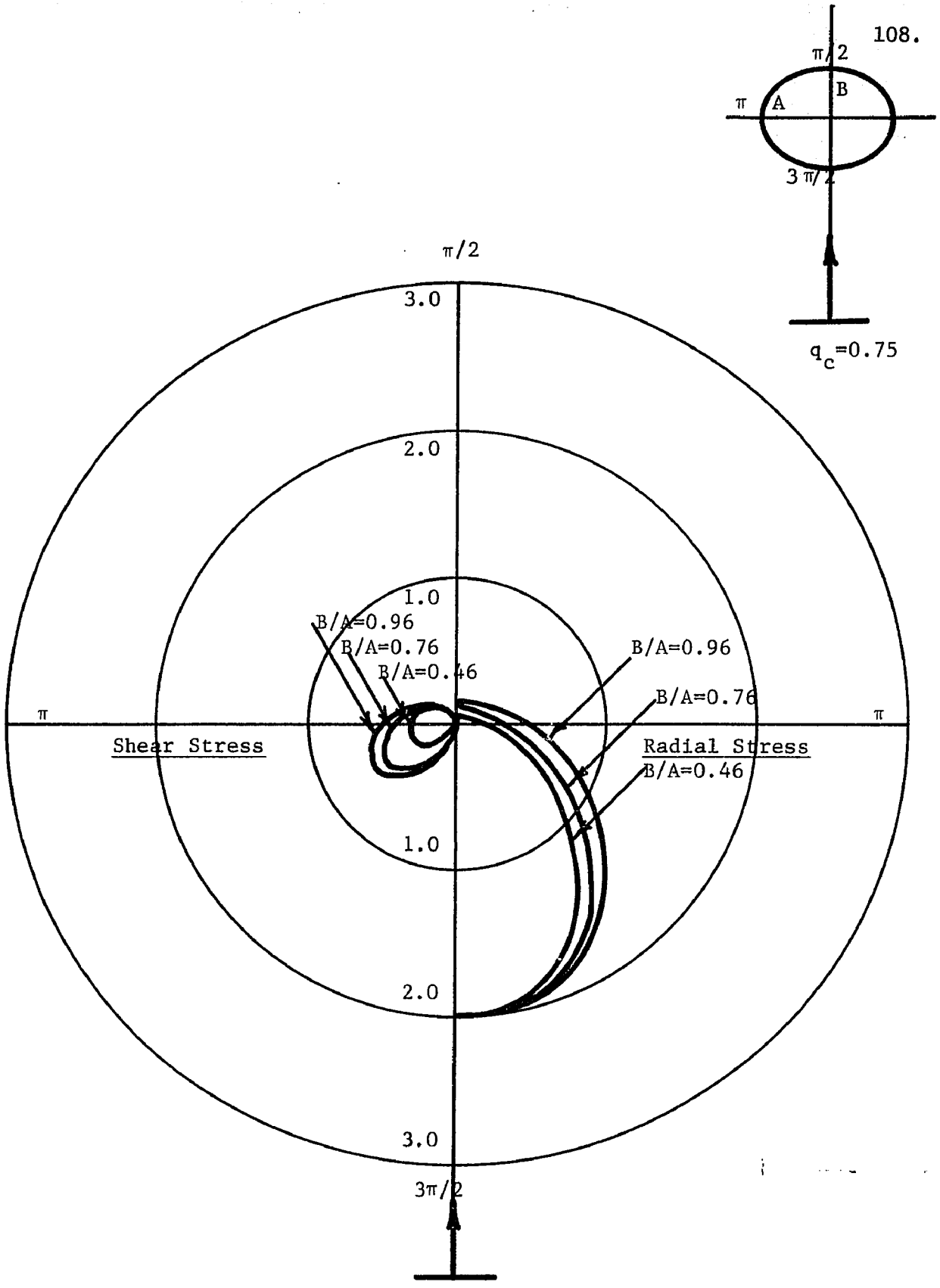


Fig. 3 Distribution of Normalized Stress vs. Ellipse Eccentricity for Incident Plane P-Wave on Minor Axis of Rigid Cylinder.

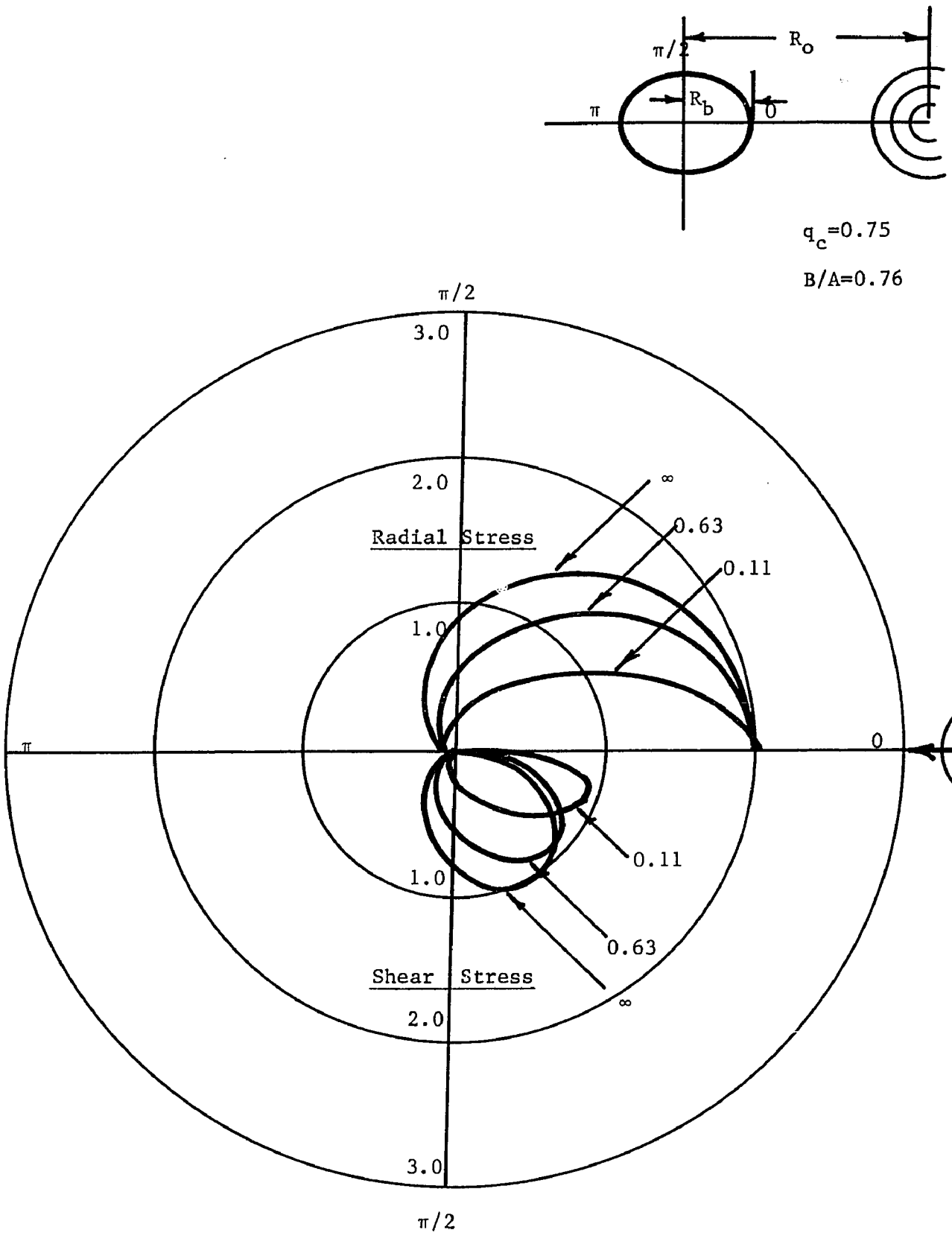


Fig. 4 Distribution of Normalized Stress on Boundary of Rigid Elliptical Cylinder vs. Normalized Source Location $(R_o-R_b)/\lambda$ of Incident P-Wave on Major Axis.

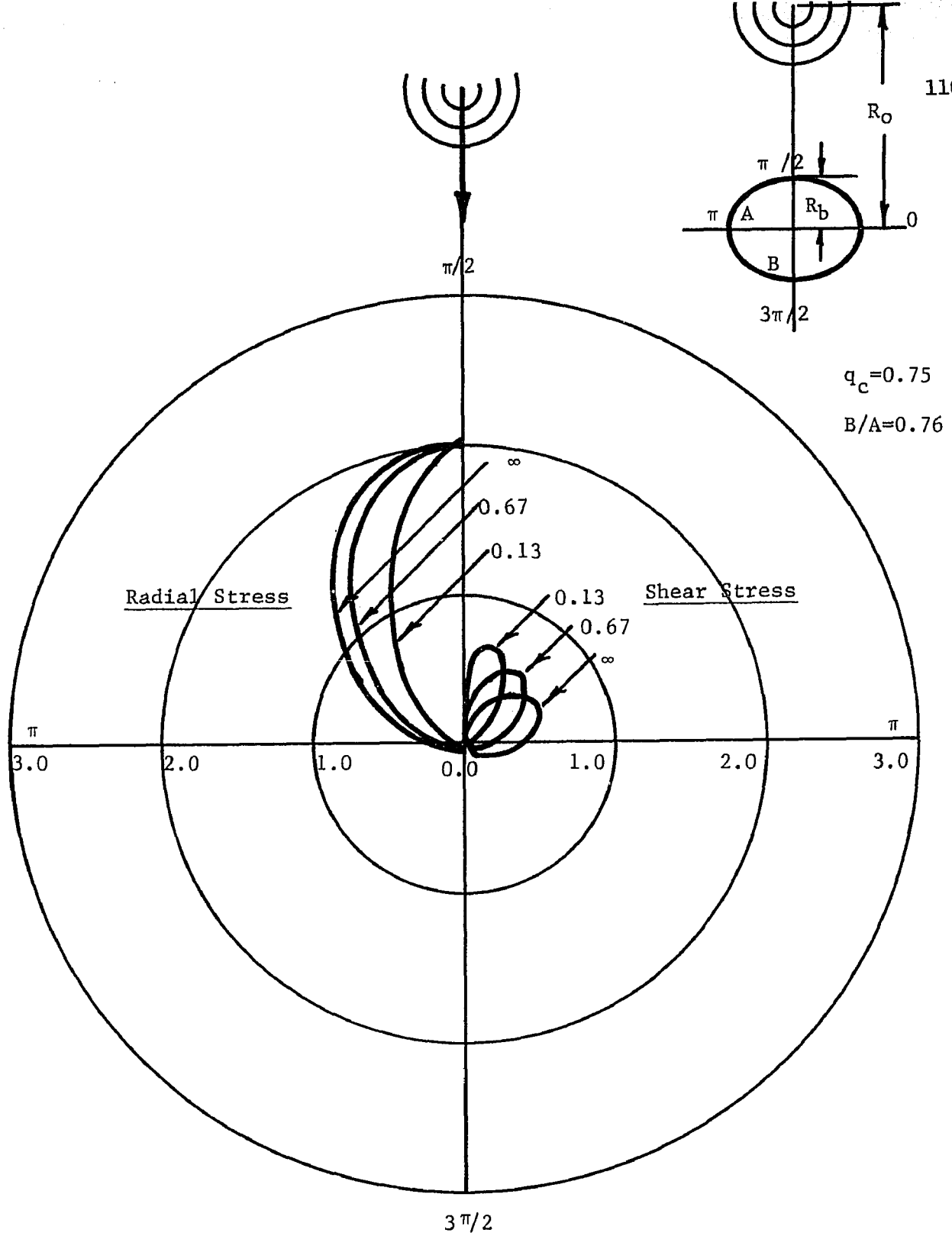


Fig. 5 Distribution of Normalized Stress on Boundary of Rigid Elliptical Cylinder vs. Normalized Source Location $(R_o-R_b)/\lambda$ of Incident P-Wave on Minor Axis.

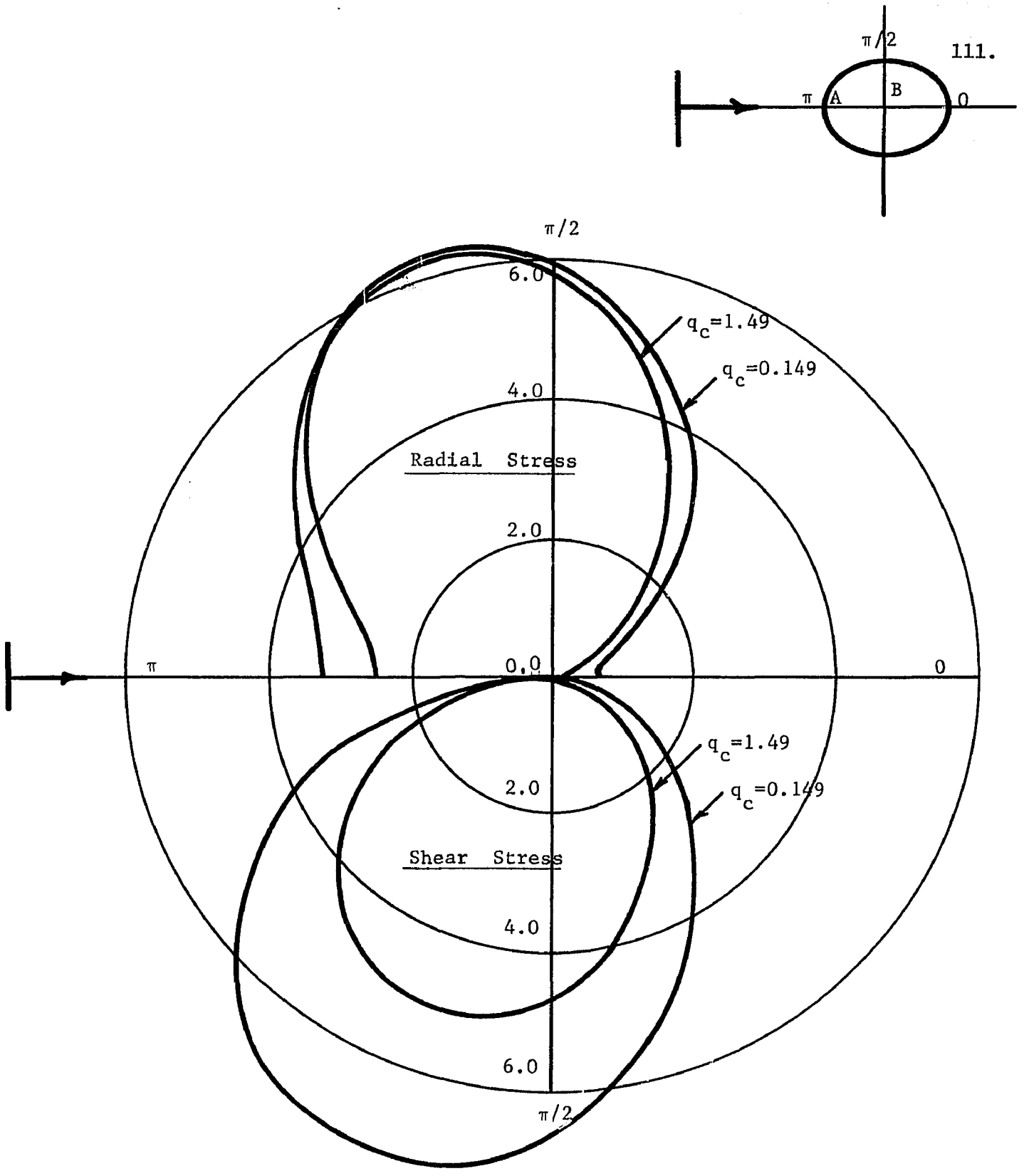


Fig. 6 Normalized stress on boundary of rigid immovable inclusion for incident plane P-wave on major axis and B/A=0.29.

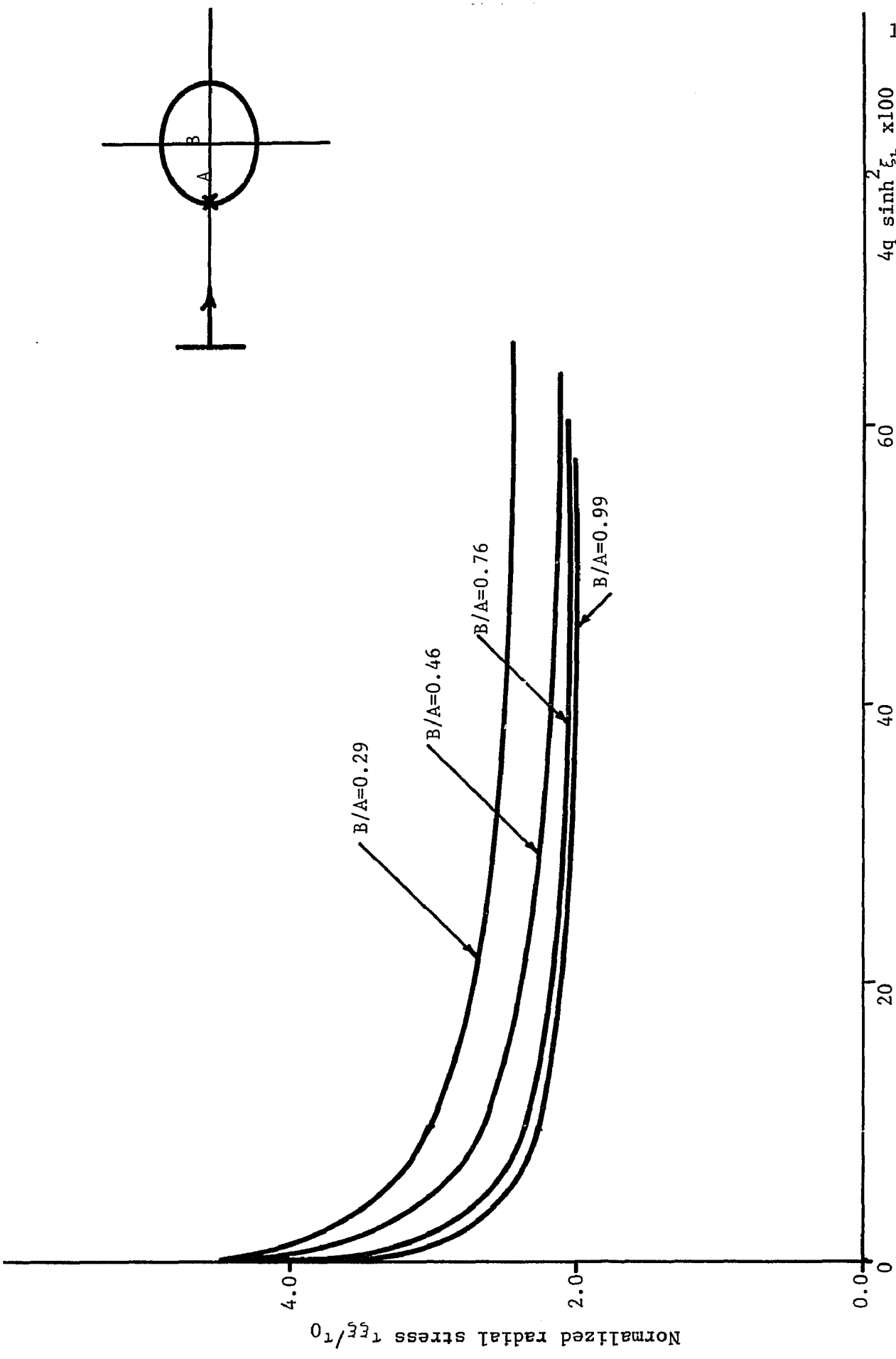


Fig. 7 Normalized radial stress at front of rigid inclusion with incident plane P-wave on major axis versus $4q_c \sinh^2 \xi_b$.

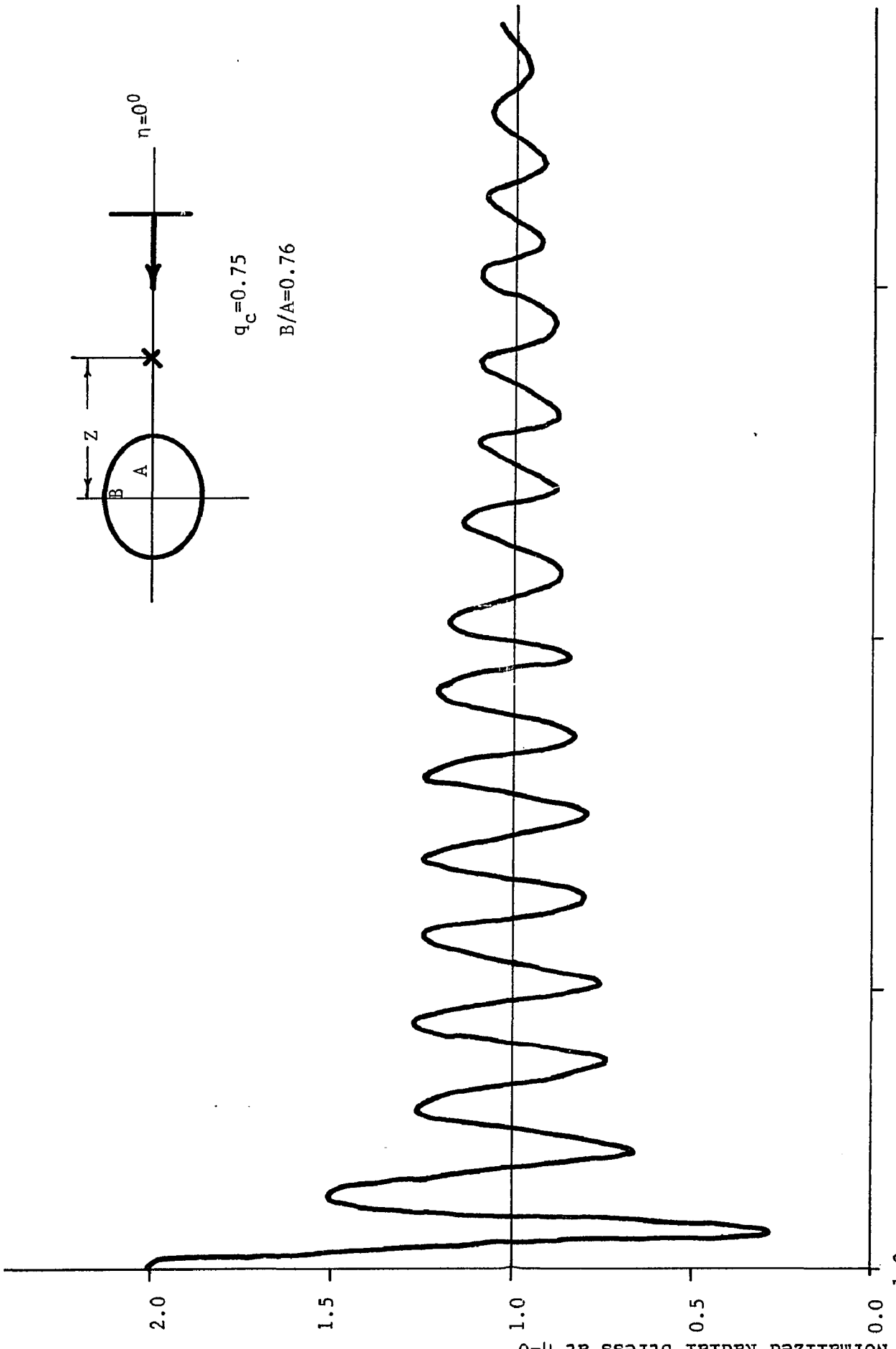


Fig 8 Normalized Distance From Boundary of Rigid Elliptical Scatterer (Z/A)

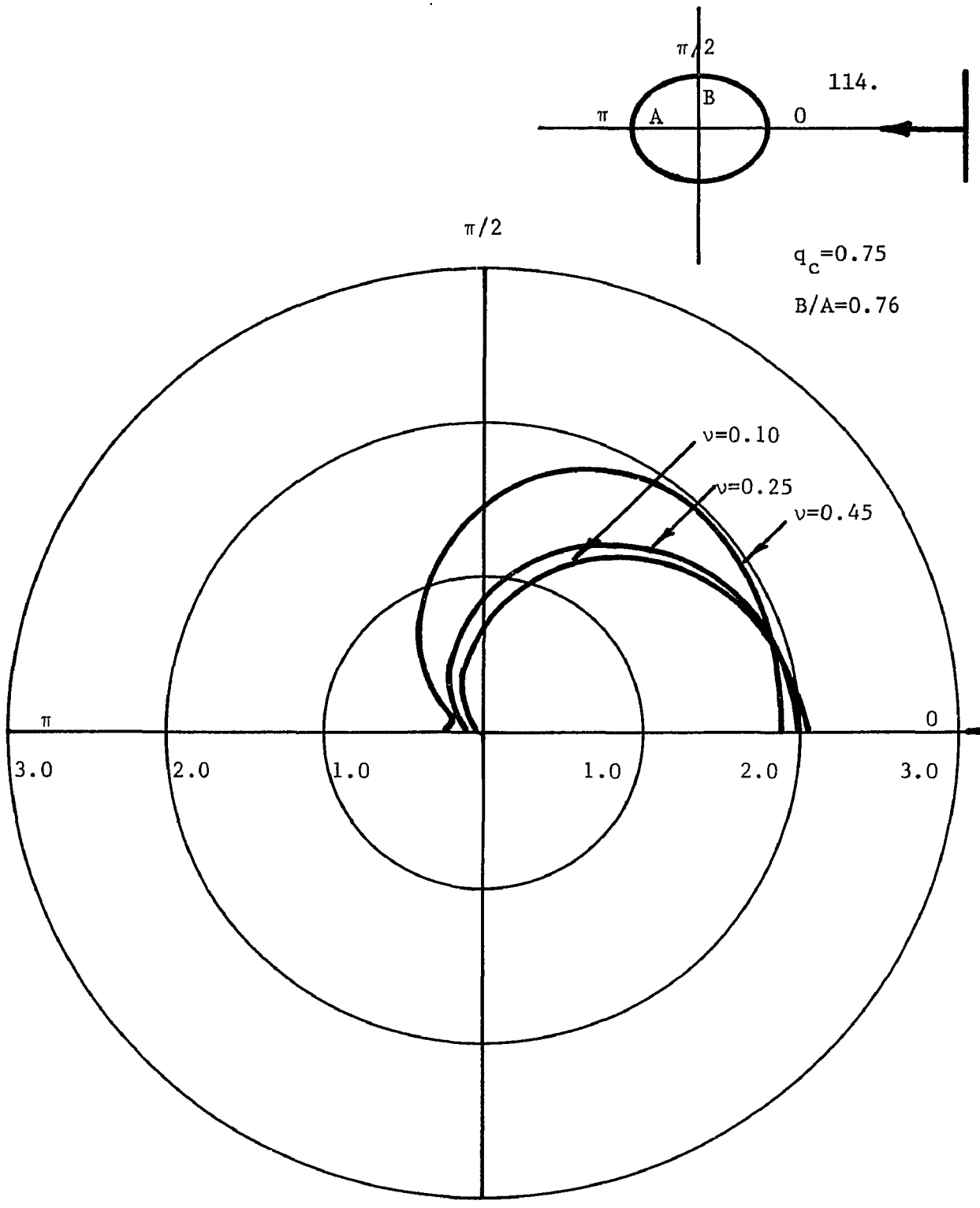


Fig. 9 Distribution of Normalized Radial Stress on Rigid Inclusion vs. Poisson's Ratio for an Incident Plane P-Wave on the Major Axis.

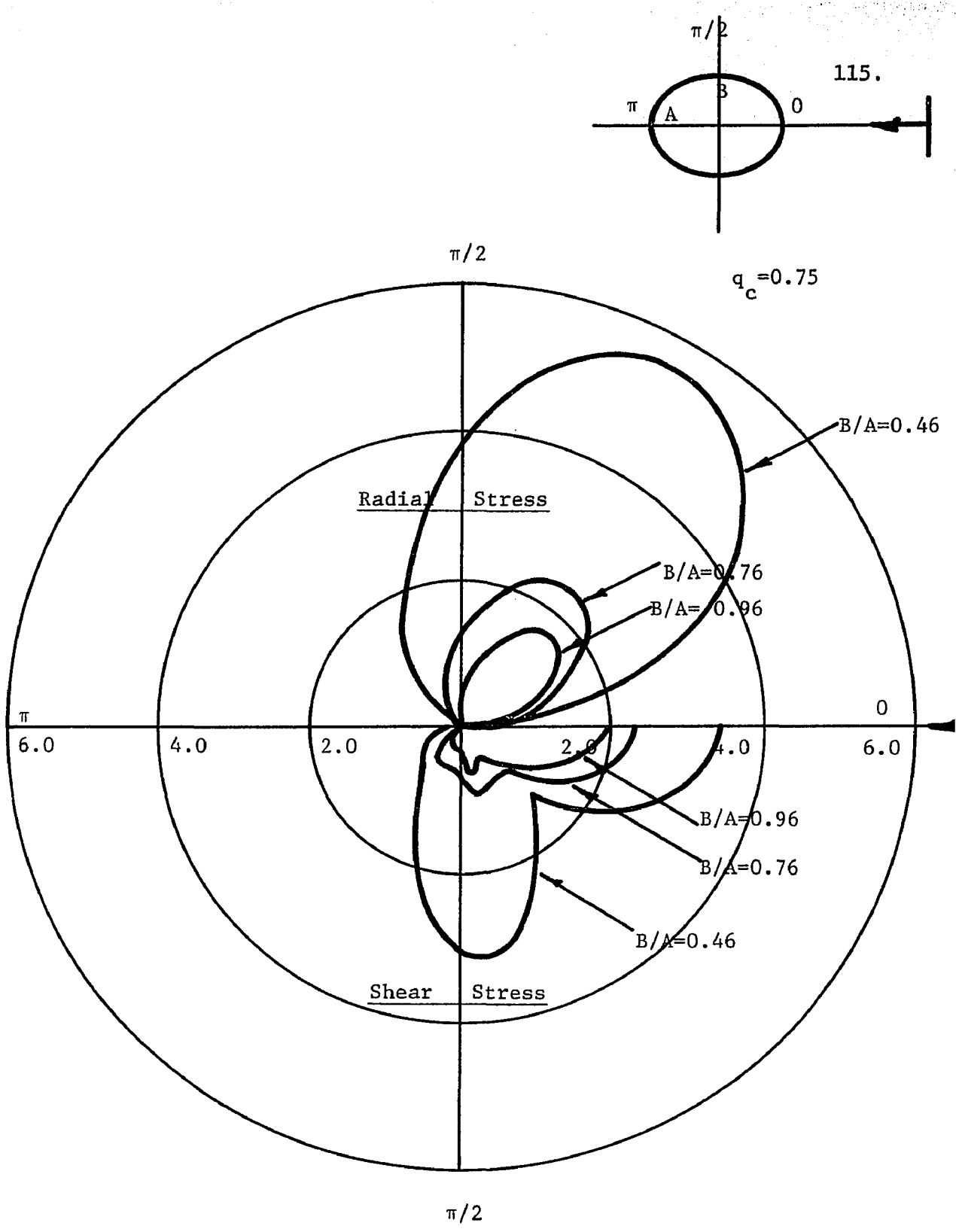


Fig. 10 Distribution of Normalized Stress vs. Ellipse Eccentricity for Incident Plane SV-Wave on Major Axis of Rigid Cylinder.

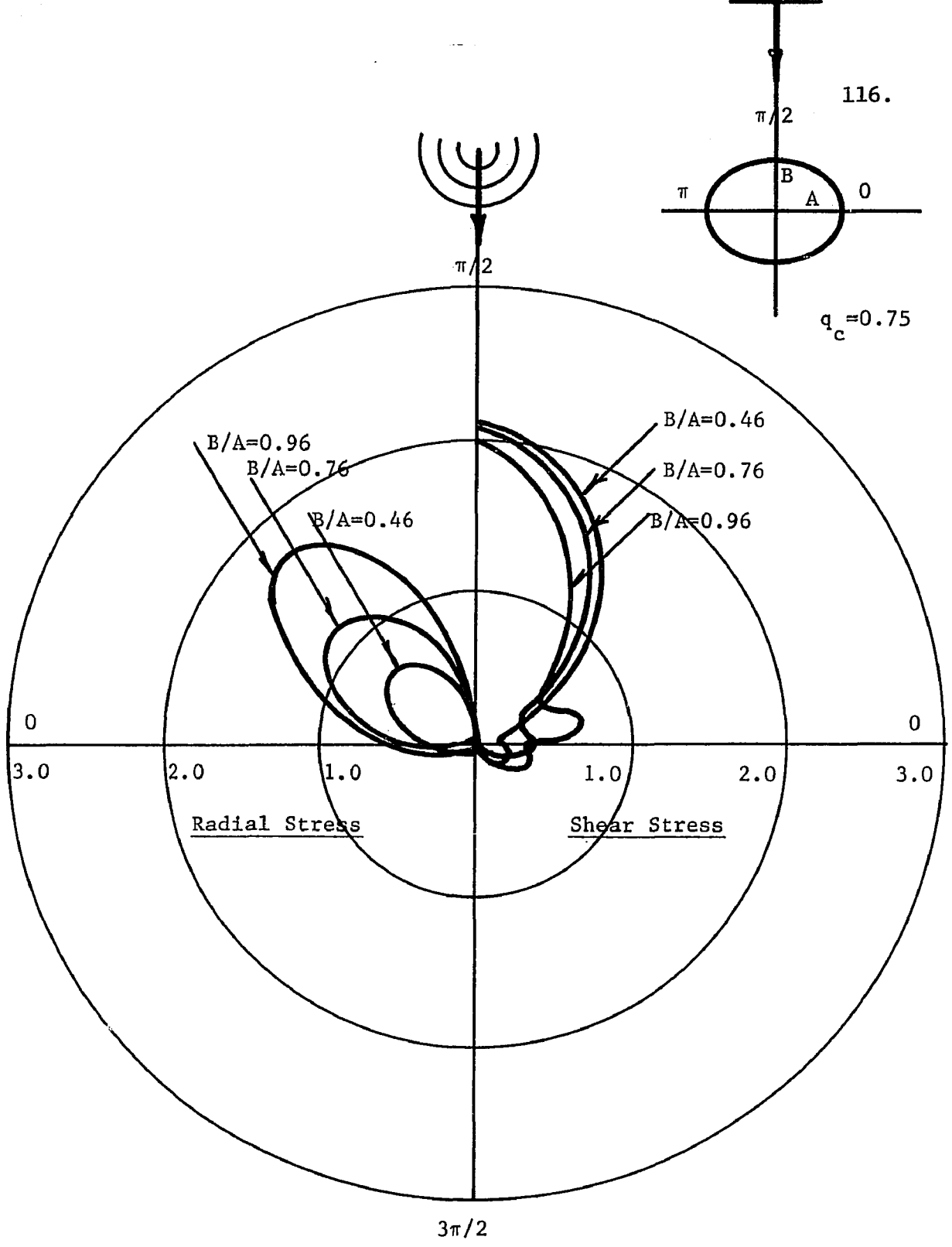


Fig.11 Distribution of Normalized Stress vs. Ellipse Eccentricity for Incident Plane SV-Wave on Minor Axis of Rigid Cylinder.

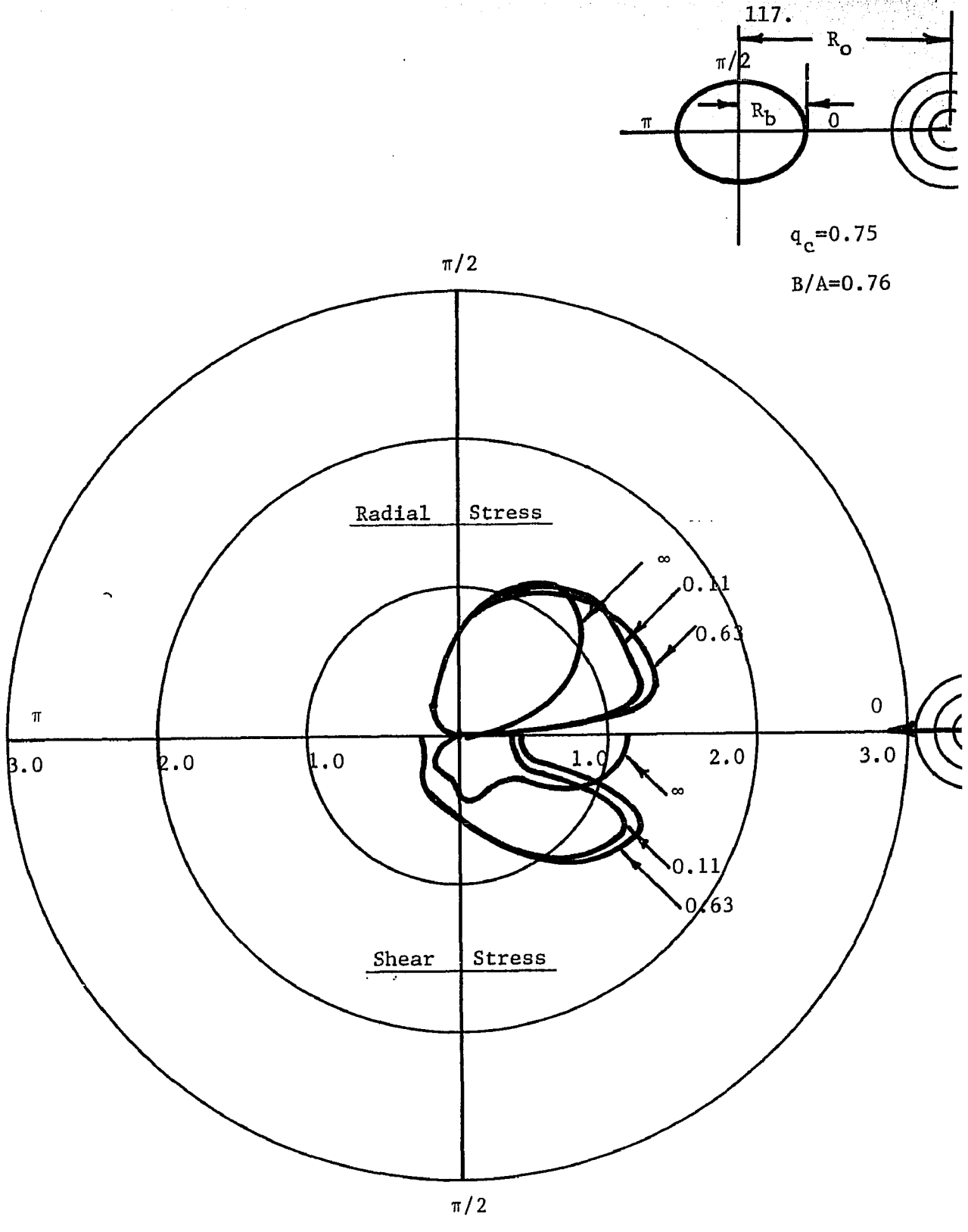


Fig.12 Distribution of Normalized Stress on Rigid Elliptical Cylinder vs. Normalized Source Location $(R_o-R_b)/\lambda$ of Incident SV-Wave on Major Axis.

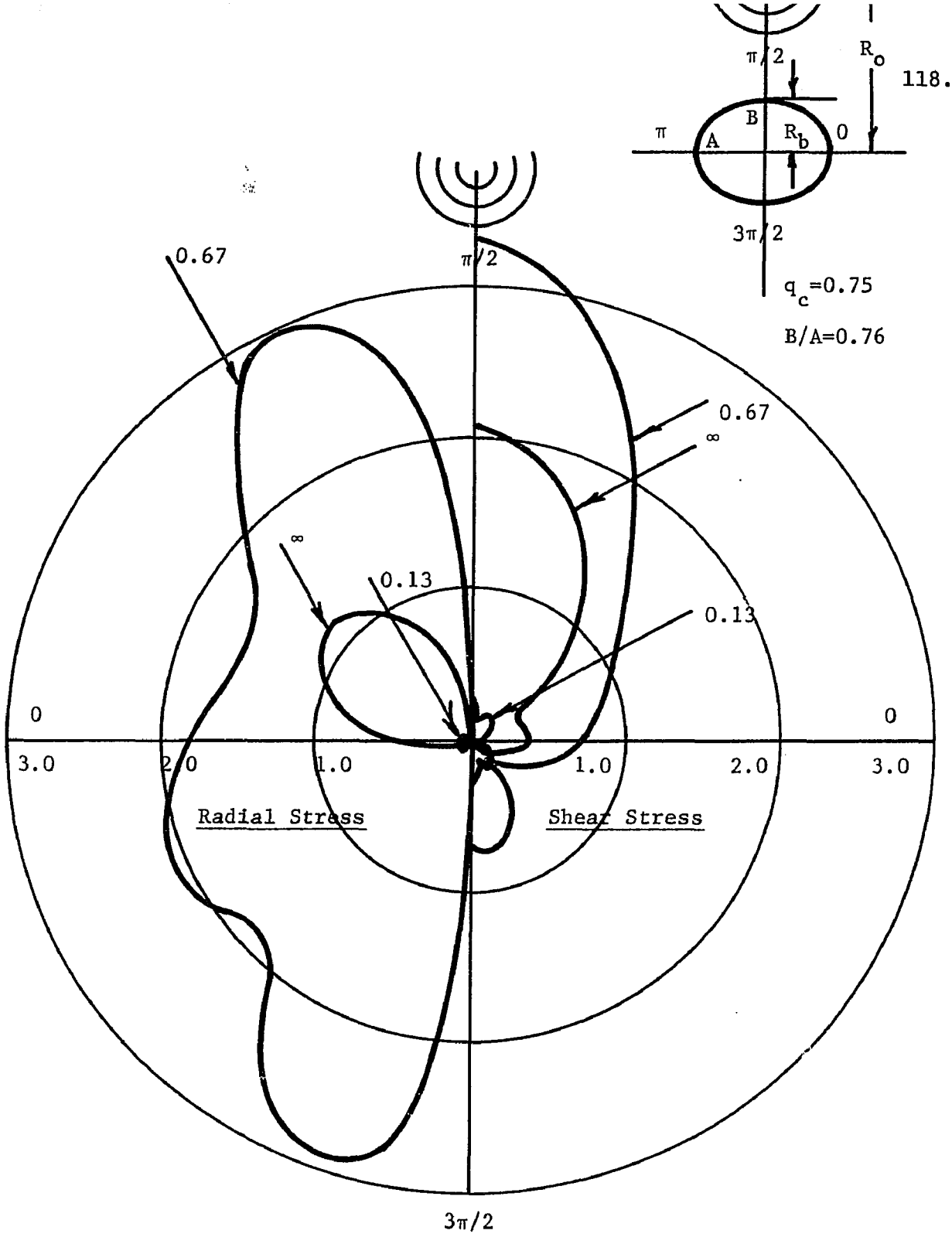


Fig.13 Distribution of Normalized Stress on Rigid Elliptical Cylinder vs. Normalized Source Location $(R_o-R_b)/\lambda$ of Incident SV-Wave on Minor Axis.

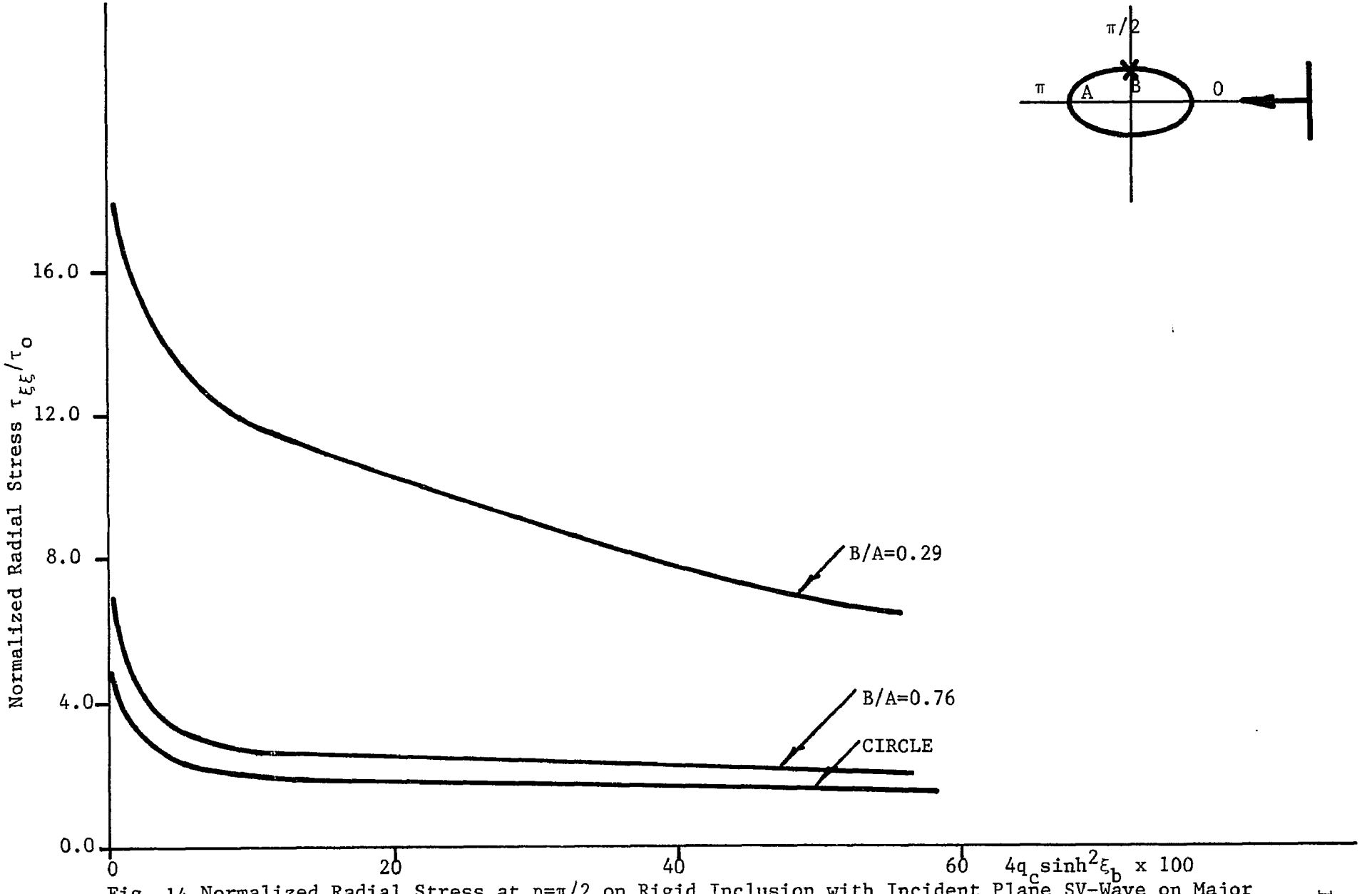


Fig. 14 Normalized Radial Stress at $\eta=\pi/2$ on Rigid Inclusion with Incident Plane SV-Wave on Major Axis vs. $4q_c \sinh^2 \xi_b$.

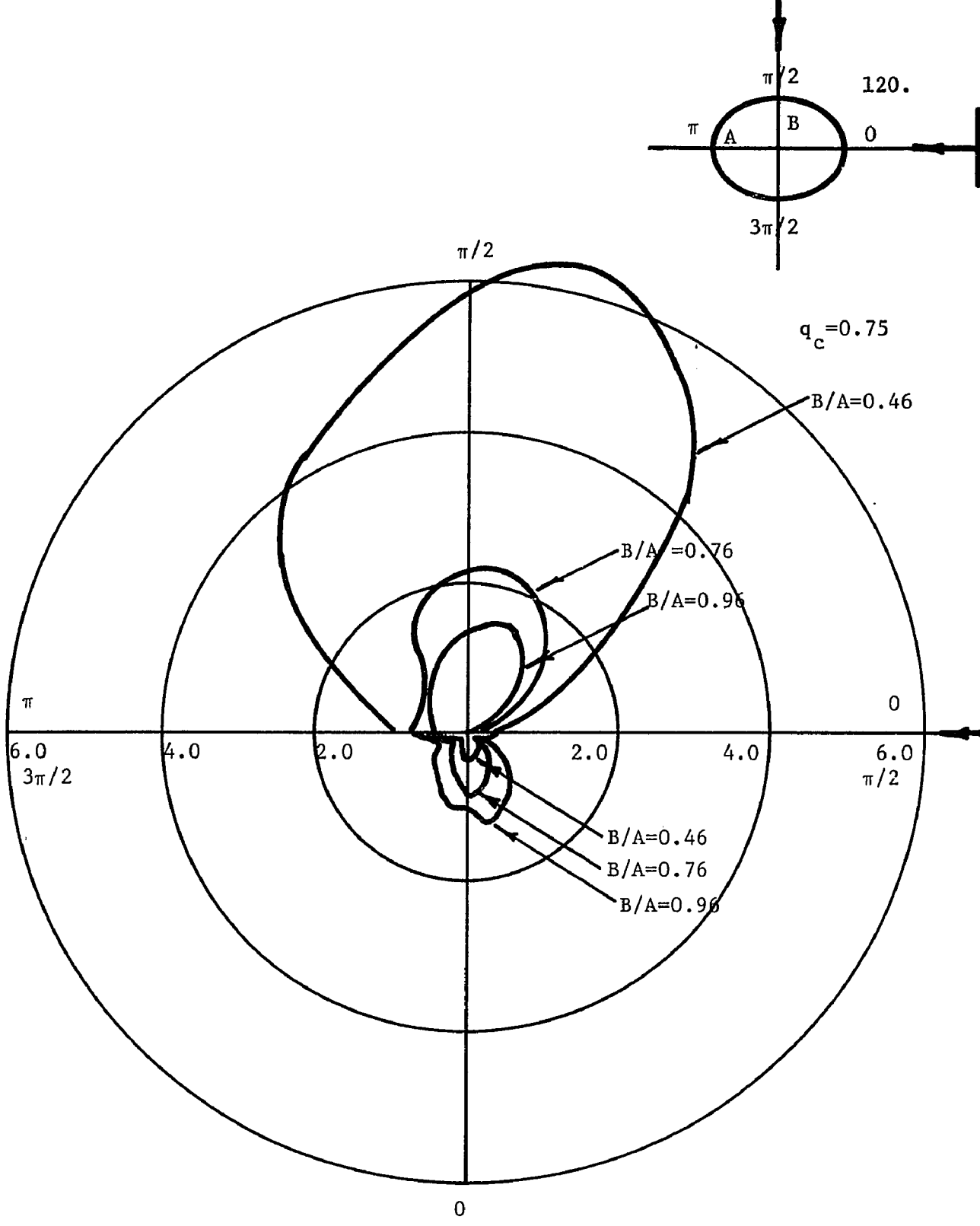


Fig. 15 Distribution of Normalized Hoop Stress vs. Ellipse Eccentricity for Incident Plane P-Wave on Major Axis (upper plot) and Minor Axis (lower plot) of Cavity.

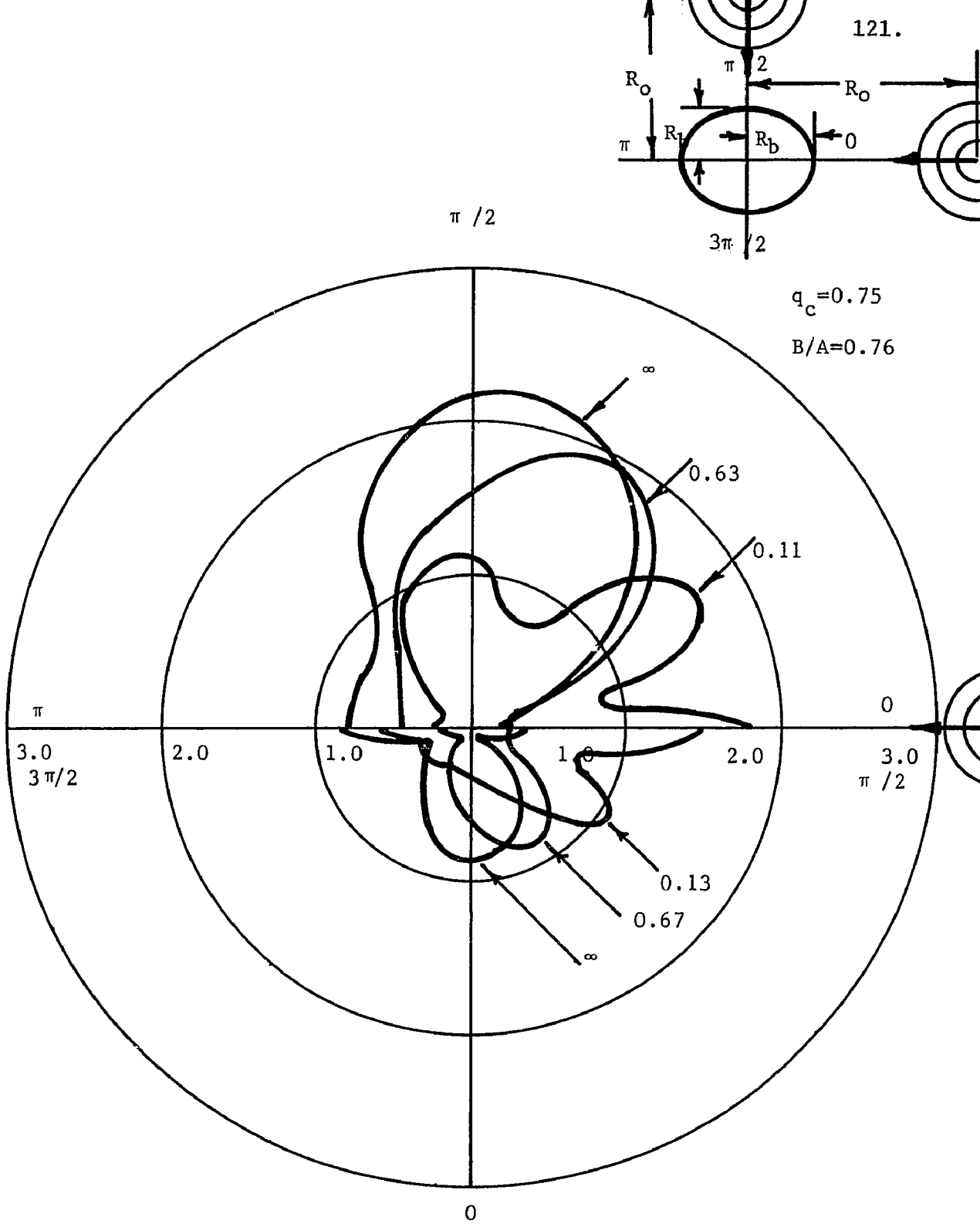


Fig. 16 Distribution of Normalized Hoop Stress vs. Normalized Source Location $(R_o-R_b)/\lambda$ of Incident P-Wave on Major Axis (upper plot) and Minor Axis (lower plot) of Cavity.

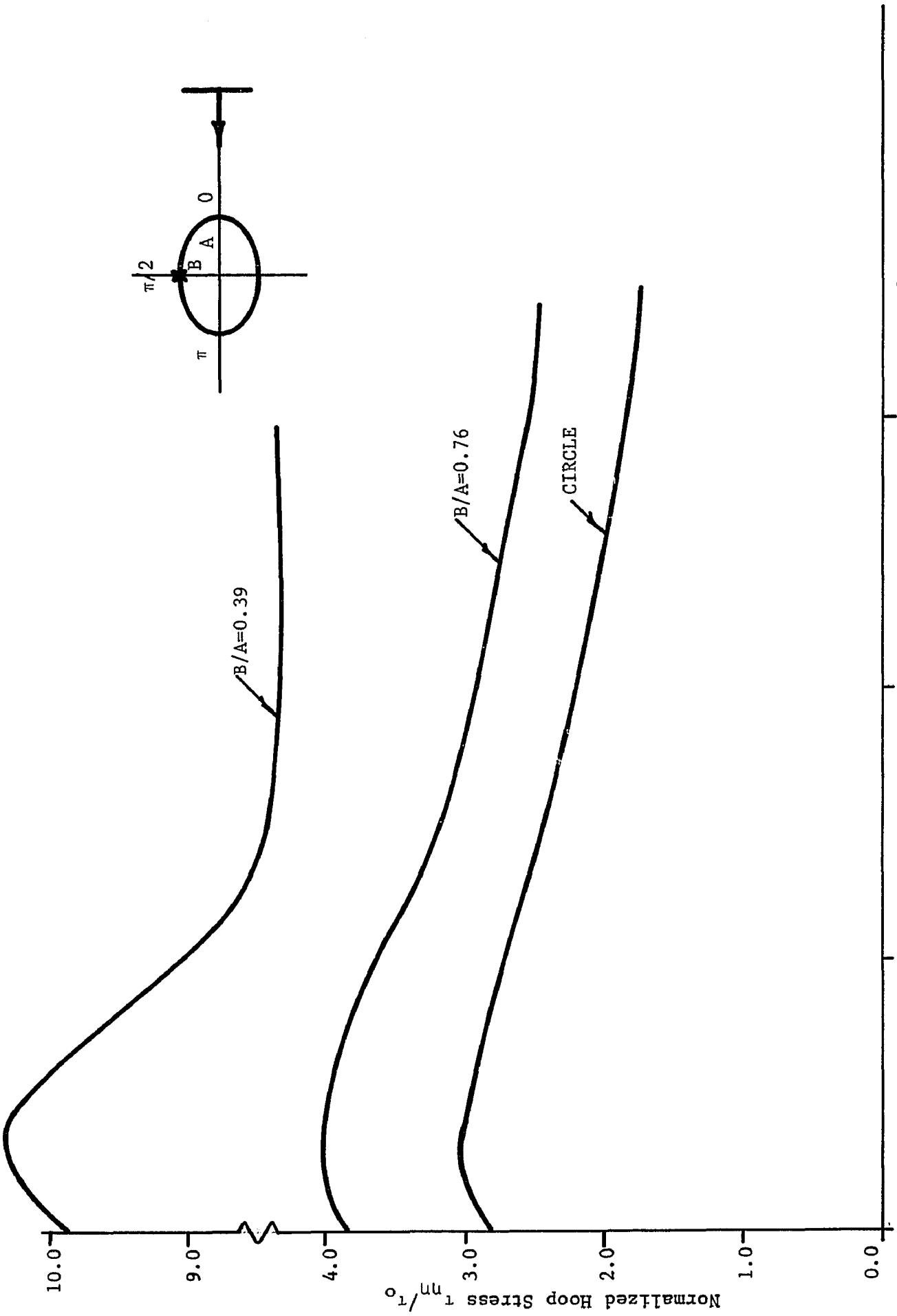


Fig. 17 Normalized Hoop Stress at $\eta=\pi/2$ on Cavity with Incident Plane P-Wave on Major Axis vs. $4q_c \sinh^2 \xi_b$.

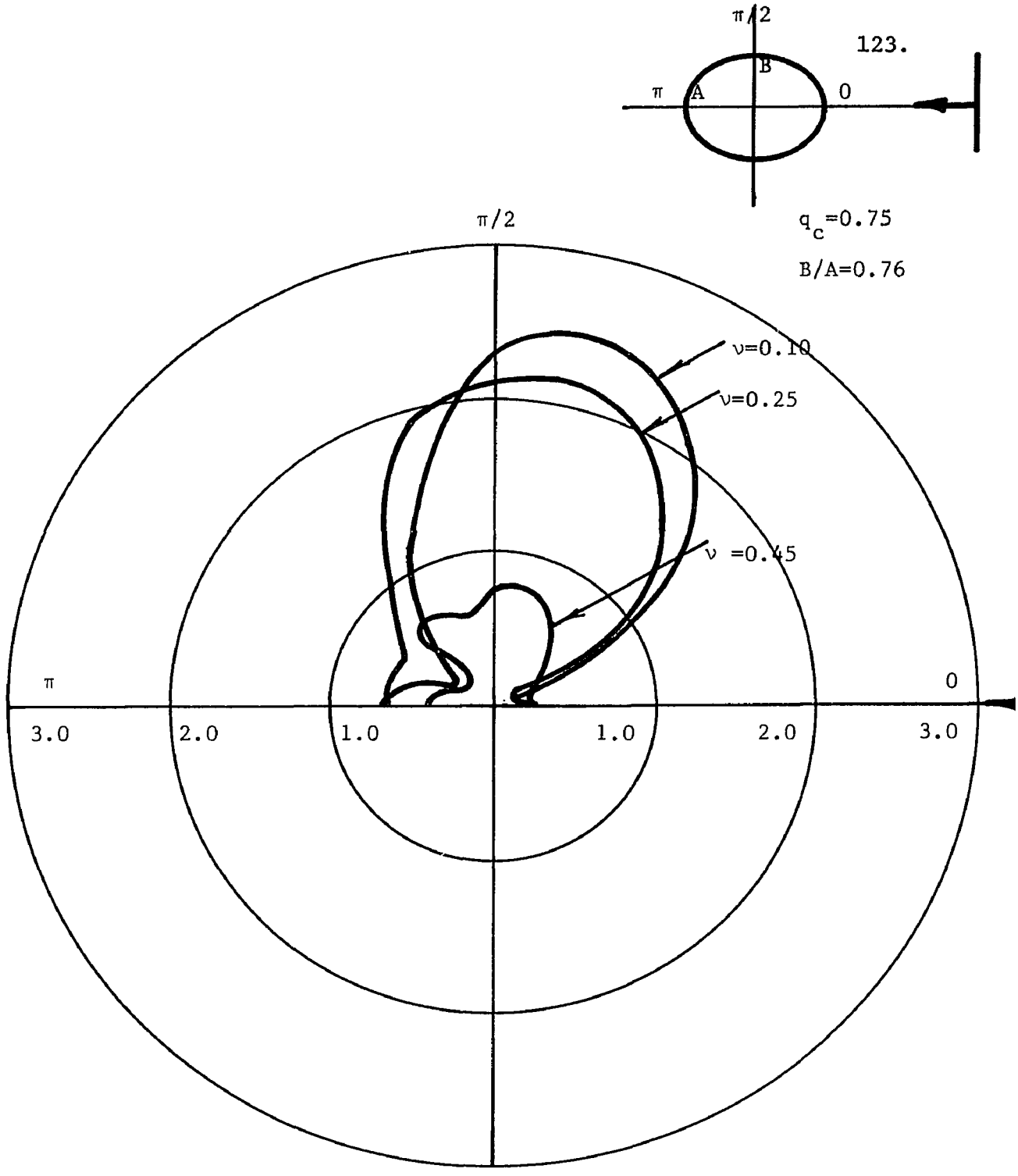


Fig. 18 Distribution of Normalized Hoop Stress on Cavity vs. Poisson's Ratio ν for an Incident Plane P-Wave on the Major Axis.

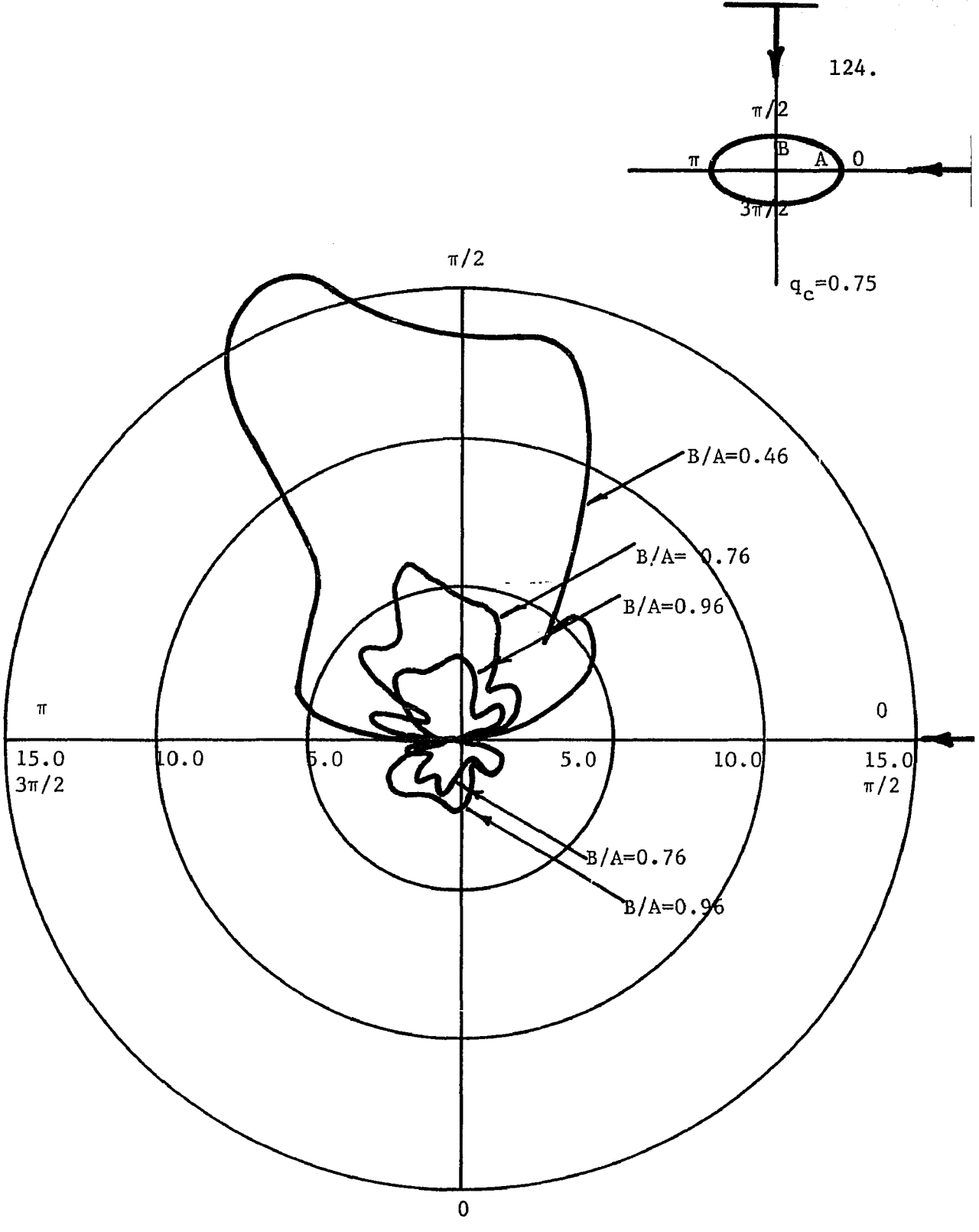


Fig. 19 Distribution of Normalized Hoop Stress vs. Ellipse Eccentricity for Incident Plane SV-Wave on Major Axis (upper plot) and Minor Axis (lower plot) of Cavity.

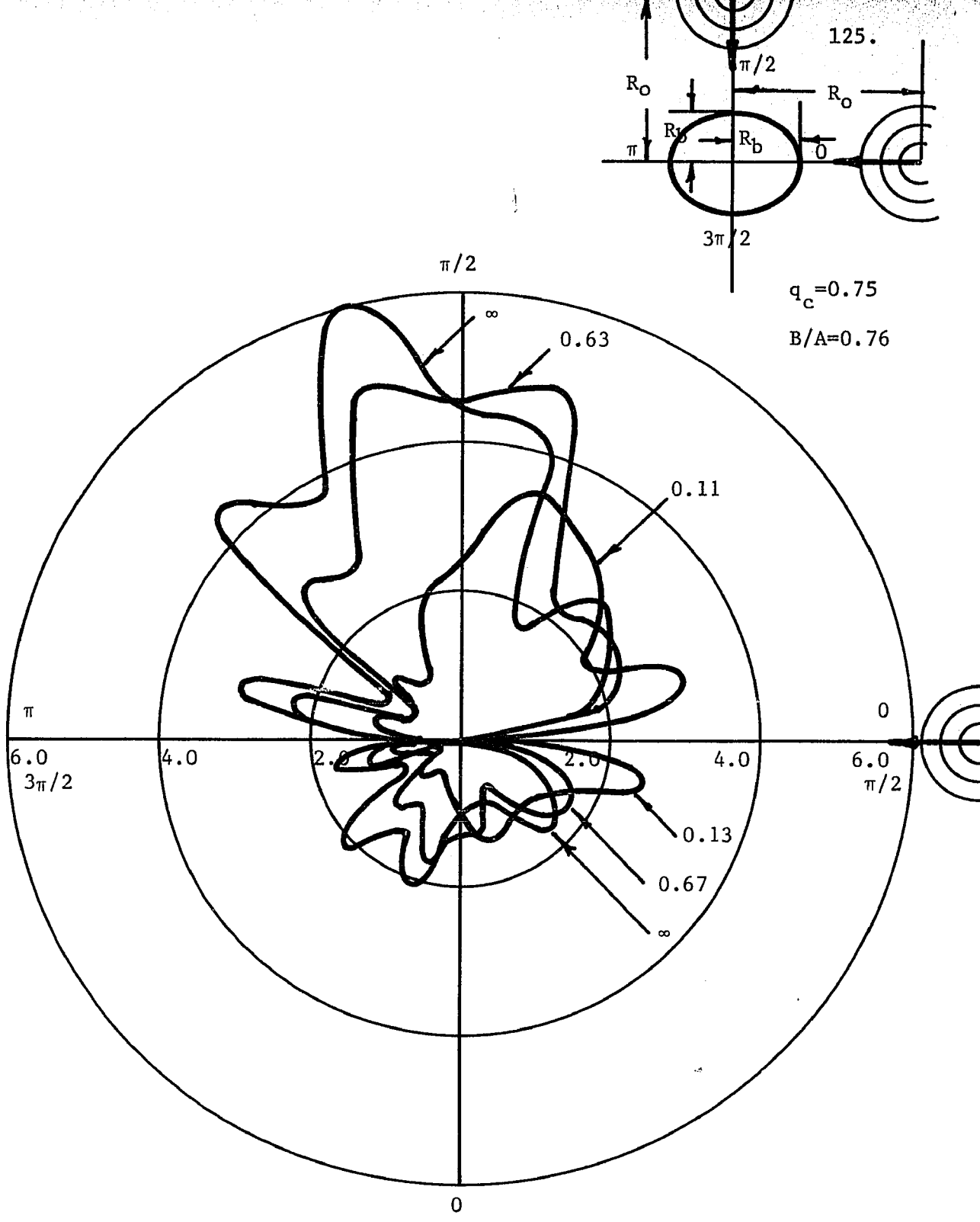


Fig. 20 Distribution of Normalized Hoop Stress vs. Normalized Source Location $(R_o-R_b)/\lambda$ of Incident SV-Wave on Major Axis (upper plot) and Minor Axis (lower plot) of Cavity.

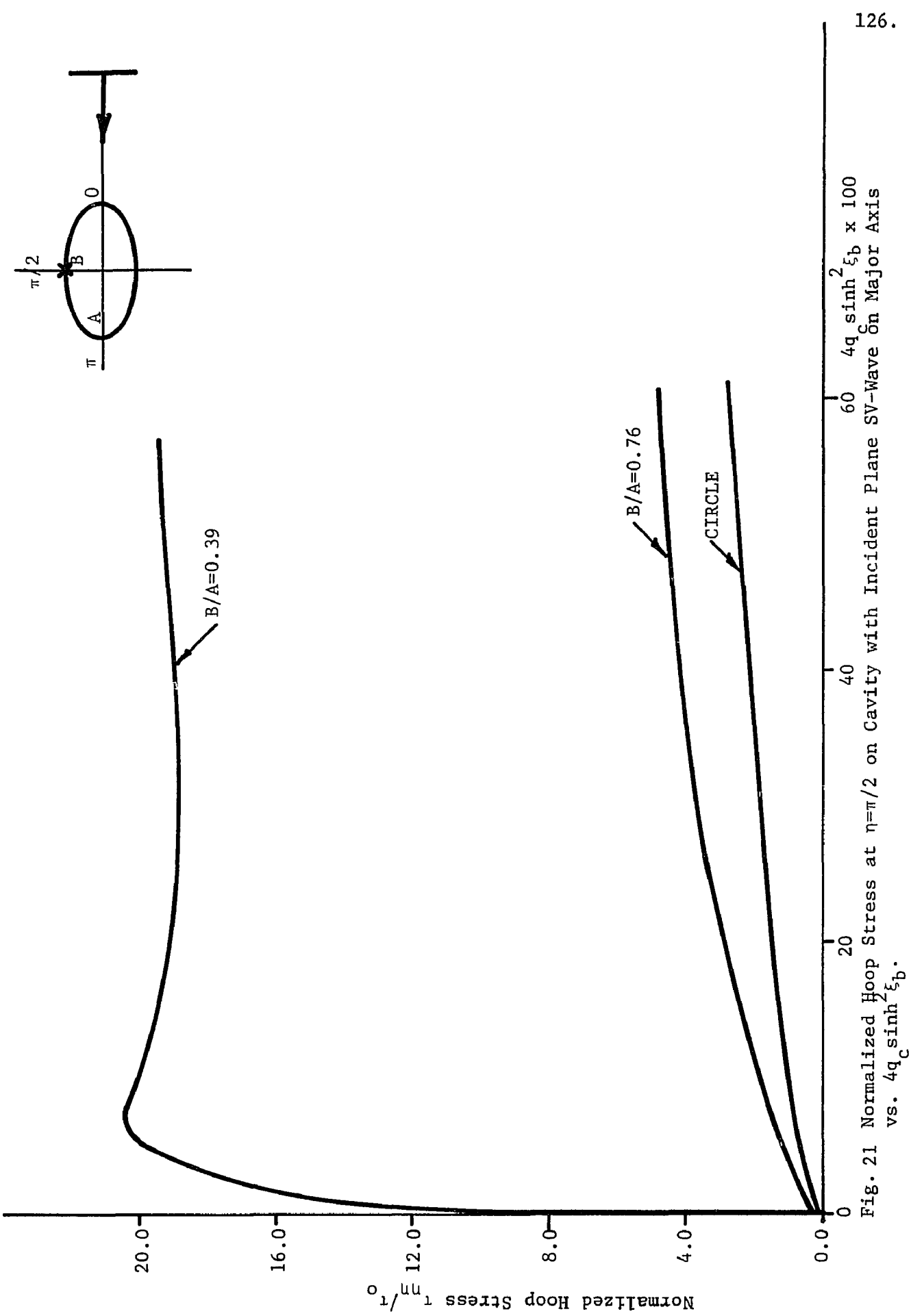


Fig. 21 Normalized Hoop Stress at $\eta=\pi/2$ on Cavity with Incident Plane SV-Wave on Major Axis vs. $4q_c \sinh^2 \xi_b$.